Polymer/Clay Nanocomposites as Barrier Materials Used for VOC Removal

By

Jose M. Herrera-Alonso

Dissertation submitted to the Faculty of

Virginia Polytechnic Institute and State University

in partial fulfillment of the requirements for the degree of

DOCTOR OF PHILOSOPHY

in

Chemical Engineering

Eva Marand, Chair

Donald G. Baird
John C. Little
Stephen M. Martin

August 31, 2009

Blacksburg, VA

Keywords: Thermoplastic polyurethane**,** polymer/clay nanocomposites, barrier membranes, gas permeation, VOC removal

Polymer/Clay Nanocomposites as Barrier Materials Used for VOC Removal

Jose M. Herrera-Alonso

(Abstract)

The objective of this study was to determine if the method of incorporation of a silicate layered nanoclay into a polymer matrix can affect the barrier properties of the pristine polymer in order to decrease the transport of volatile organic compounds (VOC) in indoor air. Building materials are a primary source for VOCs. These emissions are a probable cause of acute health effects and discomfort among occupants and are known to diminish productivity. The predicted concentrations of several of the VOCs emitted by structural insulated panels (SIP) are of concern with respect to health and comfort of occupants. The main issue related to the barrier membranes is the dispersion properties of the nanoclays in the polymer matrix, and the generation of a tortuous pathway that will decrease gas permeation. The tortuous pathway is created by a nanoclay filler, whose ideal exfoliated structure has high surface area, and high aspect ratio. By choosing the appropriate surfactants, the nanoclays can be modified to allow improved molecular interactions between the nanoclay and the polymer matrix.

Several studies were performed in order to evaluate the dispersion properties of the nanoclay in the polymer matrix. Polymer/clay nanocomposites barrier membranes were generated via different synthesis methods. In the first study, barrier membranes were composed of a polyurethane, Estane ® 58315, and different nanoclays, Cloisite ® 10A, Cloisite ® 20A, Cloisite ® 30B. The interaction of the polyurethane and the different surfactants used to organically modify the nanoclay was evaluated. The dispersion of the clay platelets was analyzed by varying the pre-processing method; sonication vs stirring. The decrease in gas permeability results was enhanced by the effect of pre-processing via sonciation in comparison to plain stirring. These results also suggest that nanoclay platelets modified with alkylammonium groups with one tallow tail Cloisite ® 10A and Cloisite ® 30B, allow better dispersion and penetration of the polymer within the basal spacing of the nanoclays. Once the decrease in gas permeability was confirmed, the next challenge was to study and evaluate the performance of the polyurethane/clay nanocomposites barrier membranes in the determination of diffusivity coefficients for volatile organic compounds (VOCs). This was achieved via gravimetric sorption characterization. This method allowed for characterization of the sorption and desorption phenomena of VOC in barrier membranes. Barrier membranes pretreated with sonication demonstrated lower diffusivity coefficients than those only treated with stirring. At high clay loadings, 50 wt% of nanoclay in the polymer, the decrease in diffusivity coefficients for VOCs such as butanol and toluene, was found to be one order of magnitude. Other VOCs such as decane and tetradecane also showed a significant decrease in diffusivity coefficient. The results for VOC sorption studies suggest that there is some variability.

In order to enhance the exfoliation of the clay, we decided to examine *in situ* polymerization of poly (n-butyl methacrylate) in the presence of nanoclay. In this study the clay wt% was kept at a low concentration of 1-5 wt%. The surface modification of natural

montmorillonite, Cloisite ® Na+, was achieved via ion exchange, and the effect of pre-processing was also explored. The modification rendered a tethered group on the surface of the clay that was able to react with the monomer/oligomer chains and thus expand and exfoliate the clay platelets. Gas permeation data suggest that sonication also produced better barrier properties than its counterpart stirring. XRD diffractograms also confirmed exfoliation of the clay platelets in the poly (n-butyl methacrylate) polymer matrix. Thermogravimetric analysis (TGA) suggested that exfoliation of the clay platelets led to improved thermal stability by increasing the decomposition temperature of the membranes. A small increase in T_g also suggested restricted segmental chain motion within the clay platelets. Overall gas permeation decreased even at low clay content. Phenomenological models such as those of Cussler and Nielsen were used to model the experimental permeation results. These models suggest that although the aspect ratio of the clay platelets is within the specifications provided by the manufacturer, it does not reflect the ideal behavior of the models. The last step of this work was to achieve exfoliation of the modified nanoclay platelets via emulsion polymerization of poly (n-butyl methacrylate). The clay concentration in the emulsion was kept the same as in the *in situ* polymerization. DLS results suggest a uniform distribution of the polymer/clay nanocomposites particles in the emulsion. Permeation data indicated higher permeation values than the *in situ* method of synthesis of the nanocomposite membranes. This led us to explore the use of glassy co-polymer of poly(n-butyl methacrylate)-poly(methyl methacrylate) as the matrix. The addition of a more glassy component in the polymer matrix led to improved barrier properties of the nanocomposite membranes. As expected, the copolymer had a higher Tg than the PMMA polymer. Analysis via phenomenological models, also suggested that the chemistry of the co-polymer played an important role in decreasing gas permeability within the polymer/clay nanocomposite membranes, although the effect of the glassy component in the matrix was not quatified by the phenomenological models.

Acknowledgements

I would like to thank my advisor Dr. Eva Marand without whom this work would not be possible. Thank you for all the encouragement, support and guidance throughout this ordeal. Thank you for allowing me the opportunity to grow as a scientist, but also the opportunity to grow as a person.

Thank you to my committee Dr. Baird, Dr. Little and Dr. Martin for proving sound and interesting feedback and also guidance on this project. A special thank you to Steven S. Cox and the staff in the Department of Civil and Environmental Engineering for all help. Thanks to Dr. Zdenka Sedlakova, Jakub Peter and the people at the Macromolecular Institute in Prague, for all interesting exchange of knowledge and the hospitality. My time in Prague will always be a defining and beautiful moment. Děkuji.

I would like to thank the staff in the department of Chemical Engineering, Diane Cannaday, Chris Moore, Jane Price, Tina Kirk, Nora Bentley, Mike Vaught and Riley Chan.

A special thank you to my lab mates, past and present, to my friend and “lab guru” Charles William James Jr., to my lab mentors, Ben Vaughan and Sangil Kim, and to the young ones, Feras Rabie and Anil Surapathi, for all the lessons learned and for the opportunity to get to know all of you. I would also like to thank my incoming class, Chris, John, Ai Fu, Sandeep and Will for their support and friendship.

Thank you to Steve McCartney for the helping collect the TEM and SEM data for this project. Thanks also to Rick Caudill at the department of Wood Science for the XRD data. Also thanks to Dr. Oyama and especially to Travis Gott for their help with the initial XRD data.

A special thanks to my wife Gaby for all the love and support throughout these past couple of years. I know that without her this “important” document would not exist. "Ninguna persona merece tus lágrimas, y quien se las merezca no te hará llorar." Gracias Pietro.

Thanks to my parents Rafael and Margarita, for their constant love and for all their support, “Cuando un recién nacido aprieta con su pequeño puño, por primera vez, el dedo de su padre, lo tiene atrapado para siempre”. Also a special thanks to my sister, brother and their families, Margarita, Rafael, Manuel and Julia. Los quiero no importa como sean o donde esten, siempre los llevo conmigo. To my friend Alfonso “Tito” Ramon, “Un amigo es una persona con la que se puede pensar en voz alta.”

Table of Contents

List of Figures

Chapter 1

Chapter 2

Chapter 3

Chapter 4

Chapter 5

Chapter 6

Chapter 7

List of Tables

Chapter 2

Chapter 3

Chapter 4

Chapter 5

Chapter 6

Chapter 1 Introduction and Objectives

1.1 Introduction and Objectives

For the past 20 years the study of polymer/clay nanocomposites has been an important area of research with direct impact on new technologies. The wide range of applications of polymer/clay nanocomposites has lead to a mass productions and utilization of these products. The nanocomposites products have found a home within the construction, electronic, and transportation industries, as well as within the consumer products area [1, 2]. These types of polymer/clay composites are attractive and offer potential growth because of their improved properties when compared to traditional polymers.

The good synergy of the polymer/clay nanocomposites, has created materials with increased mechanical [3], chemical and thermal properties [4], therefore generating higher resistance to gas permeability [5-7], flammability [8, 9], higher modulus, increases strength, and in some cases increased biodegradability [10, 11]. The origin of these composites materials can be attributed to the Toyota group [12] and their studies on clay/nylon-6 interactions. This group was the first to document the overall improvements of the nanocomposite polymers compared to their counterparts, the pristine polymers. The commercial application of the nylon-6/clay nanocomposites was used in the timing belt covers utilized by the Toyota Corporation in the automotive industry [13-15].

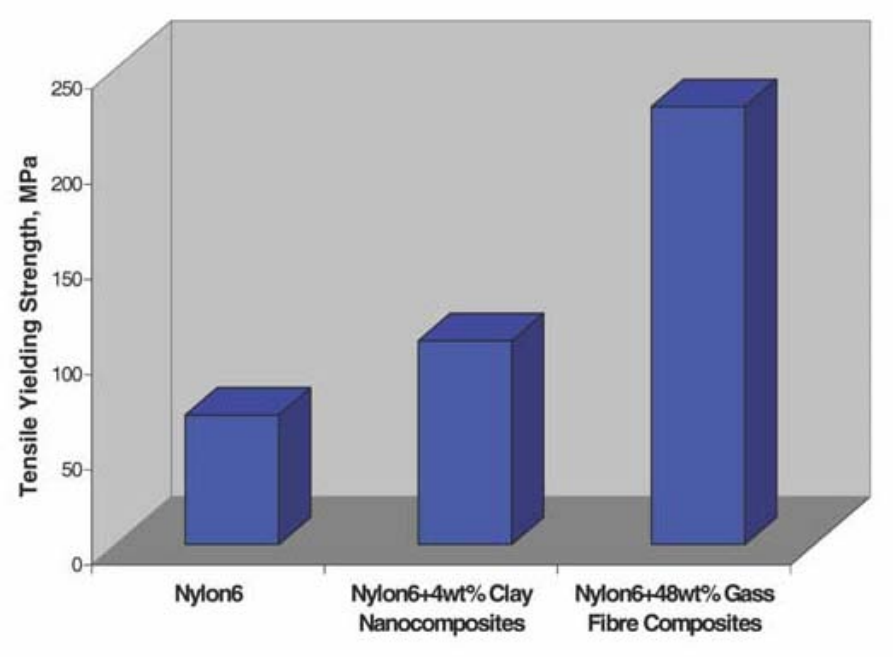

Figure 1.1 Variation and comparison of the tensile properties of nylon-6 and the further addition of clay composites in the matrix [16].

The utilization of polymer/clay nanoparticles prompted the use of clays in order to reinforce the physical properties of nylon. With the addition of clay particles this group found an increase in tensile strength, modulus, and heat distortion [13-15]. They also noticed that nanocomposites had a decrease in water uptake and improved gas barrier properties when compared to the pure nylon.

The enhanced permeation properties shown by these materials also promoted more corporations to study the benefits of the polymer/clay composites. According to the review by Gao [16], Honeywell, Alcoa CSI, Mitsubishi Gas Chemical and Nanocor have developed new technology for barrier line materials, drink packaging applications and bottle applications. These corporations have not only stayed in the area of nylon-6/clay composites, but they have also branched out to different polymers, such as multilayered

PET. Barrier membranes can be produced via three basic strategies which are: first, the use of polymers with low permeabilites [17]; second, the incorporation of sacrificial fillers or reactive groups in the polymer matrix [18]; third, loading of polymers with aligned and impermeable flake like layered materials [19].

The objective of this work is to develop polymer/clay nanocomposites as barrier membranes using dispersed and/or exfoliated phyllosilicates in a polymer matrix to decrease permeation of volatile organic compounds (VOCs) as well as gas permeating molecules. The high aspect ratio, high surface area, and impermeable properties of layered materials, such as montmorillonite $M_x(Al_{4-x}Mg_x)Si_8O_{20}(OH)_4$ will allow the design of barrier membranes. This project examines the synthesis of these materials as well the evaluation of their respective transport properties. The ultimate goal is to incorporate these barrier films into structural insulating panels.

In his extensive review regarding the mechanical and structural properties of polymer clay nanocomposites, Tjong [20] suggested that the exfoliated morphology in a nanocomposite matrix is a rare phenomena. The delicate balance between exfoliated morphologies and intercalated morphologies may depend on the close monitoring of the dispersion properties of clay platelets in the polymer matrix. According to Tjong, the proper selection of an adequate solvent is the first criteria for exfoliating clay composites in the matrix. Another property that may improve the dispersion of the layered materials is the interactions of the clays and the surfactants. The chemical modification of the clay surface may render improved polymer/clay or polymer/surfactant interactions yielding a

different morphology in the matrix. The three possible morphologies in polymer/clay nanocomposties can be seen in figure 1.2.

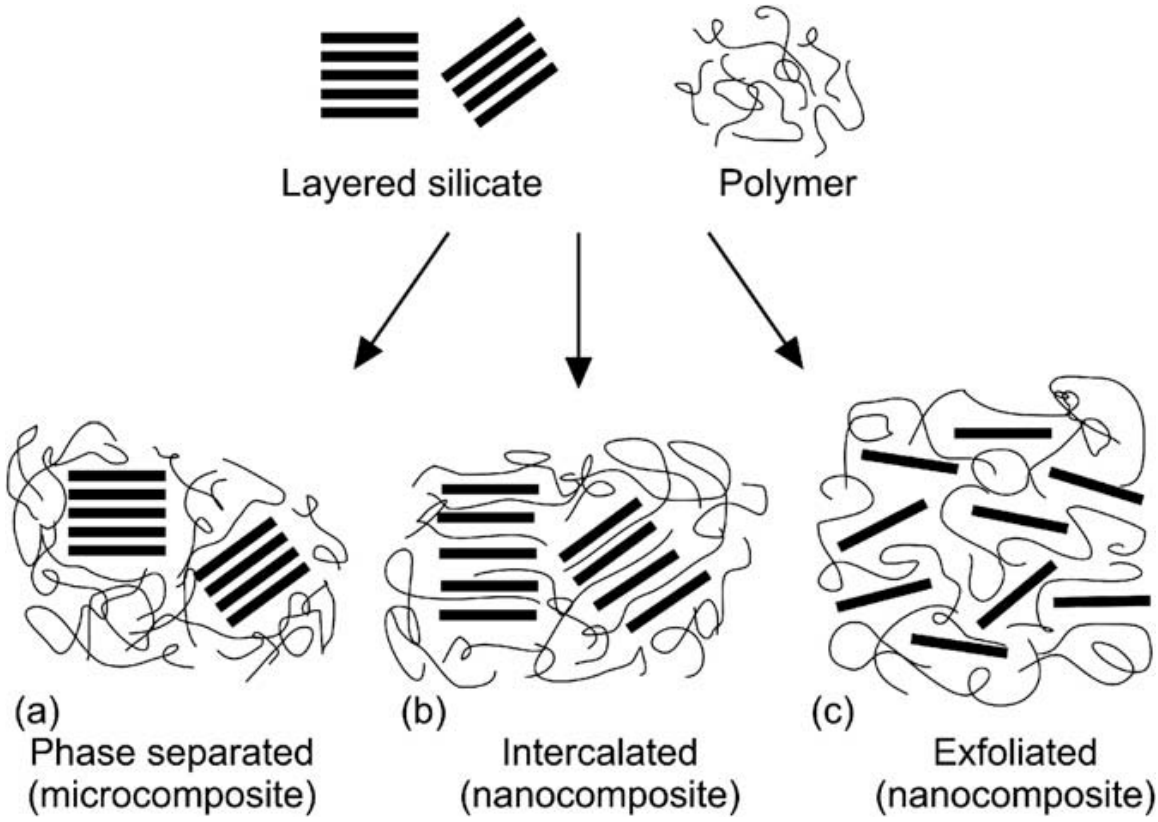

Figure 1.2 Different morphologies for polymer/clay nancomposites [21].

The interactions of polymer/layered materials may affect the crystallinity of the polymer, the molecular orientation of the chains and also the packing of the molecules near the platelets [22]. Incompatibility problems between the polymer and the layered material may produce voids at the interface, thus yielding increasing free volume in the matrix which in turn can lead to a higher permeability [23]. This phase separation in the matrix was also reported by Giannelis [24]. This group stated the different processing methods, such as extrusion, injection molding and casting maybe used to achieve intercalated and/or exfoliated morphology. The dispersion of the layered materials in the

matrix will affect the transport properties of the barrier membrane. Different models have been used to analyze and predict permeation properties of polymer/clay nanocomposites [19, 25-29]. Most notably Cussler et al. [26, 27, 30], have studied extensively the phenomena of dispersion in the matrix [19], alignment of layered materials [31], and the ideal distribution of the layered materials perpendicular to the direction of the permeating particle. The ideal distribution of the model may be seen in figure 1.3. The layered materials in the polymer matrix produce a tortuous pathway, thus increasing the length of the diffusion path for the penetrating molecules. The presence of the layered materials in the polymer matrix also decrease the cross-sectional area by which permeation may be achieved [32]. Initial studies of barrier membranes containing impermeable flakes were aimed at modeling permeation of micron-size platelets, such as mica [26, 33], but the versatility this model has allowed for the modeling of nanosize flake like structures as well [34]. Phenomenological models like Cussler's, are important tools that allow to predict permeability of a polymer/layered materials.

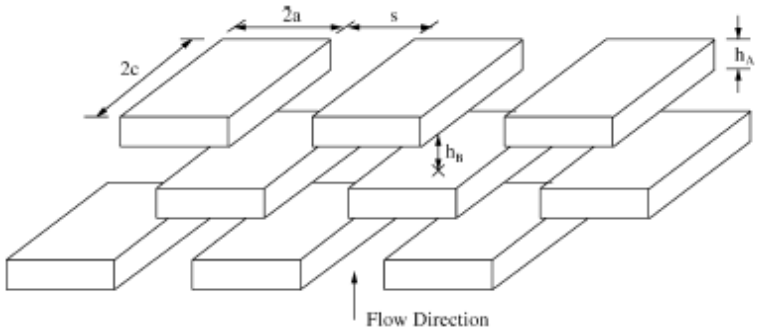

Figure 1.3 3D model of dispersed flake like platelets. Idealized structure used in Cussler's permeation model [35].

References

1. Meneghetti, P. and S. Qutubuddin, *Synthessis, thermal properties and applications of polymer-clay nanocomposites.* Thermochimica Acata, 2006. **442**(1-2): p. 74-77.
2. Tien, Y.I. and K.H. Wei, *Hydrogen bonding and mechanical properties in segmented montmorillonite/polyurethane nanocomposites of different hard segment ratios.* Polymer, 2001. **42**(7): p. 3213-3221.
3. Wang, Z. and T.J. Pinnavaia, *Nanolayer Reinforcement of Elastomeric Polyurethane.* Chemistry of Materials, 1998. **10**(12): p. 3769-3771.
4. Yoon, P.J., T.D. Fornes, and D.R. Paul, *Thermal expansion behavior of nylon 6 nanocomposites.* Polymer, 2002. **43**(25): p. 6727-6741.
5. Jeong, H.K., et al., *Fabrication of Polymer/Selective-Flake Nanocomposite Membranes and Their Use in Gas Separation.* Chemistry of Materials, 2004. **16**(20): p. 3838-3845.
6. Ogasawara, T., et al., *Helium gas permeability of montmorillonite/epoxy nanocomposites.* Composites Part A: Applied Science and Manufacturing, 2006. **37**(12): p. 2236-2240.
7. Xu, B., et al., *Calculating barrier properties of polymer/clay nanocomposites: Effects of clay layers.* Polymer, 2006. **47**(8): p. 2904-2910.
8. Beyer, G., *Nanocomposites: a new class of flame retardants for polymers.* Plastics, Additives and Compounding, 2002. **4**(10): p. 22-28.
9. Zheng, X. and C.A. Wilkie, *Flame retardancy of polystyrene nanocomposites based on an oligomeric organically-modified clay containing phosphate.* Polymer Degradation and Stability, 2003. **81**(3): p. 539-550.
10. Ray, S.S., K. Okamoto, and M. Okamoto, *Structure-Property Relationship in Biodegradable Poly(butylene succinate)/Layered Silicate Nanocomposites.* Macromolecules, 2003. **36**(7): p. 2355-2367.
11. Jeon, H.S., et al., *Characterization of polyisoprene-clay nanocomposites prepared by solution blending.* Polymer, 2003. **44**: p. 5749-5758.
12. Usuki, A., et al., *Synthesis of nylon 6-clay hybrid.* Journal of Materials Research, 1993. **8**(5): p. 1179-1184.
13. Kojima, Y., et al., *Mechanical properties of nylon 6-clay hybrid.* Journal of Materials Research, 1993. **8**(5): p. 1179-1184.
14. Kojima, Y., et al., *Sorption of water in nylon 6-clay hybrid.* Journal of Applied Polymer Science, 1993. **49**: p. 1259-1264.
15. Kojima, Y., et al., *Crystallization of a nylon-6-clay hybrid by injection moulding under elevated pressure.* Journal of Materials Science Letters, 1993. **12**(12): p. 889.
16. Gao, F., *Clay/polymer composites: the story.* Materials Today, 2004. **7**(11): p. 50-55.
17. Koros, W.J., ed. *Barrier polymers and structures*. Vol. 423. 1990, ACS Symposium Series: Washington, D. C.

18. Nuxoll, E.E., R.A. Siegel, and E.L. Cussler, *Layered reactive barrier film.* Journal of Membrane Science, 2005. **252**(1-2): p. 29-36.
19. Lape, N.K., E.E. Nuxoll, and E.L. Cussler, *Polydisperse flakes in barrier films.* Journal of Membrane Science, 2004. **236**(1-2): p. 29-37.
20. Tjong, S.C., *Structural and mechanical properties of polymer nanocomposites.* Materials Science and Engineering: R: Reports, 2006. **53**(3-4): p. 73-197.
21. Alexandre, M. and P. Dubois, *Polymer-layered silicate nanocomposites: preparation, properties and uses of a new class of materials.* Material Science and Engineering R, 2000. **28**.
22. Incarnato, L., et al., *Preparation and characterization of new melt compounded copolyamide nanocomposites.* Polymer, 2003. **44**(16): p. 4625-4634.
23. George, S.C. and S. Thomas, *Transport phenomena through polymeric systems.* Progress in Polymer Science, 2001. **26**(6): p. 985-1017.
24. Giannelis, E., *Polymer layered silicated nanocomposites.* Advanced Materials, 1996. **8**(1): p. 29-35.
25. Bharadwaj, R.K., *Modeling the Barrier Properties of Polymer-Layered Silicate Nanocomposites.* Macromolecules, 2001. **34**(26): p. 9189-9192.
26. Cussler, E.L., et al., *Barrier Membranes.* Journal of Membrane Science, 1988. **38**(2): p. 161-174.
27. Eitzman, D.M., R.R. Melkote, and E.L. Cussler, *Barrier membranes with tipped impermeable flakes.* AIChE Journal, 1996. **42**(1): p. 2-9.
28. Nielsen, L.E., *Models for the permeability of filled polymer systems.* J. Macromol. Sci., Chem., 1967. **A1**.
29. Gusev, A.A. and H.R. Lusti, *Rational Design of Nanocomposites for Barrier Applications.* Advanced Materials, 2001. **13**(21): p. 1641-1643.
30. Falla, W.R., M. Mulski, and E.L. Cussler, *Estimating diffusion through flake-filler membranes.* Journal of Membrane Science, 1996. **119**(1): p. 129-138.
31. Yang, C., W.H. Smyrl, and E.L. Cussler, *Flake alignment in composite coatings.* Journal of Membrane Science, 2004. **231**(1-2): p. 1-12.
32. Liu, Q. and E.L. Cussler, *Barrier membranes made with lithographically printed flakes.* Journal of Membrane Science, 2006. **285**(1-2): p. 56-67.
33. Perry, D., W.J. Ward, and E.L. Cussler, *Unsteady diffusion in barrier membranes.* Journal of Membrane Science, 1989. **44**(2-3): p. 305-311.
34. Sridhar, L.N., R.K. Gupta, and M. Bhardwaj, *Barrier properties of polymer nanocomposites.* Industrial and Engineering Chemistry Research, 2006. **45**(25): p. 8282-8289.
35. Swannack, C., et al., *A three-dimensional simulation of barrier properties of nanocomposite films.* Journal of Membrane Science, 2005. **263**(1-2): p. 47-56.

Chapter 2 Literature review of barrier membrane models, layered materials, polymer/clay nanocomposites, indoor air quality and emulsion polymerization

2.1 Permeation

The gas permeation phenomenon in polymer membranes is explained as a three step process [1, 2], known as the solution-diffusion mechanism. The first step in the process deals with the penetrant molecules, which dissolve into the face of the membrane at the high pressure upstream side. In the second stage, diffusion of the molecules takes place through the membrane to the low pressure side or the downstream. The last stage deals with desorption of the molecules from the surface of the downstream part of the membrane.

There are three fundamental parameters that describe the capability of a membrane to transport gas, which are:

- Permeability Coefficient
- Diffusion Coefficient
- Solubility

Utilizing the three previous fundamental parameters it is possible to model the performance of a polymeric membrane under certain simplifying assumptions [2-5]. This model is established with the following equation:

$$P = D \cdot S \qquad \text{Eq (2.1)}$$

Where P is the permeability, D is the diffusivity coefficient, and S is the solubility coefficient. These three parameters will be discussed in depth in the following section.

The permeability coefficient is also referred to as the permeability of a sample, and is defined by the rate at which the penetrant can pass through a membrane. In mathematical terms the permeability can be defined by the following equation:

$$P_i = \frac{J_i}{p_u - p_d} l \qquad \text{Eq (2.2)}$$

Where J_i is the steady state gas flux of the i-th penetrant component through the membrane, l is defined as the thickness of the membrane; p_u and p_d are defined as the up-stream and down-stream pressures of the i-th component. When dealing with a gas mixture, the down-stream and up-stream pressures are referred to as the partial pressures of each component in the mixture. In a non-ideal gas mixture the partial pressures of the i-th components are replaced by fugacities of each component.

Permeability is most commonly reported in units of Barrers, defined by the following units:

$$1\ Barrer = 1\times 10^{-10}\ \frac{cm^3\ (STP)\cdot cm}{cm^2\cdot \sec\cdot cmHg}$$

The diffusivity coefficient is a measure of the rate at which a permeant moves through the polymer material and has the units of cm^2/s. The diffusion coefficient is a kinetic parameter that depends on the properties such as the size of the penetrant, polymer segmental dynamics, the morphology of the polymer, time and temperature [2, 3].

According to Yi-Yan et al. [6] the geometry and the permeate size will motivate a change in the diffusivity coefficient For example, the diffusivity maybe 1000 times faster

for elongated molecules than for spherical molecules in glassy polymers. Vieth [7], indicated that there are two ways of evaluating molecular diffusion in polymers; the first method is the transmission through a thin membrane, the second method is the sorption of gases or vapors by a “thick” slab.

2.2 Time Lag Method

The time lag method is a useful tool that permits the calculation of the diffusion coefficient of pure gases or vapors through a membrane. The time lag is the amount of time for a gas or a vapor to permeate through a membrane. The time lag is a function of system parameters as well as operating conditions. Experimentally this method is achieved by mounting a membrane between two parallel chambers. The first chamber is filled with penetrant molecules, and its volume is large enough so that the pressure can be constant during the course of the experiment. This initial chamber represents the upstream current. The second chamber is also known as the downstream current will be isolated from the penetrant.

At t = 0 the current containing the penetrant species permeates through the membrane and into the downstream side of the system, the pressure at the downstream side remains zero for a certain time. The change in pressure is a direct result of the accumulation of the penetrant molecules in the membrane and the diffusion to the downstream current. There exists an increase in pressure and as time progresses this relationship achieves a linear asymptote. This linear asymptote intersect the time axis at the time lag. Figure 2.1. is an example of the use of the Time lag method.

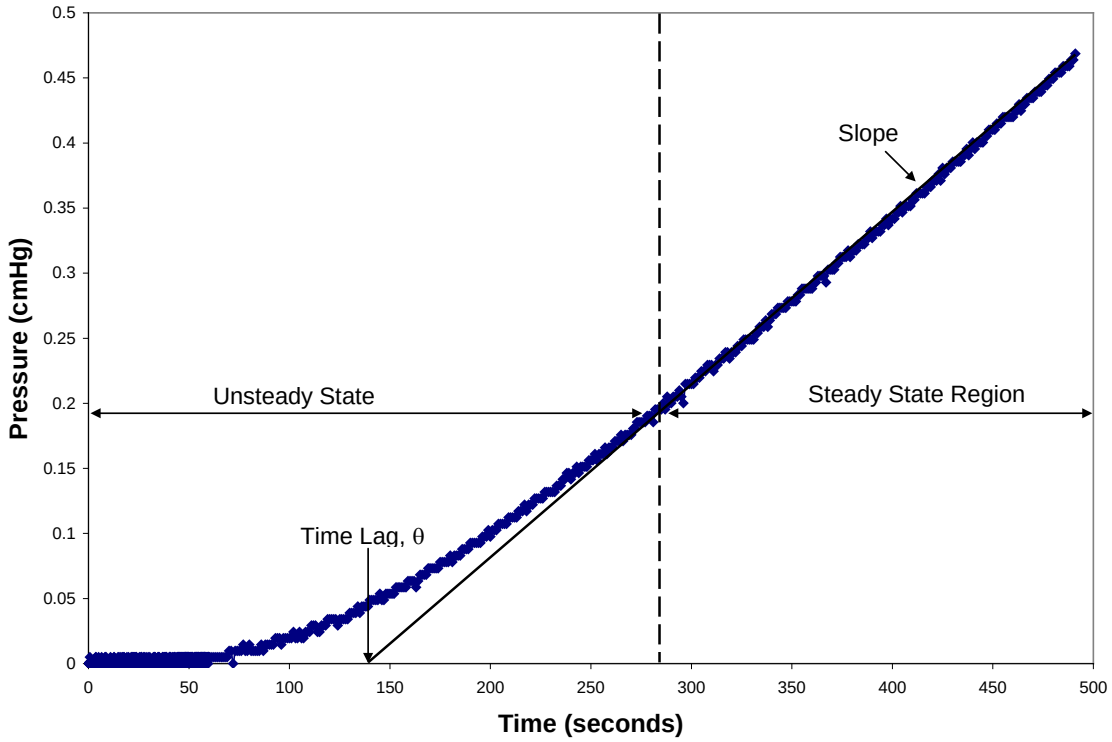

Figure 2.1. Typical experimental data analyzed using the Time Lag Method.

The pressure data can be divided into two regions: unsteady state region and steady state region. The unsteady state region exists at shorter times, and encompasses portions where the permeate pressure is zero. The steady state region includes the linear relationship between the permeate pressure and time.

In order to establish the mathematical representation of the time lag method, the first step recalls Fick's second law of diffusion. This model fits experimental data of unsteady state permeation and adsorption.

$$\frac{\partial C}{\partial t} = D\frac{\partial^2 C}{\partial x^2} \qquad \text{Eq (2.3)}$$

By applying the following boundary conditions equation 2.3 can be solved. The boundary conditions corresponding to the experimental set-up are the following:

$t < 0$	$0 \leq x \leq l$	$C = 0$
$t \geq 0$	$x = 0$	$C = C_{2,m} = Sp_2$
$t \geq 0$	$x = l$	$C = \partial C/\partial t = 0$

The solution to the Fick's second law of diffusion with the above boundary conditions is given by Equation (2.4). This is also referred to as a one-dimensional flow through a membrane and makes the assumption that the diffusion coefficient, D, is constant and independent of temperature and penetrant concentration in the membrane.

$$\frac{Q}{lC_2} = \frac{Dt}{l^2} - \frac{1}{6} - \frac{2}{\pi^2}\sum_{n=1}^{\infty}\frac{(-1)^n}{n^2}\exp\left(-\frac{Dn^2\pi^2 t}{l^2}\right) \qquad \text{Eq (2.4)}$$

From Eq 2.4 we can identify Q, which is the total permeate passing through the membrane, and l is referred to the thickness of the film. The other 3 variables that must be accounted for in Eq 2.4, are the time dependence t, the diffusion coefficient D and the concentration of the film on the feed side C_2. It can be shown that as $t \rightarrow \infty$, the amount of vapor that permeates through the membrane becomes a linear function of time.

$$\frac{2}{\pi^2}\sum_{n=1}^{\infty}\frac{(-1)^n}{n^2}\exp\left(-\frac{Dn^2\pi^2 t}{l^2}\right) = 0 \qquad \text{Eq (2.5)}$$

By analyzing the different regions in the pressure vs time curve, the steady state part implies that the t has approaches infinity, and $\partial C/\partial t = 0$. Establishing Eq 2.5 will reduce Eq 2. 4 to the following:

$$\frac{Q}{lC_2} = \frac{Dt}{l^2} - \frac{1}{6} \qquad \text{Eq (2.6)}$$

The diffusivity is calculated by extrapolating the steady state permeation curve to the time axis, where the intercept θ is called the time lag However, in order to establish the time lag term in Eq 2.6, this equation must be rearranged in terms of Q. Equation 2.7, indicates that the total gas passing through the membrane, which is Q, is zero until a time t has elapsed. This time must be greater than the time lag value θ. From Equation 2.7 the Q value is also referred to as the accumulation term, due to a trapped gas permeate within the fixed volume.

$$Q = \frac{DC_2 t}{l} - \frac{lC_2}{6} = \frac{DC_2}{l}\left(t - \frac{l^2}{6D}\right) = \frac{DC_2}{l}(t - \theta) \qquad \text{Eq (2.7)}$$

$$\theta = \frac{l^2}{6D} \qquad \text{Eq (2.8)}$$

Once the diffusivity coefficient is established, the permeability is obtained from the slope in the steady state region. Solving for the flux, J, is the starting point for the solution of the permeability coefficient, P. The following expression is the solution for the flux J through the membrane.

$$J = \frac{Slope}{RT} \cdot \frac{V}{A}\left(\frac{22414\ cm^3(STP)}{mol}\right) \qquad \text{Eq (2.9)}$$

The volume V in Eq 2.9 is the volume of the evacuated chamber into which the gas permeates, A, is the cross sectional area of the membrane, T, is the experimental temperature, R, is the ideal gas constant, and, l, is the thickness of the membrane. The solution for the flux, J, is converted to STP conditions. The slope obtained during the permeation experiment is within the steady state region. Further manipulation of Eq 2.9 will yield Eq 2.10, which is in terms of pressure. The downstream pressure, P_1, in the

system is much smaller than the feed pressure, P_2, and the difference in pressure can be replaced with the, P_2, value.

$$J = P\frac{\Delta p}{l} \cong P\frac{p_2}{l} \qquad \text{Eq (2.10)}$$

A further rearrangement of equation 2.10 will provide the permeability coefficient.

$$P \cong J\frac{l}{p_2} \qquad \text{Eq (2.11)}$$

By establishing the time lag and its relationship with the permeability coefficient, P, the solubility and diffusion coefficients are defined by the following expressions.

$$D_{eff} = \frac{l^2}{6\theta} \qquad \text{Eq (2.12)}$$

$$S_{eff} = \frac{P}{D} \qquad \text{Eq (2.13)}$$

Another way of obtaining diffusivity coefficient in a film was developed by Crank [8] based on an equilibrium sorption method. Crank provided a non steady state solution of uniform initial distribution, where surface concentrations of the “slab” or “film” are equal and kept constant. This solution is also based on Fick’s second law of diffusion, Eq. 2.3, and the following initial conditions:

$C = C_1$	$x = 0$	$t \geq 0$
$C = C_2$	$x = l$	$t \geq 0$
$C = f(x)$	$0 < x < l$	$t = 0$

The solution for equation 2.3., is in the form of trigonometrical series as presented below:

$$C = C_1 + (C_2 - C_1)\left(\frac{x}{l}\right) + \frac{2}{\pi}\sum_1^{\infty}\frac{C_2\cos n\pi - C_1}{n}\sin\frac{n\pi x}{l}\exp\left(\frac{-Dn^2\pi^2 t}{l^2}\right) + \frac{2}{l}\sum_1^{\infty}\sin\frac{n\pi x}{l}\exp\left(\frac{-Dn^2\pi^2 t}{l^2}\right)\int_0^l f(x')\sin\frac{n\pi x'}{l}dx' \qquad \text{Eq (2.14)}$$

According to Crank, the most common cases lead to f(x) being either zero or constant so that the integral in equation 2.14 is readily evaluated. It's a frequent case that this problem is symmetrical about the central plane of the sheet.

The solution for equation 2.14 in the case of uniform initial distribution with surfaces of equal concentration is obtained within the region of $-l < x < l$. Assuming initially a uniform concentration, C_0, and constant surface concentration, C_1, the solution for equation 2.14 would be as follows:

$$\frac{C - C_0}{C_1 - C_0} = 1 - \frac{4}{\pi}\sum_{n=0}^{\infty}\frac{(-1)^n}{2n+1}\exp\left\{\frac{-D(2n+1)^2\pi^2 t}{4l^2}\right\}\cos\frac{(2n+1)\pi x}{2l} \qquad \text{Eq. (2.15)}$$

Equation 2.15, can be rearranged to the following form:

$$\frac{M_t}{M_\infty} = 1 - \frac{8}{\pi^2}\sum_{n=0}^{n=\infty}\frac{1}{(2n+1)^2}\exp\left\{\frac{-D(2n+1)^2\pi^2 t}{l^2}\right\} \qquad \text{Eq (2.16)}$$

M_t is the total amount of vapor absorbed at time t, M_∞ is the equilibrium sorption and n is an integer. Experimentally, these parameters can be obtained using McBain's procedure [7], where a slab or film is suspended from a quartz spring in the penetrant atmosphere and the change of length is followed with a cathetometer as the polymer sample takes up the vapor. The variation in weight is monitored by a microbalance and thus recorded.

2.3 Layered Materials

The most common clay minerals used in polymer nanocomposites are 2:1 phyllosilicates or layered silicates. These minerals are hydrous aluminum silicates. Encompassed within the family of phyllosilicates in a 2:1 ratio are smectite, vermiculite, mica and chlorite. By focusing on the smectite group, there exists a further subdivision that contains montmorillonite, nontronite, saponite, and hectorite [9]. The general formula for each layered material is listed in Table 2.1.

Table 2.1.Chemical structure of commonly used phyllosilcate 2:1[10].

2:1 Phyllosilicate	General Formula
Montmorillonite	$M_x(Al_{4-x}\ Mg_x)Si_8O_{20}(OH)_4$
Hectorite	$M_x(Mg_{6-x}\ Li_x)Si_8O_{20}(OH)_4$
Saponite	$M_xMg_6\ (Si_{8-x}\ Al_x)O_{20}(OH)_4$

The smectite group consists of tetrahedral sheets composed of corner linked tetrahedral, whose central atoms are Si^{4+}, Al^{3+} and Fe^{3+}. The basal oxygens of the tetrahedron are shared by adjacent tetrahedral atoms, which lead to the formation of hexagonal patterns. Thus the complete framework of these natural clays is based on two tetrahedrally coordinated silicon atoms fused to an edge shared octahedral sheet of either aluminum or magnesium hydroxide, as can be seen in Fig. 2.2 [11]. The natural stacking of tetrahedral and octahedral sheets occurs in specific ratios and modes, which lead to the formation of the 2:1 layer silicates called tactoids. The layer thickness is around 1 nm, and the lateral dimensions of these layers may vary from 30 nm to several microns or even larger, for montmorillonite, whose length is within 100-200 nm.

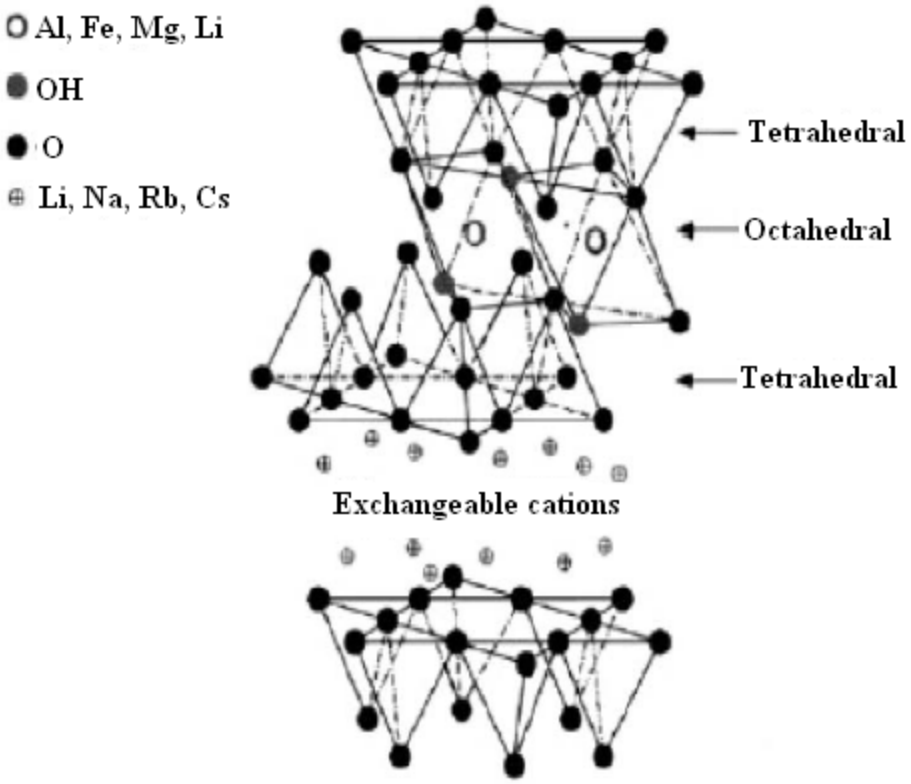

Fig. 2.2 Schematic representation of phyllosilicate crystalline structure [11].

The stacking of the layers leads to a regular van der Waals gap between the layers called interlayer or gallery. The layer charge can easily be changed by the replacement of the cations in the alumina sheet with cations of different charges. The isomorphic substitution within the layers, which can be the replacement of Al^{3+} with Mg^{2+} or Fe^{2+}, produce negative charges, which are delocalized over surrounding oxygen atoms. The charges can be counterbalanced by hydrated alkali metals and alkaline earth cations such as Na^{+}, Li^{+} or Ca^{2+}, located in the gallery between the aluminosilicate layers, and are also denominated interlayer cations [12]. The arrangement of these cations occurs in such a way that the overall electrostatic energy is minimized. This type of layered silicate contains moderate surface charge, which is known as cation exchange capacity (CEC).

This ion exchange capacity is used to characterize the degree of isomorphous substitution. The typical CEC values are within a range of 60-120 meq/100g [9]. The reactivity of the clay is a product of two different causes; the incorporation of the exchangeable cations on the interlayer sites in order to maintain a neutral charge on the crystal lattice, and the discontinuities on the edges when the periodic arrangement of atoms is terminated [13]. The charge may vary from layer to layer, and considered as an average value over the whole crystalline structure. The gallery height of the clay particles is determined by the type of cations positioned within the interlayer and the degree of hydration [14]. The compatibility of the clay platelets with the polymer can be controlled by the use of organic compounds. Smectites and silicic acids are hydrophilic, caused by the hydration of the interlayer alkali earth and alkali metal cations. The hydrophilicity renders an incompatibility of the clay with the polymeric system. Organophilic layered silicates are ion exchange reactions done with cationic surfactants like phosphonium and ammonium ions, and lead to the formation of organically modified layered silicates (OLS). According to Vaia [9], the vast majority of the OLSs utilized in polymer layers silicate nanocomposites are comprised of alkylammonium surfactants. The alkyl chains contained in the interlayer adopt different conformation, from liquid like to solid like, depending on the chain length and the exchange capacity.

2.4 Interfacial Distance and Swelling Agents

The modification of the platelet surface leads to the enlargement of interlayer gallery; this process is achieved by ion-exchange of the hydrated cations with organic cations such as bulky alky ammonium groups. Alkylammonium or alkylphosphonium cations in the organosilicates diminish the surface energy of the inorganic host and improve the wetting characteristics of the polymer matrix. This surface modification leads to a larger interlayer distance. The functional groups attached to the alkylphosphonium or alkylammonium groups present in the galley can react or interact physically with the polymer matrix, also leading to an increase the gallery distance [15]. This interspace distance is directly related to the length of alkyl chain and the ratio of the cross sectional area to available area per cation [16, 17].

Giannelis et al. [15, 18]**,** were the first group to study and elucidate a 3D arrangement of the alkyammonium groups in the interlayer. The utilization of Fourier transform infrared spectroscopy (FTIR) technique, determined that the alkyl chains can behave in two different ways: as solid-like or liquid-like structures. As temperature increased, the behavior of these chains resembled more a liquid like structure. The same type of behavior is observed when the chain length or interlayer density decreased. The reason for this behavior was due to the small differences between the gauche and trans conformations. An example of this order can be seen with the montmorillonite samples; at ambient temperatures the alkylammonium monolayers adopted a two dimensional order or disordered state, which depends on the cross sectional area of the molecules, the ratio of the area/cation available on the substrate and the alkyl chain length. At low

temperatures the chains assume a trans conformation, and as the temperature increases the chains assume a random conformation [19]. Giannelis et al. also determined that the increase of packing density or an increase in the chain length improved the order of the chains [20]. The organically modified layers self-assemble parallel to each other to form alternating, well ordered organic/inorganic multilayers [21]. The alkyl groups are attracted to the negative charge of the silicate layers and are binded in a head-to-tail conformation that yields the hydrocarbon tails filling the gallery space in between the layers.

Osman et al. [22] studied the effect of the interspacial distance related to the length of the alkyl chains in montmorillonite (MMT). When this group studied a MMT modified with an alkyl chain with four carbon atoms, there was little to no change in the basal plane gallery distance. As the length of the carbon atoms increased, from four to eight, the gallery distance increased with a linear tendency. This group also used an octadecyl series, which also increases the gallery length, but it did not maintain the linear relationship that was previously established. This group quantified this interspacial distance or gallery distance by the use of the XRD, which yields a d-spacing measurement.

Commercially it is possible to obtain many different types of clay at a low cost; companies like Southern Clay Products, Elementis Specialties Company, Nanocor Inc., Sud-Chemia and Laviosa Chimica Mineraria are suppliers for these products. Table 2.2, shows some alkylammonium groups present in the Cloisite® family from Southern Clay Products. HT is a hydrogenated tallow group with a variable composition of ~65% C18:

~30% C16: ~5% C14. T is a tallow group with the same ratio of C18, C16 and C14, where C18, for example stands for a hydrocarbon with 18 carbon units.

Table 2.2 Southern Clay Company products, Cloisite® [23].

Cloisite® 10A	Cloisite® 20A	Cloisite® 30B	Cloisite® 93
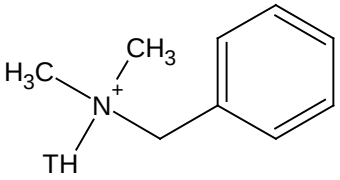	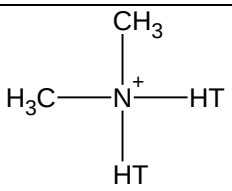	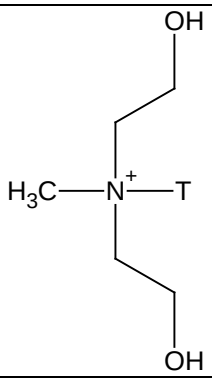	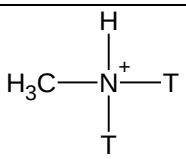

2.5 Polymer/Clay Synthesis Methods

According to Oriakhi [24] and to Zhang [25], polymer/clay composites can be prepared by four major processes, which are: (1) Exfoliation/adsorption: in this method the silicate layers are exfoliated through the use of a solvent in the polymer. After the exfoliation, the polymer adsorbes onto the surface of the silicate layers and when the solvent evaporates the silicate layers reconfigure into sandwiched structures with the polymer in the interspacial galleries; (2) In-situ intercalative polymerization or in-situ polymerization, this method is based on the swelling of the silicate layers with the liquid polymer and the application of heat or radiation can be used to promote the polymerization between the silicate layers. A proper selection of the functional groups within the silicate layers may control the polymerization rates and the initiation points so the layer separation process may occur before or during polymerization [9]; In the Melt

intercalation process (3), the polymer in the molten state is mixed with the clay, and due to favorable interactions between the clay and the polymer, the latter introduces itself between the silicate layers exfoliates the layers or simply intercalates the layers. Shear flows from the melt process may facilitate a homogenous morphology of the polymer layered silicate nanocomposites, as well as a global alignment of the layers. The final method is the Template Synthesis (4); in this method the precursors of the silicate layers are mixed with the polymer, and by self-assembly forces the polymer will help the growth of the inorganic crystals, by helping the crystals grow the polymer will be trapped between the formation of the crystals [10].

2.6 Clay Dispersion and Exfoliation

The two idealized morphologies within the polymer-layered silicate composites are exfoliated and intercalated. The intercalated structure can be considered as guest-host compounds that result from the polymer penetration into the interlayer and the subsequent expansion to a thermodynamically defined equilibrium spacing [26, 27]. The inter layer expansion will range between 1 to 4 nm, and is associated with the incorporation of individual polymer chains. Exfoliated morphology consists of individual silicate layers suspended in the polymer matrix, and is a direct result from polymer penetration within the crystallites, which eventually leads to delamination.

Polymer/clay interactions are a fundamental parameter to determine the degree of exfoliation and dispersion of layered materials. Polymers have the ability to intercalate the gallery of layered materials by interacting with the clay surface trough ion-dipole,

dipole-dipole and hydrogen bonding [28, 29] molecular interactions. In order to quantify the dispersion of the clay platelets in the polymer matrix, solubility parameters are used to characterize these interactions. Ho et al. [28, 29] used the Hansen solubility parameters to correlate the degree of exfoliation of organically modified clays and the solvent in which these clays were dispersed. The original definition of the solubility parameter was established by Hildebrand and Scott [30], these researchers proposed the following definition for solubility parameter, δ:

$$\delta = \sqrt{\frac{E}{V}} \qquad \text{Eq.2.17}$$

Where, V, is the molar volume, and, E, is the molar cohesive energy, this energy is associated with the net attractive interactions of the material. The importance of Hansen's contribution is based on the extension of the Hildebrand parameter and its application to a polymer-solvent systems. The Hansen parameter takes into consideration the dispersive forces (δ_d), the polar forces (δ_p) and the hydrogen-bonding forces (δ_h) acting together.

$$\delta_0^2 = \delta_d^2 + \delta_p^2 + \delta_h^2 \qquad \text{Eq. 2.18}$$

The proper paring of the solvent and clay particles is fundamental in order to assure a proper dispersion and exfoliation in the polymer/clay matrix.

Within these methods of synthesis the polymer/clay interaction and dispersion that is obtained can be categorized in three major categories: intercalated, exfoliated and phase separated, a graphical representation of these three different systems is depicted in Fig. 2.3. Intercalated structures are self assembled multilayered structures where the

polymer chains insert themselves in the gallery space and eventually generate an expansion of the silica interlayer. The intercalated structure generates a well ordered multilayer morphology built with alternating polymeric and inorganic layers maintain the same clay layer registry. Exfoliation on the other hand is a result of a deep penetration of the polymer in the interlayer gallery space and generates a delamination and disperses the clay palates in the matrix [10, 11, 31, 32].

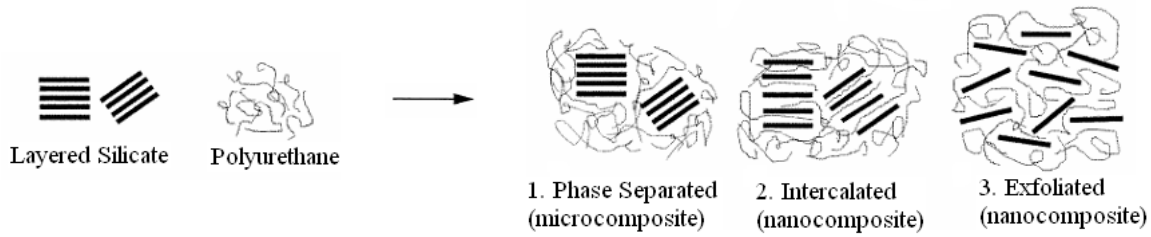

Figure 2.3. Schematic representation of different structures for the polymer/matrix[10].

An intercalated system can be determined through indexing of the d-spacing peak in an X-ray diffraction analysis (XRD). This method is based on the recurring order of the crystal structures. In this case they are assigned to the laminated phyllosilicates. The XRD analysis of powders shows peaks with lower 2θ values, which indicates a large spacing between clay platelets in comparison to the basal laminated structures. As the spacing between the layers increases, there is a shift in the diffraction peaks towards lower angle values [10], broadening of the peaks and loss of intensity. When dealing with the exfoliated structure, this property implies a complete and uniform separation of the clay platelets. The exfoliated structure does not appear on the XRD powder spectra, due to the fact that the spacing between the platelets exceeded 80Å or a random spacing or loss of order of the phyllosilicates. Powdered diffraction spectra exhibit the absence of basal reflections and are often interpreted as evidence of an exfoliated structure. This type

of physical evidence can be seen in Fig. 2.4, which provides a schematic of powdered XRD found in the different morphologies of polymer layered silicates.

Structure	Initial XRD Spectra	Final XRD Spectra
Immiscible System	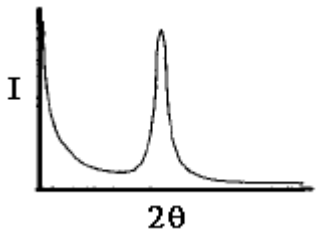	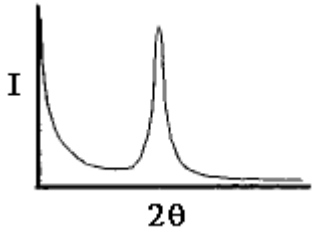
Intercalated Hybrid		
Ordered	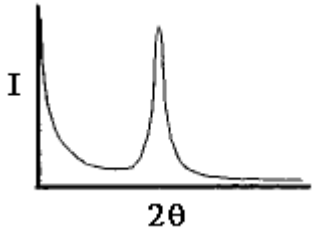	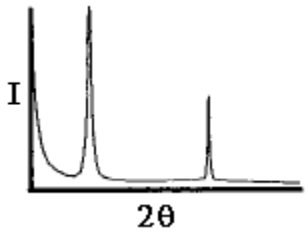
Disordered		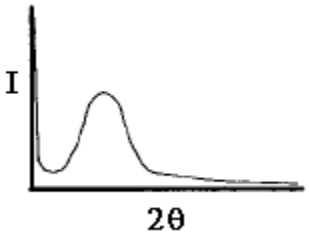
Exfoliated Hybrid	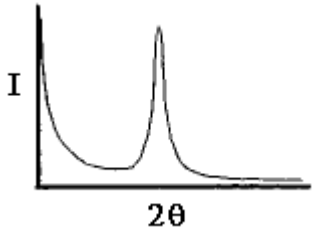	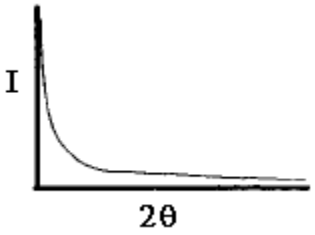

Figure 2.4. Powder XRD spectra for various polymer layered silicate nanocomposites [26].

XRD is considered the main characterization technique to determine exfoliated and intercalated structures in polymer/clay nanocomposites. Another auxiliary technique used to characterize polymer/clay morphology is transmission electron microscopy (TEM). The combination of these two techniques must be used to confirm the existence of an exfoliated system.

Another possibility to achieve exfoliation and intercalation of nanoclay platelets in the polymer matrix is via use of supercritical carbon dioxide ($scCO_2$). The use of the $scCO_2$ is a greener and more environmentally friendly approach to processing polymers for industrial applications [33, 34]. Supercritical fluids have been used in such areas as polymer blending, microcellular foaming, polymer synthesis, particle production and finally polymer composites [35-38]. Zerda, et al. [39], studied the polymerization of methyl methacrylate/clay nanocomposites using $scCO_2$ as solvent. The use of $scCO_2$ allowed for homogenous dispersion of clay platelets throughout the matrix, as well as the production of intercalated and/or exfoliated morphologies. This group suggests that at high nanoclay concentrations, 40 wt %, where prevalent morphology in the matrix is intercalated due to the restriction of the polymer chains and the high penetration of the latter in the basal spacing of the nanoclay platelets. This group also suggests that the problems related to high polymer viscosities may be avoided by the use of $scCO_2$ as a solvent. Baird et al. [40], studied the use of $scCO_2$ in the dispersion of clay platelets in a polymer/clay nanocomposite. This group compared the use of $scCO_2$ to melt processing and also to twin extrusion processing, and found an improvement in the dispersion properties of the nanoclay platelets. The use of this pre-processing also improved the mechanical properties of the polymer, by allowing a higher interaction of the polymer

with the clay platelets, thus restricting the segmental chain motion of the polymer and increasing Tg. Ma et al. [41] also prepared polymer/clay nanocomposites with the use of $scCO_2$. This group prepared polypropylene/sepiolite, by treating the nanoclay with $scCO_2$ and then combining it with the polymer via melt extrusion. The results indicate that pretreating the samples with $scCO_2$ allowed for a more homogenous distribution of the clay platelets in the matrix. The mechanical properties of the polymer/clay composites also were improved by the addition of the sepiolite, and the the sepiolite may act as a nucleating agent, thus increasing the crystallization temperature of the matrix. In a recent study, Naveau et al. [42] also used $scCO_2$ to prepared polymer/clay nanocomposites via melt blending. This group analyzed the interaction of $scCO_2$ with various types of organically modified nanoclays. Natural montmorillonite and hectorite were used as nanoclays and were modified via ion exchange with alkylphosphonium and alkylammonium salts. Polyamide 6 was used as the polymer matrix host for the nanoclays. Thermogravimetric analysis results suggest that hectorite polymer/clay nanocomposites modified with phosphonium salts are more thermally stable at higher temperature than their montmorillonite counterparts. These results also indicated that phosphonium modified clays have a higher thermal stability than ammonium modified clays. Polyamide 6/clay composites modified with phosphonium salts also had higher ignition temperatures. According to the authors this thermal stability will improve processing properties in the melt. Morphological analysis, via XRD and TEM suggest intercalated and/or exfoliated morphologies of the clay platelets in the matrix, thus indicating good dispersion properties of the clay platelets in the matrix and also suggesting some degree of penetration of polymer chains in to the basal spacing of the

nanoclay. Horsch, et al. [43], analyzed the chemical interactions of scCO2 in the expansion and/or exfoliation of organically modified nanoclays and non modified nanoclays. This group compared the degree of expansion of the basal spacing in the clay platelets when treated with $scCO_2$, and the further interaction of the pretreated clays with a polymer matrix, which in this case was polydimethyl siloxane (PDMS). The nanoclays used in this study were Cloiste ® Na+ and Cloisite ® 93A. Cloisite ® Na+ is natural montmorillonite and Cloisite 93A, is a montmorillonite modified with a methyl dihydrogenated tallow ammonium. The data obtained from this group indicates that the degree of exfoliation and/or intercalation in the matrix may be determined by the organic modifier used in the nanoclay. This group also suggests that the CO_2-philicity of the nanoclay will play an important role in the dispersion and ultimately the exfoliation of the platelets [44]. The CO_2-philicity is due to an increased positive charge on the N of the ammonium salt, or the presence of an acidic hydrogen on the ammonium salt. XRD analysis of the nanoclays treated with $scCO_2$ suggests a decrease of stacked platelets. XRD difractograms of the polymer/clay nanocomposites films suggests an exfoliated morphology in the matrix. The d_{001} peak was not present in the difractograms.

2.7 Diffusion through flake filled barriers

Polymer/clay nanocomposites reduce the diffusion coefficient by increasing the path length encountered by a permeating molecule due to the presence of barrier particles obstructing the mass transfer. According to Cussler et al. and other research groups [45-49], the use and development of polymer barriers containing impermeable flakes decreases the permeability 10 fold, and also increases the lag time. An idealized model of

the “tortuous pathway” created by the clay particles is represented in Fig.2.5. The diffusion through a heterogeneous or two phase medium depends on the individual properties of the phases and the amount of phase, the size, shape, size distribution and orientation of the dispersed phase [50].

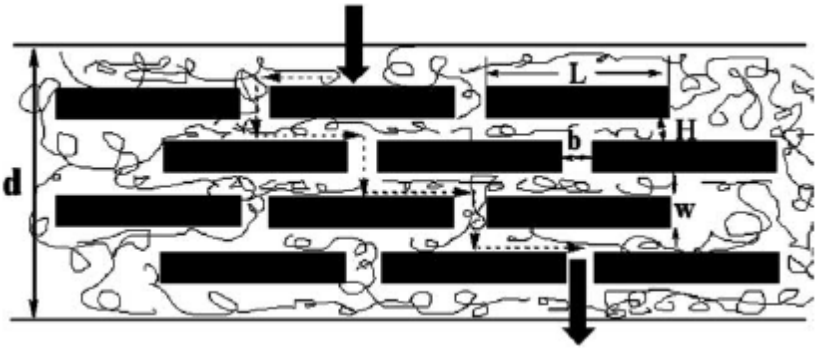

Fig. 2.5 Ideal crystalline structure of layers dispersed clay particles in a polymer matrix, and tortuous pathway of molecules [51].

Throughout the years the study and analysis of permeation and diffusion has been an important research topic. In 1873 Clerk Maxwell published data [52] that dealt with transport in periodic layers of neutrally buoyant spheres immersed in a continuum. This publication set two important concepts. The first concept established an equation dealing with the permeation around impermeable spheres

$$\frac{P_0}{P} = \frac{1+\frac{\phi}{2}}{1-\phi} \qquad \text{Eq. 2.19}$$

P_0 is the permeability of the continuum, P that of the composite, and ϕ is the volume fraction of the spheres. The second concept led to the equation dealing with highly permeable spheres;

$$\frac{P_0}{P} = \frac{1-\phi}{1+2\phi} \qquad \text{Eq. 2.20}$$

The terms in Eq 2.19 are the same as in Eq. 2.20. Strutt and Rayleigh [53] also proposed a model to determine permeability, but with impermeable cylinder. These cylinders are idealized and set perpendicular to the mass transfer.

$$\frac{P_0}{P} = \frac{1+\phi}{1-\phi} \qquad \text{Eq. 2.21}$$

The variation that exists in this equation is related to the geometry of the particles, where ϕ is the volume fraction of cylinders. Eq. 2.19 and 2.21, have three similarities; the first point states that the permeability in the continuum is independent of the geometry of the particles. The second feature indicates that the permeability varies according to the volume of the particles and not according to their size. The third feature states that the geometry of cylinders and spheres do not have a mayor effect on the permeability. This effect can be seen in Fig. 2.6, where the permeability is related to the geometry or the particles.

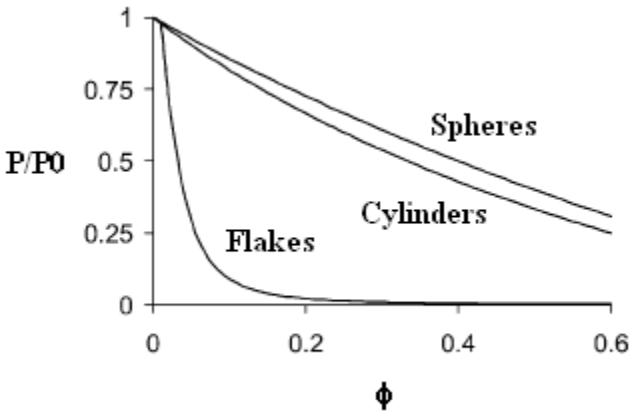

Fig. 2.6 Relationship between permeability and geometry of clay particles [46].

Another model that predicts permeation, and one of the first models discussing polymer/clay diffusion and its mathematical modeling was published by Nielsen [54], who analyzed a two dimensional diffusion phenomena through a polymer with uniformly dispersed rectangular platelets. The importance of this model stems from the introduction of the tortuosity factor. This model also predicts the effective permeability as a function of the volume fraction. The tortuosity factor is defined as the ratio of the distance a molecule must travel to get through the polymer film to the thickness of the film, as seen in equation 2.22.

$$\tau = 1 + \left(\frac{L}{2W} \right) \phi_F \qquad \text{Eq. 2.22}$$

Where ϕ_F is the volume fraction, W is the thickness of the filler, and L is the length of the filler. This model is based on the idea that the impermeable flakes are aligned perpendicular to the direction to mass transfer. The equation for this model is a follows

$$\frac{P}{P_0} = \frac{\phi_P}{1 + \left(\frac{L}{2W} \right) \phi_F} \qquad \text{Eq. 2.23}$$

In Eq. 2.23, P and P_0 are the permeability of the composite film and that of the pristine polymer respectively; ϕ_P is defined as the volume fraction of the pristine polymer.

Within the same realm of predicting permeation in polymer nancomposites, another model used to describe gaseous diffusion through membranes containing impermeable flakes was proposed by Cussler et al. [45, 47] This model incorporates the previous concepts as the tortousity factor, volume fraction and also establishes the aspect

ratio term, and studies unsteady state diffusion. This model is based on the idealization of infinitely long impermeable flakes as well as regular spacing between them. The model also states that the diffusion of the penetrating gas molecules occurs through the slits located between the impermeable flakes, as seen in Figure 2.7.

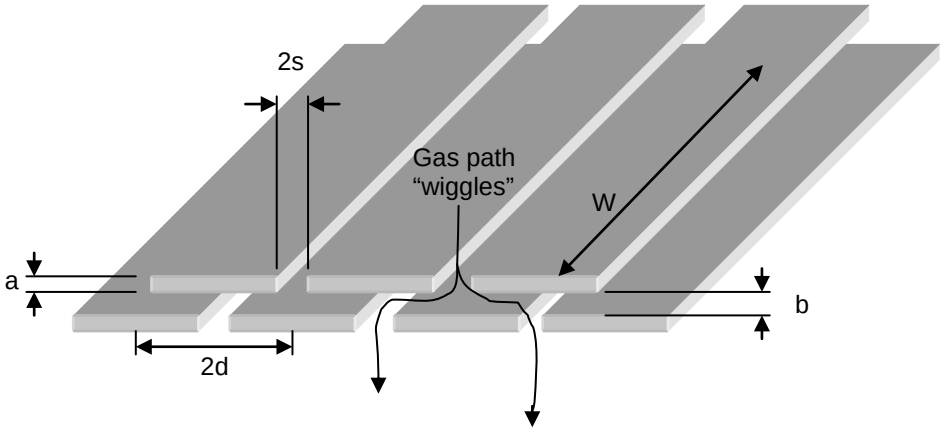

Figure 2.7 Idealized permeation as proposed Permeation of gas molecules through polymer/clay nanocomposites [55].

$$\frac{P_0}{P} = 1 + \frac{\alpha^2 \phi^2}{1 - \phi} \qquad \text{Eq. 2.24}$$

Where P_0 and P, respectively, are the permeability of the pristine polymer and the composite film; φ is defined as the volume fraction of the filler and α is the aspect ratio of the rectangle that forms the barrier cross section. Cussler’s model generates questions regarding the accurate measurement of permeation properties, due to the fact that this model estimates permeation independent of the polymer species used and only depends on the geometry and amount of clay in the barrier membrane and not the size of the flakes [47, 48].

Cussler's group continued pursing new ideas to determine and quantify permeation through polymer/clay nanocomposites. One of the proposed models set forth by Falla et al. [47], was based on Equation 2.24. Falla examined the resistance to diffusion around the flakes. This model also incorporates the resistance to diffusion in the slits between the adjacent flakes within the same horizontal plane, and also the resistance due to necking. These two last terms can be seen in Equation 2.25, as the third and forth terms. Wakeham and Manson [56], also proposed an equation with similar characteristics as Equation 2.24, but the difference is contained within the last term, which suggests that the "necking" term is independent of the aspect ratio. This justification is seen in the forth term of Equation 2.26. Falla proved that these terms could in fact be significant, but only in certain cases [47].

$$\frac{D_0}{D} = 1 + \frac{\alpha\phi^2}{1-\phi} + \frac{\alpha\phi}{\sigma} + \frac{4}{\pi}\frac{\alpha\phi}{1-\phi}\ln\left[\frac{\pi\alpha^2\phi}{\sigma(1-\phi)}\right] \qquad \text{Eq. 2.25}$$

$$\frac{D_0}{D} = 1 + \frac{\alpha\phi^2}{1-\phi} + \frac{\alpha\phi}{\sigma} + 2(1-\phi)\ln\left[\frac{1-\phi}{2\sigma\phi}\right] \qquad \text{Eq. 2.26}$$

Cussler's initial equation is based on the idea of impermeable flakes carefully aligned and of a single size, Lape et al [48], another of Cussler's students, proposed another equation that considers monodisperse flakes in a random array. The equation for this modified model is presented below Equation 2.27. The effect of random spacing is denoted by the 2/3 factor, and the decrease in total permeation area by addition of nanoclay to the barrier is denoted by the modification of the numerator, as seen below.

$$\frac{P_0}{P} = \frac{\left[1 + \left(\frac{2}{3}\right)\alpha\phi\right]^2}{1-\phi}$$ Eq. 2.27

Nielsen's model has also been modified to determine permeation properties, as stated by Lan et al. [57]. This group determined barrier properties for CO_2 permeability in polyamic acid films containing polyimide montmorillonite nanocomposites. Equation 2.28 is the proposed modification. This model has the inclusion of the aspect ratio, α, term proposed by Cussler [45].

$$\frac{P_0}{P} = \frac{1 + \frac{\phi\alpha}{2}}{1-\phi}$$ Eq. 2.28

Another assumption made by the previous models is based on the fact that the permeating gas is considered to always be perpendicular to the alignment of the impermeable flakes within the nanocomposites. This idealization of the models generates the highest tortousity for the penetrating molecules. Bharadwaj [58], analyzed this effect and proposed a modification, based on Nielsen's original model, to evaluate gas permeation depending on the orientation of the impermeable flakes. Bharadwaj introduced the parameter, (S), seen in Equation 2.29 to account for the orientation differences.

$$S = \frac{1}{2}\left\langle 3\cos^2\theta - 1\right\rangle$$ Eq. 2.29

Where θ represents the angle between the normal vector of the impermeable flakes, and the direction of the gas flow. This function has a range of -1/2 to 1. The θ value of -1/2 indicates a parallel alignment of the flakes with respect to the gas flow, and

the θ value of 1 is the opposite case, this indicates a perpendicular alignment of the flakes with respect to the gas flow, as seen in Figure 2.8.

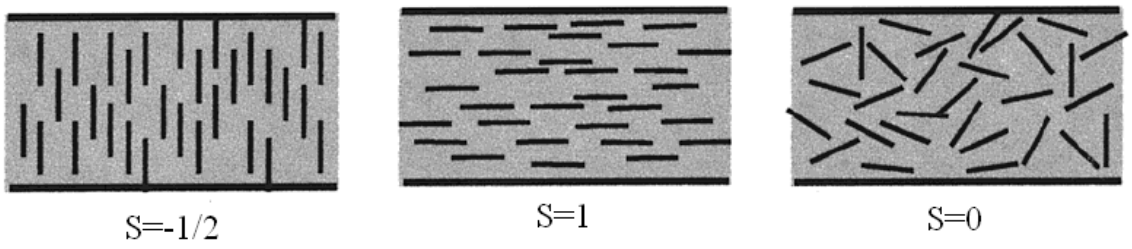

Figure 2.8 Resulting S values for different flake alignments [58].

The variation in permeability can be evaluated with Equation 2.31, Equation 2.30, is the original equation proposed by Nielsen, and is rearranged as seen below.

$$\frac{P}{P_0} = \frac{1-\phi_S}{\tau} \qquad \text{Eq. 2.30}$$

$$\frac{P}{P_0} = \frac{1-\phi_S}{1+\frac{L}{2W}\phi_S\left(\frac{2}{3}\right)\left(S+\frac{1}{2}\right)} \qquad \text{Eq. 2.31}$$

Bharadwaj's modification of Nielsen's Equation 2.30, has proved to be useful in determining permeation properties of polymer nanocomposites, as reported by Gatos et al. [59] This group reports good correlation for hydrogenated acrylonitrile butadiene rubber modified with montmorillonite and flourohectorite.

2.8 Polyurethanes

Polyurethanes were discovered in Germany by Prof. Otto Bayer in the late 1930's. This discovery was achieved while trying to generate alternative fibers that could compete with nylon fibers. The first US patent related to polyurethanes was awarded to Rinke and collaborators [60], whose research group reacted a aliphatic 1,8 octane diisocyanate with a 1,4 butanediol. This process produced a low viscosity polyurethane melt which was further processed or spun into fibers. DuPont and ICI recognized the elastomeric properties of polyurethanes, which lead to the mass production in the early 1940's. The denomination or common name polyurethane has always been a point of discussion, because urethane linkages represent a minority of the functional groups in the polymer chain. The term polyurethane is accepted as long as polymer contains a significant number of urethane linkages. Typical polyurethane may contain a wide variety of functional groups like, ethers, esters, ureas, amides, aliphatic and aromatic hydrocarbons and isocyanurate groups.

According to Szycher [60], the definition of polyurethane is any polymer with a plurality of carbamate (urethane) linkages. The repeating urethane linkage is the basis for the generic name.

Synthesis of polyurethane can be achieved by two different methods; the first is method is utilized for industrial application, and is the reaction of diisocyanates with dihydroxy compounds. This method has the particular advantage of not having byproducts. The second method is the reaction of bischloroformates with diamines. The

bischloroformates are obtained from dihydroxy compounds with an excess of phosgene [61]. Figure 2.9, illustrates the precursors of a polyurethane structure.

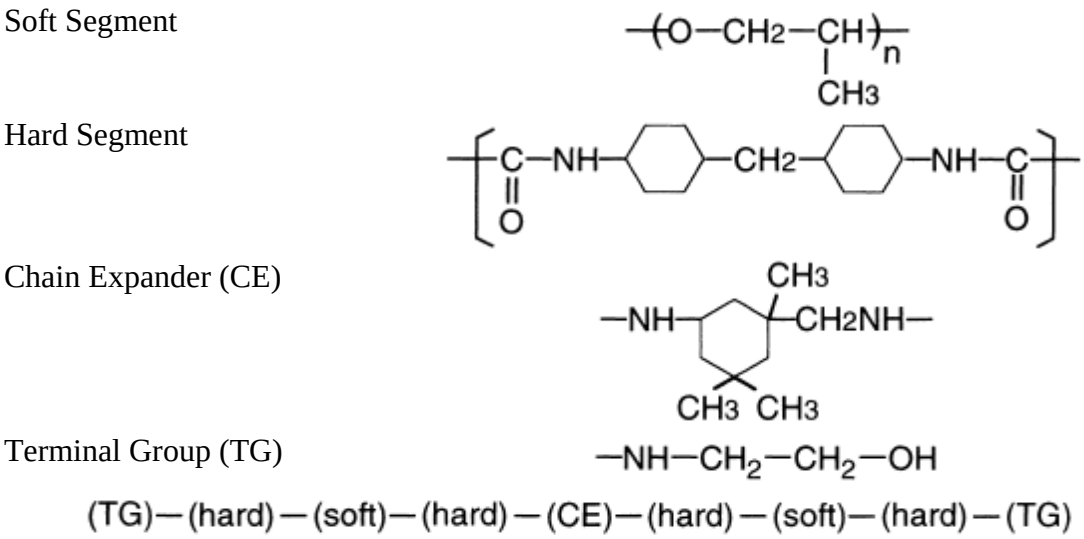

Figure 2.9. Precursors and structure of polyurethane [62].

Polyurethanes have been described as segmented elastomers composed by two different segments. The segmental composition will generate a two phase microstructure. The physical properties of the polyurethanes depend on the molecular structure caused by the interactions between the polymer clains [63], degree of flexibility/rigidity, density, hydrophobicity or hydrophilicity, cellular structure, processing characteristics and the end-use properties. Polyurethanes are linear block copolymers type $(AB)_n$, one of the blocks is constituted by a long, flexible polyester or polydiol. This block is also known as the soft segment, and has the characteristic of giving the elastomeric properties to the polymer; it also constitutes the high molecular weight of the polymer.

The second segment of the copolymer is also known as the hard phase. The composition of the hard phase is due to the reaction of the low molecular weight diol or triol chain extenders and the aromatic diisocyanates [64]. Due to the electronegativity of

nitrogen in the urethane N-H structure, the hydrogen develops a partial positive charge which can form hydrogen bonds with the adjacent oxygen atoms. The hydrogen atom from the urethane group act as a proton donor, and the carbonyl in the urethane C=O, or urea act as an acceptor group. The oxygen in the polyesters or polyether from the soft phase can also act as an acceptor [65], a physical representation of these interactions can be seen in Figure 2.10 [66].

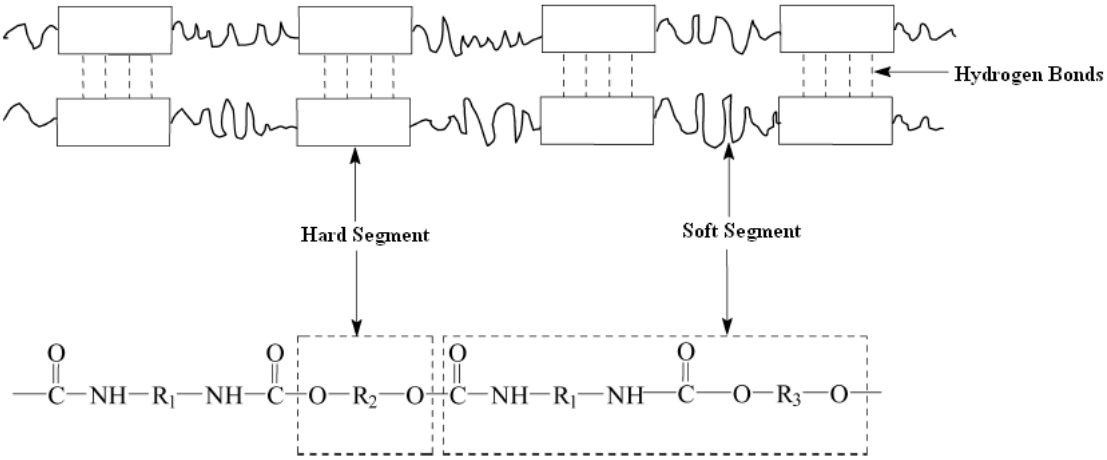

Figure 2.10 Block Structure of Polyurethane [66].

The hard phase is composed by polar materials, and has the ability to form carbonyl to amino hydrogen bonds which promote aggregation into ordered hard domains [67]. At room temperature the phases aggregate into microdomains, this same tendency is seen above and below the Tg. Analysis of the mechanical properties of polyurethanes determined that hard phase gains rigidity through hydrogen bonding between diisocyanate groups, producing physical crosslinking. This interaction also provide a filler-like reinforcement for the soft phase [68]. The basis of the microphase separation is related to the thermodynamic incompatibility of the two phases, as well as a difference in

polarity between the two phases [69]. The degree of phase separation will depend on factors like, molecular weight, chemical structure, composition and arrangement of both kinds of segments. Polyurethanes can be modified or tailored to the necessities of the researcher. The chemical structure can be exchanged due to a wide variety of precursors and synthesis conditions.

Within the realm of the polyurethane compounds, siloxane based elastomers have become very popular. When comparing conventional polyurethanes based on polyether or polyester, block copolymers composed by PDMS soft segment improve the environmental stability. Within these improved properties are better thermal and oxidative stability, improved hydrolytic stability, low moisture permeability, hydrophobic surface, low toxicity, high permeability to gases, a broader service temperature range. This range is modified by a lower glass transition temperature of PDMS (-123°C) [70, 71].

2.9 Permeation Properties of Polyurethanes

Gas permeation through a polymer membrane depends on different aspects for example; degree of crystallinity, chain stiffness, chain packing, size and ratio of the free volume and segment mobility [19, 72]. Polymers modified with impermeable nanostructure such as the nanoclay previously discussed, prove to decrease permeability when compared with the unmodified polymer matrix [11, 73]. When dealing with gas diffusion in a heterogeneous phase, the overall diffusion depends on the individual properties of the phases. In this case the clays may differ in the amount, size distribution,

orientation of the dispersed phase, shape of the clay [74]. Clays have spherical, cylindrical, ellipsoidal and platelet conformations. All of the above characteristics affect diffusion properties. The addition of clay particles to the matrix generates a tortuous pathway for the molecules with a longer diffusive path for the penetrants [11].

According to Galland et al. and other authors [75-78], the mechanical properties of a polyurethane system do in fact influence permeation properties. In their study Galland et al. proved that an increase in the concentration of the hard phase in the polyurethane/nanoclay system diminished the permeation of gases through a membrane. The increase in hard phase concentration is related to the physical properties of the polymer, which eventually lead to an increase the modulus of the polymer/clay composite.

Within the realm of gas permeation in polyurethane membranes there are certain studies that focused on the chemistry of the polyurethane membrane. Madhavan et al. [77], studied poly(dimethylsiloxane-urethane) membranes. This group used PDMS as the soft phase in these membranes and a series of three different isocyanate groups as the hard phase; hexamethylene diisocyanate (HMDI), methylenediphnyl diisocyante (MDI) and toluene diisocyanate (TDI). The variation of the ratio of hard phase to soft phase was analyzed and correlated to the gas permeation parameter. When the PDMS content increased, the density of the membrane decreased. This resulted in an increase in the free volume of the membranes and thus an increase in permeability.

On the other hand, permeation testing clearly proved that the increase in hard phase concentration diminished the permeability of the whole series of gases analyzed. The chemistry and proper selection of the hard phase within the membranes also provided an important and decisive parameter. HMDI contains only an alkane chain in the main chain of the isocyanate conformation, and due to the non polar nature of the hard phase there exists a compatibility of the hard phase with the soft phase. The compatibility generates a less segregated membrane which diminishes the permeation of the gas molecules. Figure 2.11 shows permeation data for the HMDI series of membranes.

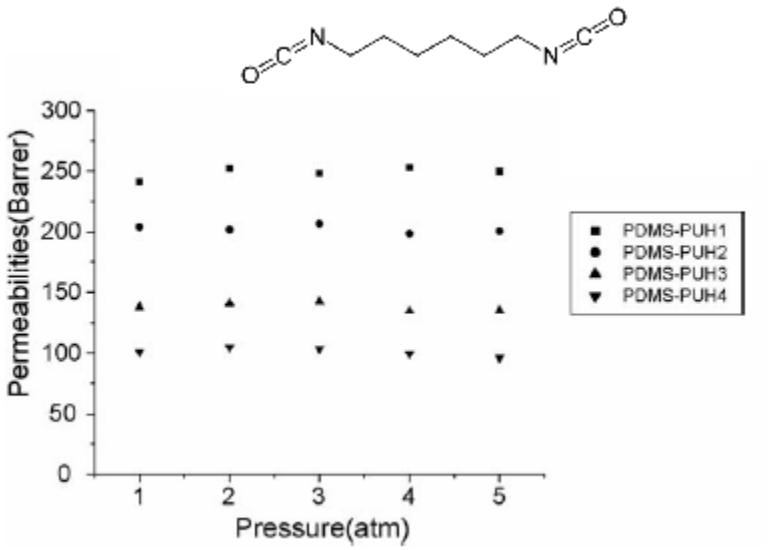

Figure 2.11 Permeation data for poly(dimethylsiloxane-urethane) membranes with different HMDI content [77].

From the analysis of the membranes composed by TDI an MDI, the permeation profiles are similar. This is due to a smiliar chemical structure of these two isocyanates. The more rigid structure of the MDI backbone allows less permeability than the more

flexible TDI structure [77]. TDI has a less ordered structure and allows a higher free volume. The increased difference in polarity of the hard phase, in both MDI and TDI, and soft phase PDMS, motivates a higher segregation of the phases which ultimately lead to higher permeation results, these permeations results can be seen in Figure 2.12.

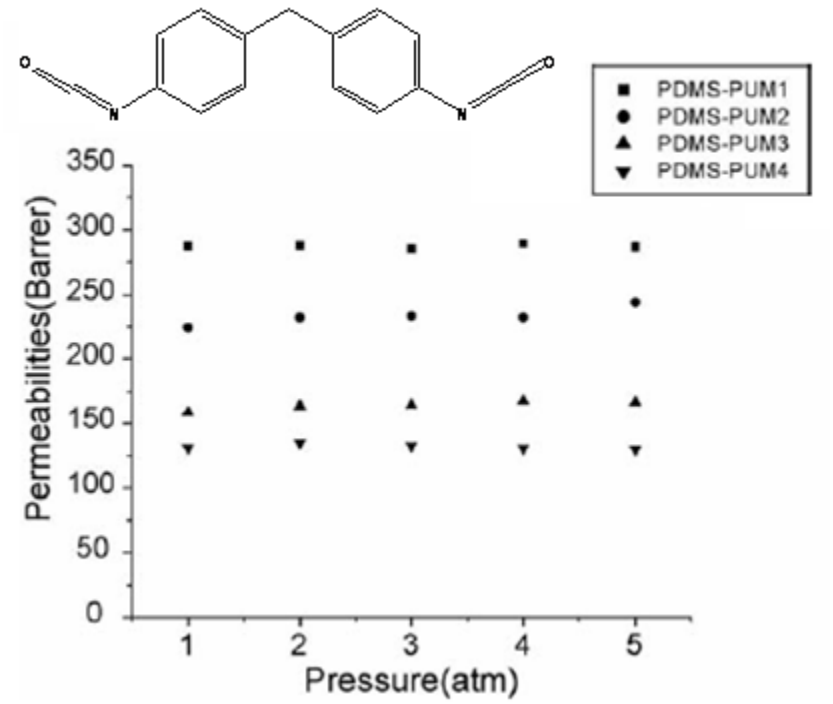

Figure 2.12 Chemical structure of methylenediphnyl diisocyante (MDI) and permeation data for N_2 permeability at 35°C [77]

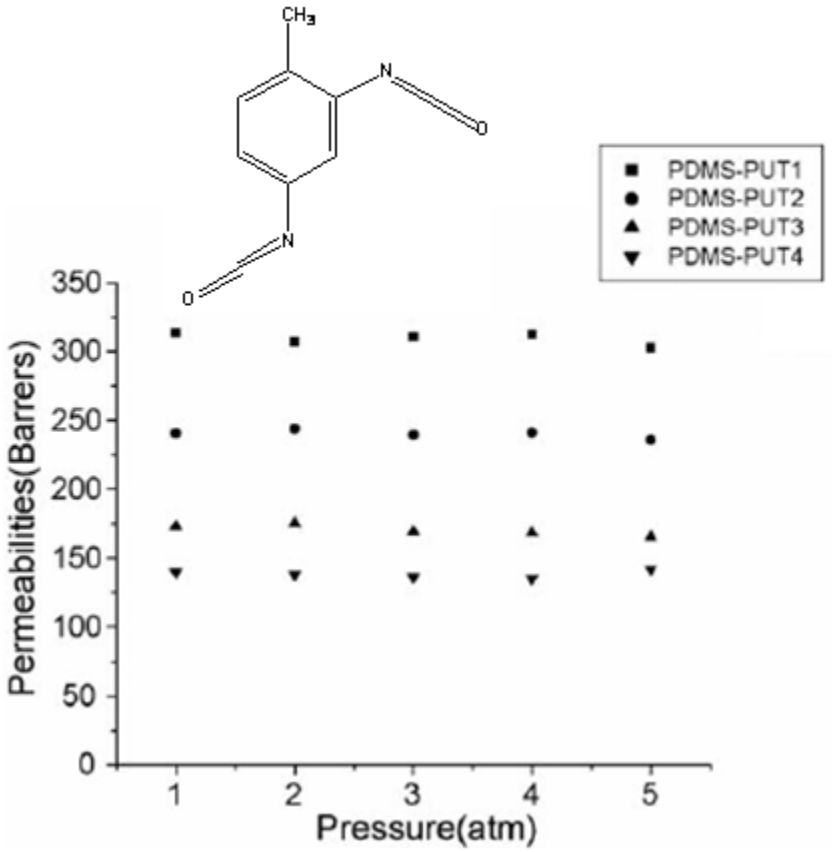

Figure 2.13 Chemical structure of toluene diisocyanate (TDI), and permeation data for N_2 permeability at 35°C [77].

2.10 Mechanical Properties of Polymer/Clay Nanocomposites

While discussing the permeation properties of polyurethanes, and the importance of the chemical composition within this property, we touched the surface of the importance of the mechanical properties of the polyurethane/nanoclay matrix and how all these elements combine in order to form a desired membrane.

Mechanical properties of polymer/clay composites are related to their microstructure, and can also be related to the degree of dispersion and exfoliation of the

clay platelets [18]. A good dispersion of the clay platelets results in an increase of the Young's modulus, storage modulus and tensile strength. There are also certain drawbacks to the polymer/clay matrix, such as reduced ductility and reduced impact strength [79]. The content or amount of clay in the polymer matrix determines the increase in the tensile strength and the modulus [80] This proclivity is seen in the tensile modulus, because at low clay content there exists a higher increase in the tensile modulus, which is attributed to the degree of exfoliation. As clay content increases the tendency to increase the modulus reaches a plateau. This point is directly related to the partial exfoliation of the clay particles and the stacking of the platelets [81]. This effect was also seen by Osman et al. [22], whose group found that the increase of the d-spacing in the clay platelets increased the relative elastic modulus and the stress at the break of the matrix. Although complete exfoliation was not achieved, the relationship between the interspatial distance and the mechanical properties of a polymer/clay matrix was established.

The reinforcement of the polymer/clay matrix leads to higher tensile properties and is related to the large interface that exists within the polymer/clay system. This is important because several chemical and physical interactions are governed by surface properties. The confinement of the polymer chains within the galleries of the clay platelets of large surface area per unit volume ultimately affects the local chain dynamics [19, 64]. Therefore composite mechanical theories of reinforcement are applied to explain the fracture toughness and mechanical properties of polymer/clay composites. Certain models are used to explain this phenomenon, and within these models are

parameters such as: aspect ratio, orientation of the reinforcements and volume fraction of the clay particles [19].

Finnigan et al. [68] also studied the effect of the hard phase to soft phase ratio in the mechanical properties of polyurethane/clay nanocomposites. This group compared two polyurethanes with different hard phase/soft phase ratio and the addition of one type of clay. The selected clay was Cloiste 30B, which contains a methyl bis-2-hydroxyethyltallow ammonium modification. This specific clay provides high exfoliation in polyurethane samples. The group also analyzed and compared two different synthesis methods; melt processing and solvent casting of films. According to this group, an important factor for clays exfoliation is centered on the soft phase of the polyurethane. The soft-phase is responsible for the separation of the platelets, due to the fact that it wants to regain entropy, and the hard phases will be attracted to the silicate layers of the clay [82]. The polyurethane with a higher soft phase content provides a better exfoliation; this was shown by the WAXD results, which record a larger distance between platelets as can be seen in Figure 2.14. Finnegan reported that clays were better dispersed in with melt processing than in solvent casting films.

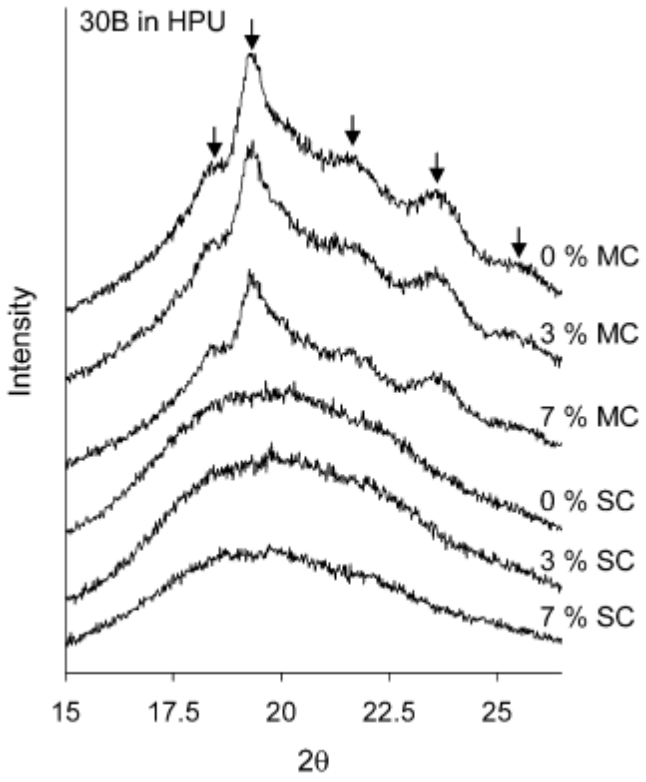

Figure 2.14. WAXD results for polyurethane based films, MC is referred to the melt casted films and SC is the solvent casted films. [68].

DMTA analysis provides evidence of the dependence between clay content and Tg of the polyurethane It is common [68, 80, 83, 84] to use the tan δ peak to determine Tg, which effect can be seen in Figure 2.15. This peak can be attributed to the backbone motion of the soft-segment phase therefore, the importance of the ratio of hard/soft phase. The addition of nanoclay increases the Tg of the matrix. The addition of the nanoclay also provided a reduction of the damping capacity, which can be directly related to a restricted molecular motion which is caused by the delaminated silicate layers [64]. The effect of restricted motion can also be connected to the hydrogen bonding between the silicate layers and the polymer. This proves the strong interaction between the polymer

and the clay. Increases in Tg with the addition of clays are reported throughout the literature [65, 83, 85].

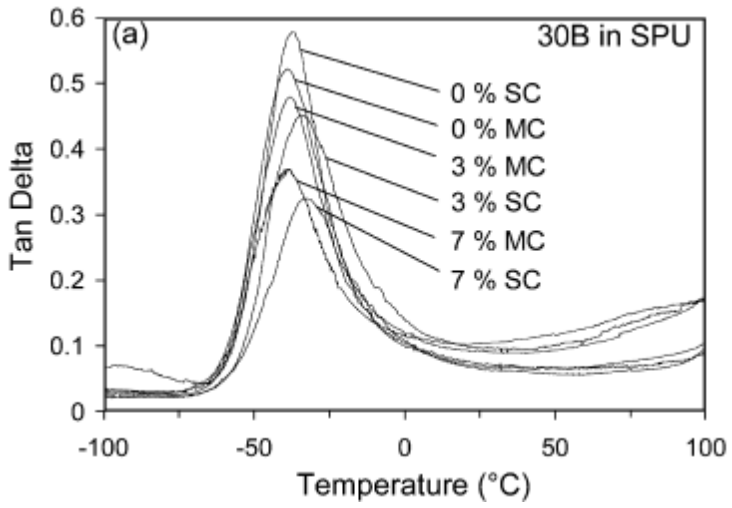

Figure 2.15 Dissipation Factor tan (δ) for Polyurethane/clay matrix [68].

Finnigan et al. [68] also reported that the impact of the clay on mechanical properties is higher for the "softer" polyurethane, due to a mismatch of the elastic constants of the polymer and the clay. Therefore the impact of clay will be higher in rubbery polymers in comparison to glassy polymers [86, 87]. These results were similar to those reported by Chavarria et al. [80].

Another study that dealt with mechanical properties of polyurethane/clay matrix was done by Chavarria et al. [80], this group developed polyurethane nanocomposite membranes by melt processing and evaluated their mechanical properties. This publication evaluated the use of two different types of polyurethanes. One was polyester based which provided medium hardness, and the other was polyether based polyurethane

which provided a higher hardness. The composition of these polyurethanes was not made available known because of trademark restrictions.

The variation of the nanoclay utilized was another parameter evaluated by this group in order to characterize the mechanical properties of these nanocomposites. This group studied 5 different quaternary ammonium nanoclays, two of these clays were similar in chemical structure but they differed on the hydrogenation of the C18 tallow group, another was an alkylammonium clay with two tail tallow groups, and the final two clays were alkylammonium clays modified with hydroxyl ethyl groups.

Chavarria found that the addition of nanoclay to the polymer matrix increased the modulus at small strains for the whole series, but depending on the nature of the nanoclay the large strain behavior was very different. The concentration of the clays and their chemical composition in the matrix affected the strain properties. While dealing with a matrix modified with a nanoclay based on hydroxy ethyl groups, the higher the concentration of the clay content, the higher the reinforcement of the strain profile. The contrary effect is seen with polyurethane/clay nanocomposites modified with alkylammonium groups containing two tallow tails. Due to strong interactions of the tallow groups with themselves and the silicate platelets within the interspacial distance, the nanocomposites containing an alkylammonium groups containg two tail tallow group did not reinforce the matrix at high strain [69].

The addition of small amounts of nanoclay increased the Young's modulus of the polymer/clay matrix [16, 80]. The difference in organically modified clay can be seen in Figure 2.16. The polyurethane/clay nanocomposites that have a better dispersion will generate a higher Young's modulus. In this case the polyurethane/clay composite

modified with an akylammonium of only one tallow group yielded a higher modulus than the two tallow alkylammonium group.

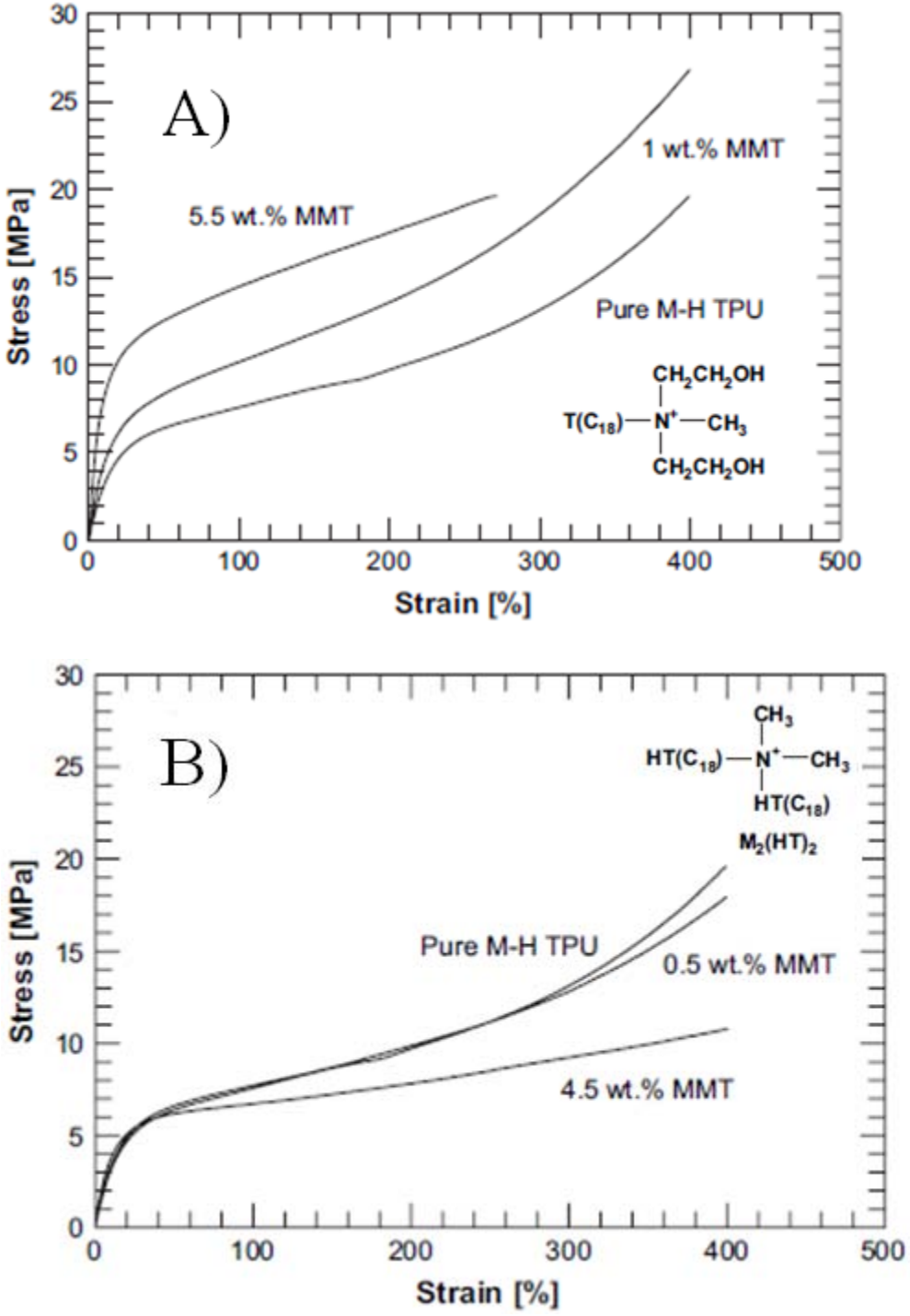

Figure 2.16 Stress-Strain behaviors for polyurethane/clays matrix. A) Cloisite® 30B, B) Cloisite® 20A [80].

According to Fornes et al. [16] polyurethanes have a good affinity for the polar clay surface and the one tallow alkylammonium clays allow a higher interaction between this surface and the polyurethane. Two tail groups will present negative dispersion effects due to two reasons: a steric hindrance effect in the penetration of the polyurethane to the gallery space and, therefore, diminishment in the interaction with the platelets and lower degree of exfoliation [17]. The hydroxyl groups present in the nanoclays increase dispersion because of the possibility of creating hydrogen bonds with the polar groups in the polymer matrix or with the surface of the clays; this type of bonding will increase exfoliation and dispersion [65, 88, 89].

Xia et al [90], studied stress relaxation and creep behavior in a polymer/clay matrix by modifying the hard phase content in the polyurethane and by the addition of clay to the matrix. Stress relaxation is attributed to chain orientation, motion, and disentanglement of the polymer chain network, and the deformation and rupture of microdomain and crosslinks. Synthesis of the polyurethane was obtained through a one-shot process. This group found that by increasing the hard phase content in the polyurethane, the initial stress, equilibrium stress, relaxation ratio and relaxation rate increased, while relaxation time decreased with increasing hard phase content. These results outline the importance of the hard phase in the relaxation of polyurethane. Once this group established the importance of hard phase in mechanical properties, they studied the addition of clay in the matrix. The hard phase content was fixed at 26% for the study with different clay content. Increasing clay content also helped increase initial stress, equilibrium stress, relaxation ratio and relaxation rate, although not in such a

dramatic way as the increase in hard phase content. The initial stress there was only a 29% for a matrix with 5% of Clay content. The addition of clay will augment the degree of microphase separation, leading increased soft phase flexibility, elasticity and therefore a slow stress relaxation process.

2.11 Indoor Air Quality

This thesis intertwines different topics such as permeation through polymer membranes, the use of nanoclay particles and the modification of permeation properties with the added clay particles, physical properties of polymer/clay nanocomposites and indoor air quality properties. In order to evaluate the latter property this study assesses and quantifies the permeation of VOCs (volatile organic compounds) in polymer/clay nanocomposites.

The Environmental Protection Agency (EPA), and the World Health Organization (WHO), have acknowledge that indoor air pollution has become an important topic and risk for workers worldwide [91]. The two major factors that may affect the indoor air quality levels are:

- Synthetic Interior Materials
- Improper Air circulation

Due to the processing and manufacturing of synthetic materials utilized in the work environment, these materials can emit a wide range of pollutants, and in particular volatile organic compounds (VOC). Some of the compounds found or determined as

VOCs are considered carcinogenic. Elevated temperatures are responsible for the degradation of cellulose, decomposition of non heat resistant additives and other thermally induced reactions such as Diels-Adler synthesis [92]. The degradation of synthetic materials, and surface reactions maybe able to form aliphatic aldehydes from the oxidation of unsaturated fatty acids. These synthetic materials are usually used to furnish the work area, and they range from carpeting to wall insulation panels.

The second topic regarding the improper circulation and delivery of fresh air to the work areas is due to energy consumption reasons. Proper ventilation in the work environment is used to create an acceptable level of humidity and temperature; this aspect is also used to remove air pollutants caused by human bioeffluents [93], tobacco smoke and building materials, in order to improve the indoor air quality [91]. Different research groups [94-96], indicate that VOCs are suspects of causing sick building syndrome (SBS) symptoms. SBS related symptoms include eye and mucous membrane irritation, fatigue, headaches, stuffiness, lethargy and certain asthmatic symptoms. The latter symptoms are responsible for a diminished and loss of productivity in the work area, as reported by Mendell [97]. Wargocki et al. [93] suggest that productivity in offices increases with a higher ventilation rate, and point out that an ideal range for ventilation per person would be between 3 to 30L/s. Within this same study Wargocki's research group [93] proves that improved ventilation diminished the intensity of some SBS symptoms and improves air quality. An increased rate of total outdoor air exchange reduces reaction time between outdoor ozone and VOCs, the reaction scheme for ozone can be seen in Table 4.2. VOCs are not only related to the work area. These contaminants are also located at home.

Saarela et al. [98] determined a higher VOC exposure in homes than in work areas. This information is specially important to people in industrialized countries, who according to Berstein et al [99]., spend approximately 22 hours indoors daily.

According Wolkoff et al. [96] to the World Health Organization (WHO) defined the term VOCs as a group or set of organic compounds with boiling points from 50°C to 260°C [100]. In 2006 Wolkoff et al [101] proposed a subdivision of VOCs into four different categories;

- Chemically Nonreactive
- Chemically Reactive
- Biologically Reactive
- Toxic

Specific compounds may be encompassed in two or more of the previous categories. In a previous publication Wolkoff et al.[102] also cites that health effects were not the main parameter to determine the classification of these compounds. The main reason for choosing this interval is due to sampling and capabilities of the analytical techniques, although these parameters are in constant evolution during the past 10 or 15 years, due to the advances in sampling and analytic techniques. There has been an alteration in the spectrum of VOCs studied and classified due to new building materials and by consequence the solvents used for these products. Table 2.3, states the major VOCs found in indoor measurements throughout the US and in European countries.

Table 2.3. VOCs present in indoor air for different countries

European Audit [103]	**US review [104]**	**BASE study [105]**	**German Study Selected VOC's [106]**
Acetone	o-Xylene	Acetone	Group 1
Isoprene	Benzene	Hexane	Phenoxyethanol
2-Methylpentane	Tetrachloroethylene	Toluene	Butyldigycol acetate
Hexane	m-, p-Xylenes	1,1,1-Trichloroethane	Longifolene
2-Methylhexane/benzene	Ethylbenzene	Methyl chloride	Dimethyl phthalate
Heptane	Trichloroethylene	Benzene	
Toluene	Toluene	Ethanol	Group 2
m-, p-Xylenes	1,1,1-Trichloroethane	2-Propanol	α-Pinene
o-Xylene	Dichlorobenzenes	Dichlorofluoromethane	Camphene
Decane	Styrene	m-, p-Xylenes	B-Pinene
Trimethylbenzene	Undecane	2-Butanone	3-Carene
Limonene	Dodecane	Trichlorofluoromethane	
	Octane	o-Xylene	Group 3
		Undecane	Styrene
		Tetrachloroethylene	o-Xylene
		Methylene chloride	C_{12}-Alkanes
		1,2,4-Trimethylbenzene	
		Decane	Group 4
			1,2,3-Trimethylbenzene
			1,2,4-Trimethylbenzene
			Methylcyclohexane

Brown et al. [107] determined an upper and lower concentration limit for VOCs; the concentration threshold is between 50 μg/m^3 and 5 μg/m^3. This concentration range is consistent with data obtained in Europe and North America, where the majority of the single VOCs were generally found at concentrations below 10 μg/m^3 [96]. But the importance of this threshold is epitomized by carcinogenic compound like benzene, who

is found to have an indoor air level concentration of 20 μg/m^3. The variation in the profiles of the organic compounds in the last decade is related to the introduction of new building materials and household products with higher boiling points. Another factor for this variation is and the replacement of aromatic and aliphatic solvents with oxygenated solvents [101]. Carbon compounds with double bonds like styrene, terpenes and 4-phenylcyclohexene undergo gas phase reactions with OH, O_3, and NO_x. The formation of new OH species within the work environment is related to the presence of O_3 and the subsequent reactions with alkenes and monoterpenes; the latter species are present due to cleaning products, timber, houseplants and fragrances [108]. Reactions with O_3 yield radical products such as OH, HO_2 and RO_2. The gas phase reaction of O_3 with unsaturated hydrocarbons is known to produce aldehydes, ketones and acids as main components [109]. The reaction scheme for the formation of reactive gases as a byproduct of secondary emissions was described by Weschler et al. [110]. Weschler cites that O_3 is responsible for the generation of significant amounts of NO_2 and NO_3, as a function of indoor air decomposition. The reaction scheme is presented in Table 2.4.

Table 2.4. reaction schemes for indoor air decomposition [92, 110].

$O_3 + NO \rightarrow NO_2 + O_2$
$O_3 + NO_2 \rightarrow NO_3 + O_2$
$NO_3 + R\text{-}H \rightarrow HNO_3 + R$
$OH + R\text{-}H \rightarrow H_2O + R$
$O_3 + R_1R_2C{=}CR_3R_4 \rightarrow [Ozonide]^*$
$[Ozonide]^* \rightarrow R_1C(O)R_2 + [R_3R_4COO]^*$
$[Ozonide]^* \rightarrow R_3C(O)R_4 + [R_1R_2COO]^*$

O_3 is known to react with indoor surfaces, and non-volatile compounds in carpeting and latex paint. Reactions with latex paints will produce aldehyde species; the

main difference between the radical species and the aldehyde is the stability of the latter species within the indoor environment. Degradation and reaction of aromatic species within the indoor environment produce ketones, alcohols, organic nitrates, PAN (peroxy-acetylnitrate)-type species and organic species [111]. PAN is an important radical present in indoor air. The reaction scheme for the formation of PAN from acetaldehyde is as follows in table 2.5:

Table 2.5. reaction schemes for indoor air decomposition of PAN

$CH_3CHO + OH \rightarrow CH_3CO + H_2O$
$CH_3CO + O_2 + M \rightarrow CH_3C(O)OO + M$
$CH_3C(O)OO + NO_2 + M \rightarrow CH_3C(O)OONO_2$

VOCs are also present in the environment due to primary or secondary emissions. The primary emissions are due to a physical release of compounds which are present in a new product, and the emission rate tends to decrease rapidly during the first six months. The secondary emissions are related to the compounds produced by chemical reaction in the product or in the indoor environment, these emissions may last long periods of time and can also increase [112].

Zhang et al. [113] states that there are basically two models in the literature that quantify emissions of VOC. The first model is the empirical model, which finds its basis on statistical analysis of emission data. The data obtained from the model comes from environmental chamber testing, and is based on the application of the first-law decay model and the power law decay model. According to Zhang et al. [113], these models are simple to use. The drawback from these models is that they do not provide information regarding the emissions mechanisms and cannot be scaled from test conditions to building conditions.

The second series of models are called the mass transfer models. The mass transfer model provides a difference from the empirical model because it can predict the VOCs emissions for different conditions from known physical parameters.

2.12 Emulsions

The evolution of our research project pointed in the direction of emulsion polymerization as a possible route for exfoliation/delamination of clay platelets in the matrix. This synthesis route provides a cleaner and greener alternative to the solvents used for *in situ* polymerization. The basic ingredients/components of an emulsion polymerization are: the dispersing medium, monomer, initiator and the surfactant. The dispersing medium or continuous phase is an inert phase which can provide good heat transfer and also provides a low viscosity. The typical monomers used for emulsion polymerization are acrylates [114, 115], methacrylates [116, 117], styrene [118], vinyl acetate and butadiene. These monomers have limited solubility in water. Sodium, ammonium and potassium persulphate salts are common water soluble initiators. The persulphates dissociate into two sulfate radical anions which may initiate the polymerization reaction. Redox initiators, such as persulfate-bisulfite, are commonly used in low temperature polymerizations. The lower temperature reactions decrease crosslinking and chain branching during the synthesis of rubbers. Redox initiators are typically a mixture of a reducing agent and an oxidizing agent whose reactions generally produce radicals.

Surfactants are amphililic, which indicates that they have hydrophobic and hydrophilic segments or moieties. This property allows the possibility to reside and effectively

interact at the interface. Surfactants are also known as stabilizers or emulsifiers. When dissolved in aqueous solution the surfactant molecules can orient and reduce the surface tension of water. According to van Herk [119], surfactant are classified according to the hydrophilic group. For anionic surfactants the hydrophilic part is the anion, common anionic surfactants are sodium dodecyl sulphate (SDS) $CH_3(CH_2)_{11}SO_4^-Na^+$ and sodium dodecyl benzene sulphonate $CH_3(CH_2)_{11}C_6H_4SO_3^-Na^+$. The cation is the hydrophilic part in cationic surfactants. Cetyltrimethylammonium bromide (CTAB) $CH_3(CH_2)_{15}N(CH_3)_3^+Br^-$ and Dodecylaine hydrochloride $CH_3(CH_2)_{11}NH_3^+Cl^-$ are the most used cation surfactants. For non-ionic surfactants, the hydrophilic part is a non-ionic component. Sugar derivatives, polyols and ethylene oxide chains are common non-ionic surfactants. The properties of the hydrophilic group will be pH dependent when dealing with amphoteric surfactants. Other important ingredients in emulsion polymerization are: chain transfer agents, electrolytes and sequestering agents. Chain transfer agents, such as mercaptans, are used in emulsion polymerization to control the molar mass of the resulting polymer. The consumption of the mercaptan should be kept in balance with the consumption of the monomer. Electrolytes maybe added to control pH, which may lead to maintaining the efficiency of the initiator and it may also prevent the hydrolysis of the surfactant. Sequestering agents help maintain metal ions in solution.

2.12.1 Emulsion Polymerization a brief introduction.

The combination of water, monomer, surfactant, initiator and added elements may provide a stable emulsion. The inclusion of surfactant to the water or dispersing media leads to the generation of micelles, which are swollen by the monomer. The typical diameter of these clusters is in the range of 5-10 nm and the number density is in the order of 10^{17}-10^{18} dm^{-3}. The generation of these swollen particles is based on the premise that the concentration of the surfactant is above its critical micelle concentration or CMC. The monomer is present in large-size droplets or monomer reservoirs, with surfactant molecules adsorbed onto its surface. The typical diameter of the monomer droplets is within the range of 1-10μm and its number density on the order of 10^{12}-$10^{14}$$dm^{-3}$. The addition of the initiator promotes the generation of radicals in aqueous solution. The radicals propagate in the aqueous phase and react with dissolved monomer molecules, leading to the formation of oligoradicals. This is considered the starting point of the particle nucleation. There exists certain controversy surrounding the mechanism of particle formation or particle nucleation. The three mayor theories related to particle formation are: micellar nucleation, homogeneous nucleation and droplet nucleation.

The micellar nucleation model was initially proposed by Harkin [120, 121], and Smith and Ewart [122, 123]. This model proposes that initiator radicals in aqueous phase enter the monomer swollen micelles, in racial form or as oligoradicals, and initiate polymerization. The growth of the monomer swollen polymer particles is due to propagation reactions. Unreacted micelles will donate their monomer particles as well as their surfactants to the growing particles. The depletion of micelles in aqueous phase indicates the termination of the particle nucleation. In this theory the monomer droplets in

aqueous phase server “feed” the swelling particles via diffusion, until they are fully consumed. According to this model, the typical polymerization reaction rate can be divided into three different intervals. Interval I is related to the nucleation state or particle formation stage. This stage is characterized by the increase of the polymerization rate with time and also by the increase of the particle number. Particle nucleation stage ends with the disappearance of the micelles in the aqueous phase. Within interval II the reaction rate and the particle number is maintained constant [119]. The monomer droplets in the aqueous phase provide the growing particles with sufficient monomer to continue the saturation and propagation reaction.

Interval III is related to the depletion of the monomer droplet in the aqueous phase [124], the disappearance of the monomer droplets leads to a decrease in the reaction rate. The particle number for interval III is considered to be constant also. There are specific cases where the polymerization rate presents an decrease-increase-decrease prolife. This profile is known as the Tromsdorff gel effect, and relates to the decrease in the termination rate between radicals inside the particles which is directly caused by an increase of interval viscosity [125].

The rate of polymerization (R_P) can be calculated with the equation 2.32:

$$R_P = k_P[M]_P\left(\frac{nN_P}{N_A}\right) \qquad \text{Eq. 2.32}$$

Where k_P is the propagation rate constant, $[M]_P$ is the monomer concentration in the particles, n the average number of free radicals per particle, N_P the number of latex particles per unit volume and N_A the Avogadro constant. Also the number-average degree of polymerization x_n, can also be calculated from equation 2.33:

$$x_n = k_p[M]_P \left(\frac{nN_P}{R_i}\right)$$ Eq. 2.33

The above parameters used for equation 2.32, can also be substituted into equation 2.33, and also R_i is the rate of radical generation. Equation 2.32 and 2.33, prove that by increasing the number of polymer particles, N_P, in the aqueous phase the molar mass and the reaction rate can be increased.

The graphical representation of the three intervals can be clearly seen in figure 2.17

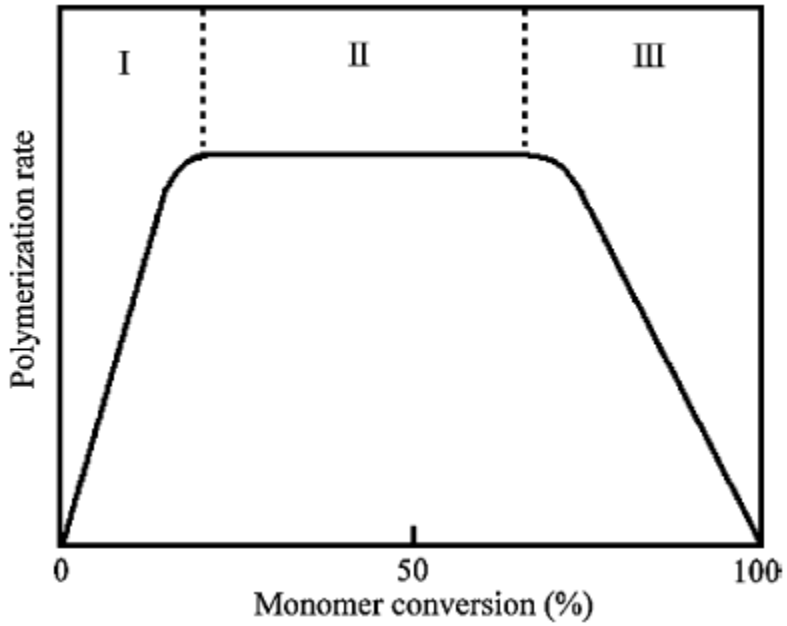

Figure 2.17 Description of the different intervals as a function of polymerization reaction rate vs monomer concentration in the aqueous phase [126].

Other research groups [127-129], presented an alternative theory know as homogeneous nucleation theory, which differs from the micelle nucleation theory in the premise that there are no particles present in the aqueous phase. Thermal decomposition of the initiator generates radicals in the aqueous phase. The radicals propagate and add

monomer units until the oligomers reached a critical chain length and become insoluble, thus precipitating the oligomer out of the solution. The precipitation of the oligomer causes a coil to globule transition of the hydrophobic chain, which is known as a primary particle. The particle becomes swollen by the monomer. This particle will also adsorb surfactant molecules thus providing stability in the aqueous phase. Final particle size as well as the profile of the particle size during the polymerization reaction depends on the amount of surfactant in the aqueous phase. Surfactant concentration will also condition the effectiveness of stabilizing and growth of the primary particles.

The droplet nucleation theory [130, 131], suggests that radicals in aqueous phase enter the monomer droplets as oligoradicals or single radicals and propagate to form particles. The adsorption of surfactant molecules to the surface of the growing particles, as well as the surface of the monomer droplets will provide the colloidal stability in the aqueous phase.

The controversy of which theory is correct still lingers within the colloidal community, but according to El-Aasser and Sudol [125] all three mechanisms operate simultaneously in the particle formation, although the specific contribution of each particle formation mechanism will depend on different factors; such as monomer solubility in the aqueous phase, surfactant concentration, and monomer droplet subdivision.

2.13 Stability in Colloidal Dispersions

The term “stable colloidal system” suggests that in an aqueous phase there are no signs of phase separation during an extended period of time. The stability of a system is characterized by the dispersity and the uniform distribution of the dispersed species in the medium [132]. Many systems remain stable through time, and are known to be in meta-stable state. The meta-stable state suggests that the aggregation of particles is prevented by the potential barrier that is sufficiently high. The term “stability” may also be related to the inability of particles to aggregate. Surface properties may be a determining factor in the colloidal behavior of the particles in the aqueous phase. Surface grouping or aggregation may be determined by different factors such as: Surfactant grafting, initiator used and grafted or adsorbed polymeric species. Polymer emulsion stability maybe controlled by the addition of low molecular weight surfactants such as sodium dodecyl sulfate and sodium dialkyl sulfosuccinates. The use of solid particles to stabilize emulsions has also been explored [133, 134]. These emulsions are known as pickering emulsions. These solid particles can function as surfactants, and the solids are located at the liquid-liquid interface and develop strong lateral interactions [133]. Different groups have used this technique to stabilize emulsions, Colver and Bon [135], studied the stabilization effect via pickering in miniemulsion. This group used laponite as a stabilizer for an emulsion polymerization of styrene. According to their findings, this technique can be applied to a wide variety of hydrophobic monomers, such as lauryl (meth)acrylate, butyl (meth)acrylate, octyl acrylate. The emulsion polymerization lead to armored droplets, as can be seen in figure 2.18, which correspond to the attachment of clay platelets to the surface of the colloidal particle.

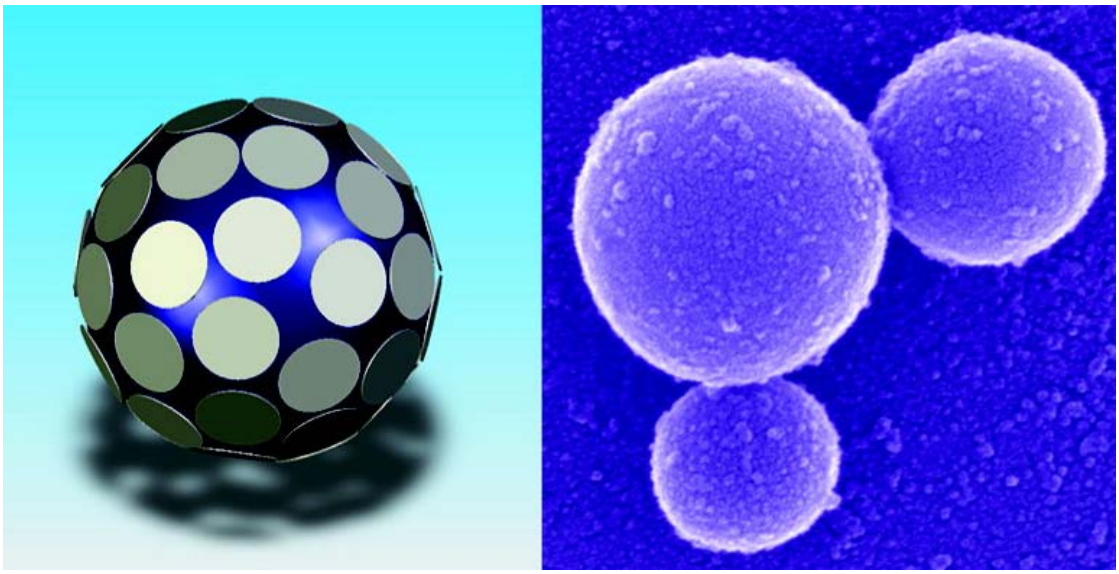

Figure 2.18 Idealized model of laponite coverage of styrene droplets in the emulsion. Actual cryo-TEM image of laponite/styrene droplets [135].

Zhang et al. [136], used pickering emulsion polymerization reactions to synthesize poly(methyl methacrylate) (PMMA) colloidal particles. Polyelectrolyte polymer brushes of poly[2-(dimethylamino) ethyl methacrylate] (PDMAEMA) were attached on to the surface of clay platelets, and used as stabilizers in the polymerization reaction. According to this group, the modified clay platelets were located at the oil/water interface. The interfacial effect caused the PMMA brushes to grow on the surface of the modified clay. Cryo-TEM imaging revealed that the PMMA particles in the emulsion were not spherical, due to physical constrains of the clay platelets, as can be seen in figure 2.19.

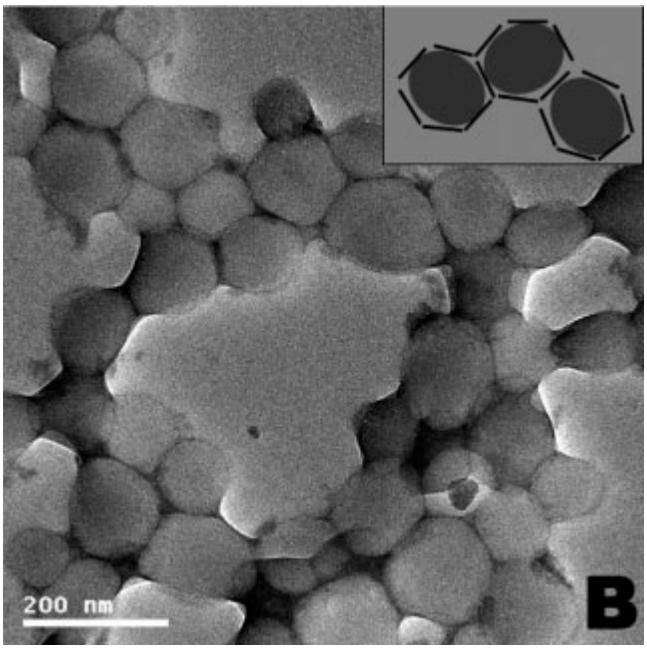

Figure 2.19. Cryo-TEM image of PMMA/clay nanocomposite synthesized via pickering emulsion polymerization, as can be seen in the figure the PMMA particles are not spherical. At the top right hand corner is an idealized structure of the nanocomposites and the physical restrictions of the clay platelets [136].

Guillot et al. [137], used natural nano size clay mineral particles, such as natural montmorillonite and laponite to evaluate the colloidal stability of a an oil-water system. This group also evaluated the surface interactions of the clay mineral particles and the colloidal particles. This group found that the addition of clay particles lead to stable dispersions and also helped the long term stabilization. The clay particles acted as a co-surfactant. Emulsion droplets are absorbed onto the flat surface of the clay particles causing an elongation of the droplets, as can be seen in figure 2.20. This group also found that the size of the droplets was not influenced by the presence of the clay, thus there was no variation of the particle size in the colloidal system.

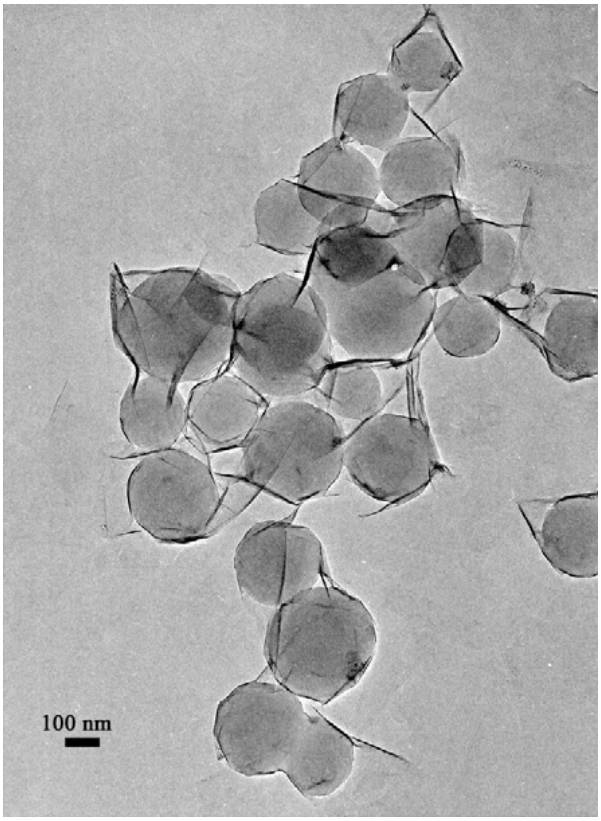

Figure 2.20 TEM image of polymerized particles of 2wt% montmorillonite-stabilized monolinolein/styrene emulsion [137].

Depending on the synthesis conditions of the emulsion, the latex droplets may be able to encapsulate clay platelets. This encapsulation effect was seen by Voorn et al. [138]. The emulsion polymerization of MMA was carried out in a surfactant free environment and at starved-feed conditions. The natural montmorillonite and laponite used in this study was organically modified to improve interactions with the polymer droplets. Characterization of cryo-TEM micrographs, suggest that the latex particles are in snowman-like conformation, and appear to be in dumbbell conformation. The authors suggest that the clay platelets were dispersed throughout the matrix, but exfoliation or delamination was not quantified. The same snowman and dumbbell morphology of the

polymer/clay particles was seen by Ianchis et al. [139]. This group studied the emulsion polymerization of polystyrene on the surface of organically modified montmorillonite platelets. The grafting of different monofunctional alkoxysilanes directly affects the particle size distribution of the emulsified polystyrene/clay particles. The particle size distribution is caused by the aggregation of modifed nanoclay platelets. The use of modified nanoclay platelets promotes a polyhedral conformation of polystyrene particles [140].

Voorn et al. [141], also synthesized polymer/clay nanocomposites latex particles via inverse pickering emulsion. This group used nanoclay montmorillonite Cloisite ® 20A as a stabilizing agent in the emulsion synthesis. The organic modification of the clay platelets improved their dispersion in the organic phase of the water-in-oil emulsion. As mentioned before the clay platelets are located at the surface of the latex particles [142]. A schematic representation of the polymerization process can be seen in figure 2.21. Stacking of the clay platelets was seen on the surface of the latex particles, thus suggesting that complete exfoliation of the clay platelets was not achieved in the emulsion polymerization. Dispersion results were later confirmed via XRD analysis of the nanocomposite films.

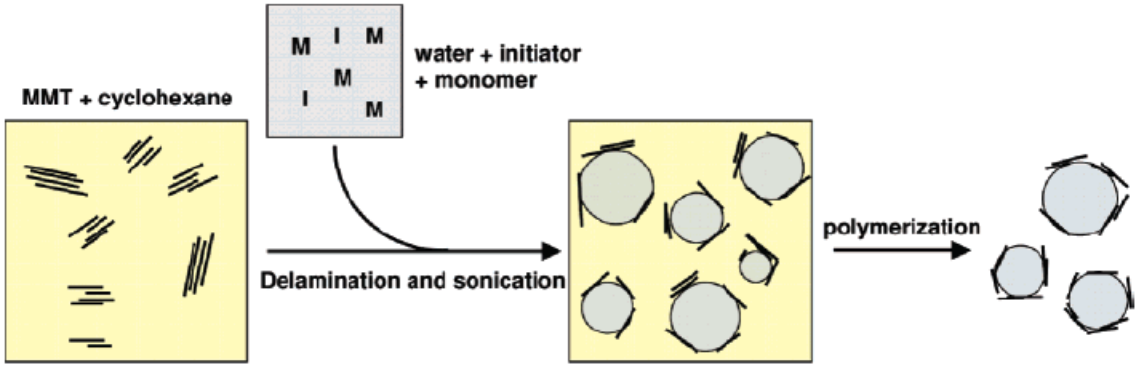

Figure 2.21. Proposed inversed emulsion polymerization mechanism of polymer/clay nanocomposites. Nanoclay platelets are used to stabilize the colloidal system. Clay platelets are distributed throughout the surface of the droplets [141].

Negrete-Herrera et al. [143, 144], reported the exfoliation of laponite clay platelets via emulsion polymerization. This group analyzed the surface modification of the nanoclay via ion exchange with cationic initiator (AIBA) and the effect the modified might have on the grafting polymerization process of poly (styrene-co butyl acrylate). This group suggests that the first step in the polymerization process is achieved in the aqueous phase. After this step the oligomeric radicals attach to the surface of the modified laponite and grow by the addition of monomers dispersed in the aqueous phase. The maximum amount of stacking of the clay platelets was limited to three or four individual platelets. The authors also suggest that the size distribution and the morphology of the polymer/clay particles is a direct result of the amount of AIBA intercalated within the platelets.

Diaconu et al. [145], reported that the enhancement of the mechanical properties of polymer/clay nanocomposites obtained via emulsion polymerization. The increase in tensile strength and storage modulus was due to the exfoliation of clay platelets. This

group also indicated that the poor dispersion of the clay platelets in the matrix will decrease the elongation at break for the composites. The stacked platelets will act as stress concentrators and which contributes to the poor elongation properties [146]. This group also reported a low increase in the glass transition temperature for the nanocomposites (Tg) when clay platelets were exfoliated in the matrix. The addition of nanoclay to the polymer matrix also enhanced the thermal stability of the system.

Refrences

1. Koros, W.J. and R.T. Chern, *Handbook of Process Separation.* 1st ed, ed. R.W. Rousseau. 1987: John Wiley & Sons.
2. Ghosal, K. and B.D. Freeman, *Gas Separation Using Polymer Membranes: An Overview*. Polymers for Advanced Technologies, 1994. **5**: p. 24.
3. Naylor, T.V., ed. *Permeation Properties*. Comprehensive Polymer Science, ed. A. Geoffrey. 1989, Pergamon Press Inc. 643-668.
4. Singh, A., B.D. Freeman, and I. Pinnau, *Pure and mixed gas acetone/nitrogen permeation properties of polydimethylsiloxane [PDMS]*. Journal of Polymer Science Part B: Polymer Physics, 1998. **36**: p. 289-301.
5. Dixon-Garrett, S.V., K. Nagai, and B.D. Freeman, *Ethylbenzene solubility. diffusivity, and permeability in poly(dimethylsiloxane).* Journal of Polymer Science Part B: Polymer Physics, 2000. **38**: p. 1461-1473.
6. Yi-Yan, N., R.M. Felder, and W.J. Koros, J. Appl. Polym. Sci., 1980. **25**.
7. Vieth, W.R., *Diffusion in a through polymers: principles and applications*. 1991, New York, N.Y.: Oxford Universtity Press.
8. Crank, J., *The mathematics of diffusion*. Second Edition ed. 1975, Bristol, England: Oxford University Press.
9. Pinnavaia, T.J. and G.W. Beall, eds. *Polymer-Clay Nanocomposites*. 2000, John Wiley & Sons Ltd.
10. Alexandre, M. and P. Dubois, *Polymer-layered silicate nanocomposites: preparation, properties and uses of a new class of materials.* Material Science and Engineering R, 2000. **28**.
11. Ray, S.S., K. Okamoto, and M. Okamoto, Macromolecules, 2003. **36**.
12. Xie, W., et al., *Thermal Degradation Chemistry of Alkyl Quaternary Ammonium Montmorillonite.* Chemistry of Materials, 2001. **13**: p. 2979-2990.
13. Wingrave, J.A., *Oxide Surfaces*. Surfactant Science Series, ed. A.T. Hubbard. Vol. 103. 2001, New York, NY: Marcel Dekker, Inc.

14. Brady, P.V. and J.L. Krumhansl, *Oxide Surface*. Surfactant Science Series, ed. J.A. Wingrave. Vol. 103. 2001, New York, N.Y.: Marcel Dekker, Inc.
15. Krishnamoorti, R., R.A. Vaia, and E.P. Giannelis, *Structure and dynamics os polymer-layered silicate nanocomposites.* Chem. Mater., 1996(8): p. 7.
16. Fornes, T.D., et al., *Effect of organoclay structure on nylon 6 nanocomposite morphology and properties.* Polymer, 2002. **43**.
17. Fornes, T.D., D.L. Hunter, and D.R. Paul, *Nylon-6 Nanocomposites from Alkylammonium-Modified Clay: The Role of Alkyl Tails on Exfoliation.* Macromolecules, 2004. **37**: p. 6.
18. Vaia, R.A., et al., Chem. Mater., 1996(8).
19. Tjong, S.C., *Structural and mechanical properties of polymer nanocomposites.* Material Science and Engineering R, 2006(53): p. 124.
20. Vaia, R.A., R.K. Teukolsky, and E.P. Giannelis, *Interlayer Structure and Molecular Environment of Alkylammonium Layered Silicates.* Chemistry of Materials, 1994. **6**(7): p. 1017-1022.
21. Hackett, E., E. Manias, and E.P. Giannelis, Chem. Phys., 1998(108).
22. Osman, M.A., M. Ploetza, and P. Skrabal, *Structure and Properties of Alkylammonium Monolayers Self-Assembled on Montmorillonite Platelets.* J. Phys. Chem. B, 2004. **108**(8): p. 2580-2588.
23. http://www.nanoclay.com/.
24. Oriakhi, C., *Nanosandwiches.* Chem. Br., 1998. **34**.
25. Zhang, Z., et al., *Synthesis and characterization of poly(butyl acrylate-co-methyl methacrylate) clay nanocomposites via emulsion polymerization.* International Journal of Nanoscience, 2006. **5**(2&3): p. 291-297.
26. Vaia, R.A. and E.P. Giannelis, *Polymer Melt Intercalation in Organically-Modified Layered Silicates: Model Predictions and Experiment.* Macromolecules, 1997. **30**: p. 8000-8009.
27. Vaia, R.A. and E.P. Giannelis, *Lattice Model of Polymer Melt Intercalation in Organically-Modified Layered Silicates.* Macromolecules, 1997. **30**: p. 7990 - 7999.
28. Ho, D.L., R.M. Briber, and C.J. Glinka, *Characterization of Organically Modified Clays Using Scattering and Microscopy Techniques.* Chem. Mater., 2001. **13**.
29. Ho, D.L. and C.J. Glinka, *Effects of Solvent Solubility Parameters on Organoclay Dispersions.* Chem. Mater., 2003. **15**.
30. Hildebrand, J.H. and R.L. Scott, *The solubility of nonelectrolytes*. 3rd ed. 1950, New York: Reinhold Pub. Corp.
31. Kong, Q., et al., *Synthesis and properties of poly(methyl methacrylate) clay nanocomposites using natural montmorillonite and synthetic Fe-montmorillonite by emulsion polymerization.* Polymer Composites, 2005. **27**(1): p. 49-54.
32. Zeng, C. and L.J. Lee, *Poly(methyl methacrylate) and Polystyrene Clay Nanocomposites Prepared by in-Situ Polymerization.* Macromolecules, 2001. **34**: p. 4098-4103.
33. Nalawade, S.P., F. Picchioni, and L.P.B.M. Janssen, *Supercritical carbon dioxide as a green solvent for processing polymer melts: Processing aspects and applications.* Progress in Polymer Science, 2006. **31**(1): p. 19-43.

34. Tomasko, D.L., et al., *A Review of CO2 Applications in the Processing of Polymers.* Industrial & Engineering Chemistry Research, 2003. **42**(25): p. 6431-6456.
35. Shenoy, S.L., et al., *Supercritical carbon dioxide aided preparation of conductive polyurethane–polypyrrole composites.* Journal of Supercritical Fluids, 2004. **28**(2-3): p. 233-239.
36. Yue, B., et al., *Particle encapsulation with polymers via in situ polymerization in supercritical CO2.* Powder Technology, 2004. **146**(1-2): p. 32-45.
37. Wang, Y., R.N. Dave, and R. Pfeffer, *Polymer coating/encapsulation of nanoparticles using a supercritical anti-solvent process.* Journal of Supercritical Fluids, 2004. **28**(1): p. 85-99.
38. Shieh, Y.T., et al., *Interaction of Supercritical Carbon Dioxide with Polymers. 1. Crystalline Polymers.* Journal of Applied Polymer Science, 1996. **59**(4): p. 695-705.
39. Zerda, A.S., T.C. Caskey, and A.J. Lesser, *Highly Concentrated, Intercalated Silicate Nanocomposites: Synthesis and Characterization.* Macromolecules, 2003. **36**(5): p. 1603-1608.
40. Nguyen, Q.T. and D.G. Baird, *An improved technique for exfoliating and dispersing nanoclay particles into polymer matrices using supercritical carbon dioxide.* Polymer, 2007. **48**(23): p. 6923-6933.
41. Ma, J., et al., *Preparation of polypropylene/sepiolite nanocomposites using supercritical CO2 assisted mixing.* European Polymer Journal, 2007. **43**(12): p. 4931-4939.
42. Naveaua, E., et al., *Supercritical CO2 as an efficient medium for layered silicate organomodification: Preparation of thermally stable organoclays and dispersion in polyamide 6.* Polymer, 2009. **50**(6): p. 1438-1446.
43. Horsch, S., et al., *Supercritical CO2 dispersion of nano-clays and clay/polymer nanocomposites.* Polymer, 2006. **47**(21): p. 7485-7496.
44. Serhatkulu, G.K., C. Dilek, and E. Gulari, *Supercritical CO2 dispersion of nano-clays and clay/polymer nanocomposites.* Journal of Supercritical Fluids, 2006. **39**(2): p. 264-270.
45. Cussler, E.L., S.E. Hughes, and W.J. Ward, *Barrier membranes.* Journal of Membrane Science, 1988. **38**.
46. DeRocher, J.P., et al., *Barrier membranes with different sizes of aligned flakes.* Journal of Membrane Science, 2005. **254**: p. 9.
47. Falla, W.R., M. Mulski, and E.L. Cussler, *Estimating diffusion through flake-filled membranes.* Journal of Membrane Science, 1996. **119**: p. 9.
48. Lape, N.K., E.E. Nuxoll, and E.L. Cussler, *Polydisperse flakes in barriers films.* Journal of Membrane Science, 2004. **236**: p. 8.
49. Yang, C., W.H. Smyrl, and E.L. Cussler, *Flake alignment in composite coatings.* Journal of Membrane Science, 2004. **231**: p. 12.
50. Sridhar, L.N., R.K. Gupta, and M. Bhardwaj, *Barrier properties of polymer nanocomposites.* Industrial and Engineering Chemistry Research, 2006: p. 8.
51. Xu, B., et al., *Calculating barrier properties of polymer/clay nanocomposites: Effects of clay layers.* Polymer, 2006. **47**: p. 7.

52. Clerk Maxwell, J., *A Treatise on Electricity and Magnetism*. Vol. 1. 1873, Oxford: Clarendon Press.
53. Strutt, W. and L. Rayleigh, *On the influence of obstacles arranged in rectangular order upon the properties of a medium.* Philos. Mag., 1892. **34**.
54. Nielsen, L.E., *Models for the permeability of filled polymer systems.* J. Macromol. Sci., Chem., 1967. **A1**.
55. Vaughan, B.R., *Polymer aluminophosphate mixed matrix membranes for gas separations*, in *Chemical Engineering*. 2007, Virginia Polytechnic Institute and State University: Blacksburg.
56. Wakeham, W.A. and E.A. Mason, *Diffusion through Multiperforate Laminae.* Industrial & Engineering Chemistry Fundamentals, 1979. **18**(4): p. 301-305.
57. Lan, T., P.D. Kaviratna, and T.J. Pinnavaia, *On the nature of polyamide-clay hybrid composites.* Chemistry of Materials, 1994. **6**(5): p. 573-575.
58. Bharadwaj, R.K., *Modeling the Barrier Properties of Polymer-Layered Silicate Nanocomposites.* Macromolecules, 2001. **34**(26): p. 9189-9192.
59. Gatos, K.G. and J. Karger-Kocsis, *Effect of the aspect ratio of silicate platelets on the mechanical and barrier properties of hydrogenated acrylonitrile butadiene rubber (HNBR)/layered silicate nanocomposites.* European Polymer Journal, 2007. **43**(4): p. 1097-1104.
60. Szycher, M., *Szycher's Handbook Of Polyurethanes*. 1st ed. 1999: CRC Press.
61. Stevens, M.P., *Polymer Chemistry An Introduction*. Third Edition ed. 1999: Oxford University Press.
62. Kusakabe, K., S. Yoneshige, and S. Morooka, *Separation of benzene/cyclohexane mixture using polyurethane-silica hybrid membranes.* Journal of Membrane Science, 1998. **149**: p. 29-37.
63. Jin, J., et al., *A Study on Viscoelasticity of Polyurethane-Organiclay Nanocomposites.* J. Appl. Polym. Sci., 2005. **99**: p. 3677-3683.
64. Gorrasi, G., M. Tortora, and V. Vittoria, *Synthesis and Physical Properties of Layered Silicates/Polyurethane Nanocomposites.* Journal of Polymer Science: Part B: Polymer Physics, 2005. **43**: p. 2454-2467.
65. Pattanayak, A. and S.C. Jana, *Properties of bulk-polymerized thermoplastic polyurethane nanocomposites.* Polymer, 2005. **46**: p. 3394–3406.
66. Njuguna, J. and K. Pielichowski, *Recent developments in polyurethane-based conducting composites.* Journal Of Material Science, 2004. **39**: p. 4081-4094.
67. Chattopadhyay, D.K. and K.V.S.N. Raju, Prog. Polym. Sci., 2007. **32**: p. 352.
68. Finnigan, B., et al., *Morphology and properties of thermoplastic polyurethane nanocomposites incorporationg hydrophilic layerd silicates.* Polymer, 2004. **45**: p. 2249-2260.
69. Xia, H., S.J. Shaw, and M. Song, *Relationship between mechanical properties and exfoliation degree of clay in polyurethanes nanocomposites.* Polymer International, 2005(54): p. 1392-1400.
70. Park, H.B., C.K. Kim, and Y.M. Lee, *Gas separation properties of polysiloxane/polyether mixed soft segment urethane urea membranes.* Journal of Membrane Science, 2002. **204**: p. 257-269.

71. Queiroz, D.P. and M.N. de Pinho, *Structural characteristics and gas permeation properties of polydimethylsiloxane/poly(propylene oxide) urethane/urea bi-soft segment membranes.* Polymer, 2005. **46**: p. 2346-2353.
72. Pixton, M.R. and D.R. Paul, *Gas Transport Properties of Polyarylates: Substituent Size and Symmetry Effects.* Macromolecules, 1995. **28**: p. 8277 - 8286.
73. Sorrentino, A., M. Tortora, and V. Vittoria, *Diffusion behavior in polymer-clay nanocomposites.* Journal of Polymer Science Part B: Polymer Physics, 2005. **44**(2): p. 265 - 274.
74. Sridhar, L.N., R.K. Gupta, and M. Bhardwaj, *Barrier Properties of Polymer Nanocomposites.* Ind. Eng. Chem. Res., 2006. **45**(25): p. 8282 -8289.
75. Galland, G. and T.M. Lam, *Permeability and diffusion of gases in segmented polyurethanes: structure-properties relations.* Journal of Applied Polymer Science 1993. **50**(6): p. 1041-1058.
76. Cao, N., et al., *Gas transport properties of polycarbonate-polyurethane membranes.* Journal of Applied Polymer Science, 1993. **48**(10): p. 1831 - 1842.
77. Madhavan, K. and B.S.R. Reddy, *Poly(dimethylsiloxane-urethane) membranes: Effect of hard segment in urethane on gas transport properties.* Journal of Membrane Science, 2005. **283**: p. 357-365.
78. Teo, L.S., J.F. Kuo, and C.Y. Chen, *Study on the morphology and permeation property of amine group-contained polyurethanes.* Polymer, 1998. **39**(15): p. 3355-3364.
79. Tjong, S.C. and Y.Z. Meng, *Impact-modified polypropylene/vermiculite nanocomposites.* J. Polym. Sci. Part B: Polym. Phys., 2003. **41**(19): p. 2332-2341.
80. Chavarria, F. and D.R. Paul, *Morphology and properties of thermoplastic polyurethane nanocomposites: Effect of organoclay structure.* Polymer, 2006. **47**(22): p. 7760-7773.
81. Lee, J.H., et al., *Properties of polyethylene-layered silicate nanocomposites prepared by melt intercalation with a PP-g-MA compatibilizer.* Composites Science and Technology, 2005. **65**(13): p. 1996-2002.
82. Balazs, A.C., C. Singh, and E. Zhulina, *Modeling the Interactions between Polymers and Clay Surfaces through Self-Consistent Field Theory.* Macromolecules, 1998. **31**(23): p. 8370-8381.
83. Finnigan, B., et al., *Effect of the average soft-segment length on the morphology and properties of segmented polyurethane nanocomposites.* Journal of Applied Polymer Science, 2006. **102**(1): p. 128-139.
84. Choi, W.J., et al., *Synthesis of chain-extended organifier and properties of polyurethane/clay composites.* Polymer, 2004. **45**: p. 6045-6057.
85. Woo, T., et al., *Effect of different preparation routes on the structure and properties of rigid polyurethane-layered silicate nanocomposites.* Journal of Applied Polymer Science, 2006. **102**(3): p. 2894-2903.
86. Buxton, G.A. and A.C. Balazs, *Lattice spring model of filled polymers and nanocomposites.* Journal of Chemical Physics, 2002. **117**(16): p. 7649-7658.
87. Gersappe, D., *Molecular Mechanisms of Failure in Polymer Nanocomposites.* Physical Review Letters, 2002. **89**(5): p. 058301/1-058301/4.

88. Choi, S., K.M. Lee, and C.D. Han, *Effects of Triblock Copolymer Architecture and the Degree of Functionalization on the Organoclay Dispersion and Rheology of Nanocomposites.* Macromolecules, 2004. **37**(20): p. 7649 - 7662.
89. Osman, M.A., et al., *Polyurethane Adhesive Nanocomposites as Gas Permeation Barrier.* Macromolecules, 2003. **36**(26): p. 9851 - 9858.
90. Xia, H., et al., *Microphase separation, stress relaxation, and creep behavior of polyurethane nanocomposites.* Journal of Applied Polymer Science, 2007. **103**(5): p. 2992-3002.
91. Yang, X., et al., *Performace of three air distribution systems in VOC removal from an area source.* Building and Environment, 2004. **39**: p. 1289-1299.
92. Uhde, E. and T. Salthammer, *Impact of reaction products from building materials and furnishings on indoor air quality—A review of recent advances in indoor chemistry.* Atmospheric Environment, 2007. **41**: p. 3111-3128.
93. Wargocki, P., et al., *The Effects of Outdoor Air Supply Rate in an Office on Perceived Air Quality, Sick Building Syndrome (SBS) Symptoms and Productivity.* Indoor Air, 2000. **10**: p. 222-236.
94. Järnström, H., et al., *Reference values for indoor air pollutants concentrations in new, residential buildings in Finland.* Atmospheric Environment, 2006. **40**: p. 7178-7191.
95. Molhave, L., *Organic compounds as indicators of air pollution.* Indoor Air, 2003. **13**: p. 12-19.
96. Wolkoff, P. and G.D. Nielsen, *Organic compounds in indoor air-their relevance for perceived indoor air quality?* Atmospheric Environment, 2001. **35**.
97. Mendell, M.J., et al., *Improving the health of workers in indoor environments: priority research needs for a national occupational research agenda.* Am. J. Public. Health., 2002. **92**: p. 1430-1440.
98. Saarela, K., et al., *Exposure of population and microenvironmental distributions of volatile organic compound concentrations in the EXPOLIS study.* Atmospheric Environment, 2003. **37**: p. 5563-5575.
99. Bernstein, J.A., et al., *The health effects of nonindustrial indoor air pollution.* Journal of Allergy and Clinical Immunology, 2008. **121**(3): p. 585-591.
100. Organization, W.H., *Indoor Air Quality: Organic Pollutants*, in *EURO Reports and Studies*. 1989, World Health Organization: Copenhagen.
101. Wolkoff, P., et al., *Organic compounds in office environments – sensory irritation, odor, measurements and the role of reactive chemistry.* Indoor Air, 2006. **16**: p. 7-19.
102. Wolkoff, P., et al., *Are we measuring the relevant indoor pollutants?* Indoor Air, 1997. **7**: p. 14.
103. Bernhard, C.A., et al. *Volatile organic compounds in 56 European office buildings*. in *Proceedings of the Healthy Buildings*. 1995. Milan.
104. Holcomb, L.C. and B.S. Seabrook, *Indoor concentrations of volatile organic compounds: implications of comfort, health and regulation.* Indoor Environment, 1995. **4**: p. 7-26.
105. Girman, J.R., et al., *Individual volatile organic compound prevalence and concentrations in 56 buildings of the building assessment survey and evaluation*

(BASE) study in *Proceedings of the 6th International Confrence on Indoor Air Quality and Climate*. 1999: Nagoya, Institute of Public Health. p. 237-242.
106. Reitzig, M., et al., *VOC emissions after building renovation: traditional and less common indoor air contaminants, potential sources, and reported health complaints.* Indoor Air, 1998. **8**: p. 91-102.
107. Brown, S.K., *Ocurrence of volatile organic compounds in indoor air* Organic Indoor Air Pollutants, ed. T. Salthammer. 1999, Wienheim: Wiley-VCH. 171-184.
108. Wolkoff, P., et al., *Formation of Strong Airway Irritants in Terpene/Ozone Mixtures.* Indoor Air, 2000. **10**: p. 82-91.
109. Grosjean, E. and D. Grosjean, *The gas-phase reaction of alkenes with ozone: formation yields of carbonyls from bi radical in ozone-alkene-cyclohexane experiments.* Atmospheric Environment, 1998. **32**: p. 3393-3402.
110. Weschler, C.J. and H.C. Shields, *Potential reactions among indoor air pollutants.* Atmospheric Environment, 1997. **31**: p. 3487-3495.
111. Carslaw, N., *New Directions: Where next with indoor air measurements?* Atmospheric Environment, 2003. **37**: p. 5645-5646.
112. Sundell, J., *On the history of indoor air quality and health.* Indoor Air, 2004. **14**(7): p. 51-58.
113. Zhang, Y. and Y. Xu, *Characteristics and correlations of VOC emissions from building materials.* International Journal of Heat and Mass Transfer, 2003. **46**: p. 4877-4883.
114. Qi, D.M., et al., *Synthesis and characterization of poly(butyl acrylate)/silica and poly(butyl acrylate)/silica/poly(methyl methacrylate) composite particles.* Journal of Applied Polymer Science, 2006. **99**(6): p. 3425 - 3432.
115. Mizutani, T., et al., *Preparation of spherical nanocomposites consisting of silica core and polyacrylate shell by emulsion polymerization.* Journal of Applied Polymer Science, 2005. **99**(3): p. 659 - 669.
116. Luna-Xavier, J.L., A. Guyot, and E. Bourgeat-Lami, *Synthesis and Characterization of Silica/Poly (Methyl Methacrylate) Nanocomposite Latex Particles through Emulsion Polymerization Using a Cationic Azo Initiator.* Journal of Colloid and Interface Science, 2002. **250**(1): p. 82-92.
117. Luna-Xavier, J.L., A. Guyot, and E. Bourgeat-Lami, *Preparation of nano-sized silica/poly(methylmethacrylate) composite latexes by heterocoagulation: comparison of three synthetic routes.* Polymer International, 2004. **53**(5): p. 609 - 617.
118. Wang, D., et al., *A comparison of various methods for preparation of polystyrene and poly(methyl methacrylate) clay nanocomposites.* Chemistry of Materials, 2002. **14**(9): p. 3837–3843.
119. van Herk, A.M., *Chemistry and technology of emulsion polymerisation*, ed. A.M. van Herk. 2005, Oxford: Blackwell Publishing Ltd.
120. Harkin, W.D., *A General Theory of the Mechanism of Emulsion Polymerization.* Journal of American Chemical Society, 1947. **69**(6): p. 1428-1444.
121. Harkin, W.D., *A general theory of the reaction loci in emulsion polymerization.* Journal of Chemical Physics, 1945. **13**: p. 381-382.

122. Smith, W.V., *The Kinetics of Styrene Emulsion Polymerization.* Journal of American Chemical Society, 1948. **70**(11): p. 3695-3702.
123. Smith, W.V. and R.H. Ewart, *Kinetics of Emulsion Polymerization.* Journal of Chemical Physics, 1948. **16**: p. 592.
124. Herrera-Ordonez, J., R. Olayo, and S. Carro, *The Kinetics of Emulsion Polymerization: Some Controversial Aspects.* Journal of Macromolecular Science, Part C: Polymer Reviews, 2004. **44**(3): p. 207-229.
125. Lovell, P.A. and M.S. El-Aasser, *Emulsion polymerization and emulsion polymers*. 1997, West Sussex, England: John Wiley & Sons Ltd.
126. Chern, C.S., *Emulsion polymerization mechanics and kinetics.* Progress in Polymer Science, 2006. **31**(5): p. 443-486.
127. Priest, W.J., *Particle growth in the aqueous polymerization of vinyl acetate.* Journal of Physical Chemistry, 1952. **56**(9): p. 1077-1082.
128. Fitch, R.M., *The homogeneous nucleation of polymer colloids.* British Polymer Journal, 1973. **5**(6): p. 467-483.
129. Roe, C.P., *Surface chemistry aspects of emulsion polymerization.* Industrial and Engineering Chemistry, 1968. **60**(9): p. 20-33.
130. Ugelstad, J., M.S. El-Aasser, and J.W. Vanderhoff, *Emulsion polymerization: Initiation of polymerization in monomer droplet.* Journal of Polymer Science: Polymer Letters Edition, 1973. **11**(8): p. 503-513.
131. Tang, P.L., et al., *Seeded emulsion polymerization of n-butyl acrylate utilizing miniemulsions.* Journal of Applied Polymer Science, 1991. **42**(7): p. 2019 - 2028.
132. Sjöblom, J., ed. *Emuslions and Emulsion Stability*. Second Edition ed. Surfactant Science Series. Vol. 132. 2006, CRC Press: Boca Raton, FL.
133. Binks, B.P., *Particles as surfactants--similarities and differences.* Current Opinion in Colloid & Interface Science, 2002. **7**(1-2): p. 21-41.
134. Pickering, S.U., *Pickering: Emulsion.* Journal of the Chemical Society, Transactions, 1907. **91**: p. 2001-2021.
135. Colver, P.J. and S.A.F. Bon, *Pickering miniemulsion polymeriztion using laponite clay as a stabilizer.* Langmuir, 2007. **23**(16): p. 8316-8322.
136. Zhang, J., K. Chen, and H. Zhao, *PMMA colloid particles armored by clay layers with PDMAEMA polymer brushes.* Journal of Polymer Science Part A: Polymer Chemistry, 2007. **46**: p. 2632-2639.
137. Guillot, S., et al., *Internally structured pickering emulsions stabilized by clay mineral particles.* Journal of Colloid and Interface Science, 2009. **333**(2): p. 563-569.
138. Voorn, D.J., W. Ming, and A.M. Van Herk, *Clay platelets encapsulated inside latex particles.* Macromolecules, 2006. **39**(14): p. 4654-4656.
139. Ianchisa, R., et al., *Surfactant-free emulsion polymerization of styrene in the presence of silylated montmorillonite.* Applied Clay Science, 2009. **45**(3): p. 164-170.
140. Negrete Herrera, N., et al., *Aqueous Dispersions of Silane-Functionalized Laponite Clay Platelets. A First Step toward the Elaboration of Water-Based Polymer/Clay Nanocomposites.* Langmuir, 2004. **20**(5): p. 1564-1571.
141. Voorn, D.J., W. Ming, and A.M. Van Herk, *Polymer-clay nanocomposite latex particles by inverse pickering emulsion polymerization stabilized with*

hydrophobic montmorillonite platelets. Macromolecules, 2006. **39**(6): p. 2137-2143.
142. Cauvin, S., P.J. Colver, and S.A.F. Bon, *Pickering Stabilized Miniemulsion Polymerization: Preparation of Clay Armored Latexes.* Macromolecules, 2005. **38**(19).
143. Negrete-Herrera, N., et al., *Polymer/Laponite Composite Colloids through Emulsion Polymerization: Influence of the Clay Modification Level on Particle Morphology.* Macromolecules, 2006. **39**(26): p. 9177-9184.
144. Bourgeat-Lami, E., et al., *Surface Assisted Nucleation and Growth of Polymer Latexes on Organically-Modified Inorganic Particles.* Macromolecular Symposia, 2005. **229**(1): p. 32-46.
145. Diaconu, G., M. Paulis, and J.R. Leiza, *Towards the synthesis of high solids content waterborne poly(methyl methacrylate-co-butyl acrylate)/montmorillonite nanocomposites.* Polymer, 2008. **49**(10): p. 2444-2454.
146. *Chemistry and technology of polymer additives*, ed. S. Al-Malaika, A. Golovoy, and C.A. Wilkie. 1999, Malden, MA: Blackwell Science.

Chapter 3: Transport properties in polyurethane/clay nanocomposites as barrier materials: Effect of processing conditions

3.1 Abstract

Polyurethane/clay nanocomposites were fabricated in solution and tested as gas barrier membranes. Natural montmorillonite was modified with various alkylammonium surfactants and incorporated into a polyurethane matrix. Permeation properties of the nanocomposites were studied as a function of processing methodology. Pre-processing clay samples with sonication instead of plain stirring led to significantly better barrier properties. Fitting the experimental permeabilities with phenomenological models, which predict the effective permeability of polymer systems filled with barrier flakes as a function of flake concentration, led to low values of calculated aspect ratios.

3.2 Introduction

In the past decade, polymer/clay nanocomposites have drawn considerable interest because of their enhanced properties, including flame resistance [1, 2], mechanical properties [3, 4], gas barrier properties [5-8], thermal stability [9] and biodegradability [10, 11], when compared to pristine polymers. Polymer/clay nanocomposites have been used in various consumer products and in the construction and transportation industry [12-14], with specific impact on technologies such as barrier layer materials, drink packaging applications, bottle applications, protective coatings, and adhesive molding compounds [15, 16]. Clay particles have been added to different

polymers including multilayered PET, epoxy composites [15], and polystyrene/polyethylene [17]. Polyurethane/nanoclay systems have also attracted attention for their barrier-like properties [18]. Polyurethanes are inherently versatile and can be processed into a wide variety of products such as fibers, foams, adhesives and coatings. The addition of clay particles into these systems allows for enhanced control of their physical properties. Polyurethanes are considered linear block co-polymers of the $(AB)_n$ type. The nature of a microphase separation, which is due to a difference in polarity and the thermodynamic incompatibility of the two phases [19], allows these polymers to be subdivided into a “soft” and “hard” phase. The soft segment is generally composed of long flexible polyester or polyether units and provides the elastomeric properties of the polymer. The hard phase or second block of the copolymer is based on isocyanates and triol or diol chain extenders. The hard phase is in an amorphous glassy state or in a crystalline state with hydrogen bonding within the hard segments, and will acts as a physical crosslink. The alternating blocks and the variety of monomers used to synthesize the copolymer structure permits tailoring the properties of these thermoplastic polyurethanes [20, 21]. Chen-Yang, et al. [22], proposed the use of polyurethane nanocomposites as thermal an anticorrosive films. The use of these composites has also extended to the coating [23] and adhesive area [18]. The use of coatings with barrier properties has been proposed to reduce volatile organic compounds emissions in structural insulated panels [24].

In this study we investigate the effect of processing on the gas barrier properties of polyurethane/clay nanocomposite systems. In particular we compare the effects of clay platelet sonication versus plain stirring during processing. We also examine the role of

various alkyl ammonium surface groups present in the montmorillonite clays in the dispersion of clay layers in the polyurethane.

3.3 Experimental

3.3.1 Materials

Tetrahydrofuran (THF) was purchased from Sigma Aldrich and used as received. The grade purchased was high purity liquid chromatography and inhibitor free. THF was used as a solvent in the casting of the polyurethane/clay membranes. The thermoplastic polyurethane used in this study was polyether-based TPU Estane® 58315 supplied by Estane®, a unit of Noveon Inc. The commercially available nanoclays were purchased from Southern Clay Products. For nomenclature purposes the different Cloisite® series will be referred as C10A, C20A and C30B as indicated in Table 3.1.

Table 3.1 Nomenclature for thermoplastic polyurethane/nanoclay composite.

Commercial Name	Cloisite ® 10A	Cloisite ® 20A	Cloisite ® 30B
Denomination for this chapter	C10A	C20A	C30B

The specifications of the nanoclays used in this study are presented in Table 3.2. The average concentration of the tallow (T) and/or hydrogenated tallow (HT) groups was as follows: ~65% C18; ~30% C16: ~5% C14, where the number following C refers to the number of carbon atoms in the tallow group.

Table 3.2. Nanoclay specifications as provided by Southern Clay Products.

Denomination		Chemical Structure	Specifications
Cloisite ® 10A	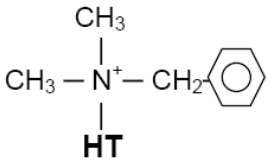	Dimethyl benzyl hydrogenated-tallow ammonium montmorillonite	125 MER, Organic Content = 39.6%, d_{001} spacing = 19.2 Å, ρ = 1.9 g/cc
Cloisite ® 20A	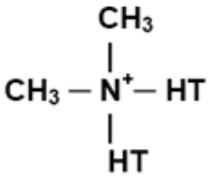	Dimethyl bis(hydrogenated-tallow) ammonium montmorillonite	95 MER, Organic Content = 39.6%, d_{001} spacing = 24.2 Å, ρ = 1.77 g/cc
Cloisite ® 30B	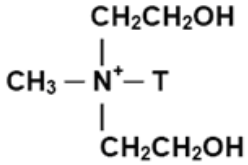	Bis(2-hydroxy-ethyl)methyl tallow ammonium montmorillonite	90 MER, Organic Content = 31.5%, d_{001} spacing = 18.5 Å, ρ = 1.98 g/cc

3.3.2 Membrane Preparation

All clay samples were dried for a period of 24 hours at 100°C and kept in a desiccator. Membranes composed from the polyether based thermoplastic polyurethane and the different nanoclays, were prepared as follows. In the first stage, the nanoclay was mixed in 5 ml of THF in a 20 ml flask, the composition of the nanoclay in THF was varied from 1 wt % to 5 wt %. The solution was mixed for 8 hours. The second stage involved the addition of 0.22 g of the polymer to the clay/THF solution. The polymer/clay solution was mixed for 8 hours, and then cast on to a nonstick circular Teflon pan with a diameter of 5 cm. Immediately after casting, a flat glass plate was placed over the pan to decrease the rate of evaporation. A controlled evaporation rate allowed the reduction of solvent concentration within the film and prevented the

formation of bubbles within the membrane, and curling of the film. The solution was allowed to dry for 1 day. Once dry the polymer/clay membranes were removed from the pan and placed in a vacuum oven at 80 °C for 24 hours.

The preparation for the sonicated membranes was similar to that for the stirred membranes, with the exception that in the first step the THF solution containing the nanoclay was set in a sonication bath at 25 °C for a period of 30 minutes. The sonication bath used was VWR model 50HT. After sonication was completed, a pre-determined amount of the polyurethane was added to the flask and stirred for 8 hours. The casting and annealing of the membranes remained the same as for the preparation of the stirred samples. The average thickness of the membranes was 91 μm ± 10μm.

3.4 Characterization

Gas permeabilities in the pure polyurethane, stirred polyurethane/clay and sonicated polyurethane/clay membranes were measured in a constant volume-variable pressure system. The membranes are placed in a stainless steel cell with volumetric chambers on each side. The upstream side of the membrane is set at 25 °C and 4 atm with the penetrating gas specie. The downstream side is initially evacuated to $P < 0.001$ atm. The variation in downstream pressure is monitored in real time and is analyzed only after steady state is achieved [25]. The steady-state behavior allows for time-lag method analysis. All gases employed (He, O_2, N_2, and CH_4) were ultra-high purity (minimum purity 99.999%) and were obtained from Airgas, Inc.. X-Ray diffractometry, XRD, was used to determine the interspacial distance within the clay platelets. The system was a Sintag XDS 2000 powder diffractometer using Ni filtered Cu KαX-ray radiation

(λ=1.54Å) at voltage of 45KV, 40mA current, and filament current of 3.30A. The scanning rate for the low angle samples was done at 0.25°/min over a range of 2θ = 1-10°. For the wide angle samples, the scanning rate was 1°/min over a range of 2θ = 10-90°. The XRD measurements were conducted on the membrane samples, while the clay was analyzed in the powder form. Dynamic mechanical thermal analysis (DMTA) was performed on a Rheometric Scientific DMTA IV with a ramp rate of 2°C/min and a frequency of 1 Hz. Transmission electron microscopic (TEM) images were obtained with the use of FEI Titan 300, Scanning Transmission Electron Microscope, equipped with a field-emission electron gun, with variable accelerating voltages from 80 kV to 300 kV.

3.5 Results and Discussion

3.5.1 X-Ray Analysis and TEM

The X-ray diffractograms for the polyurethane/clay nanocomposite for the C10A sonicated series and the pristine organically modified clay can be seen in Figure 3.1. Pure C10A displays a peak at 2θ = 4.7°, which corresponds to the d_{001} basal spacing of 18.8 Å. The C10A nanocomposites have d_{001} basal spacing values within the region of 2θ = 2.4-2.6. The shift to lower values indicates an expansion of the basal spacing, which suggests a penetration of the polymer chains within the gallery space. In case of the stirred samples containing the highest concentration of clay, 5% wt., the calculated interspatial distance was 35.9 Å. This corresponds to a 91% increase in the basal spacing of the nanocomposite compared to the pristine clay. The maximum value of the basal spacing in the sonicated samples was 35.3 Å. Both stirred and sonicated samples show a weak peak in the range of 2θ = 5.14 to 5.18. This d_{002} spacing corresponds to an interfacial distance

of approximately 17 Å. The indexing of samples in the 2θ region, confirms the presence of polymer intercalated structures in the C10A series.

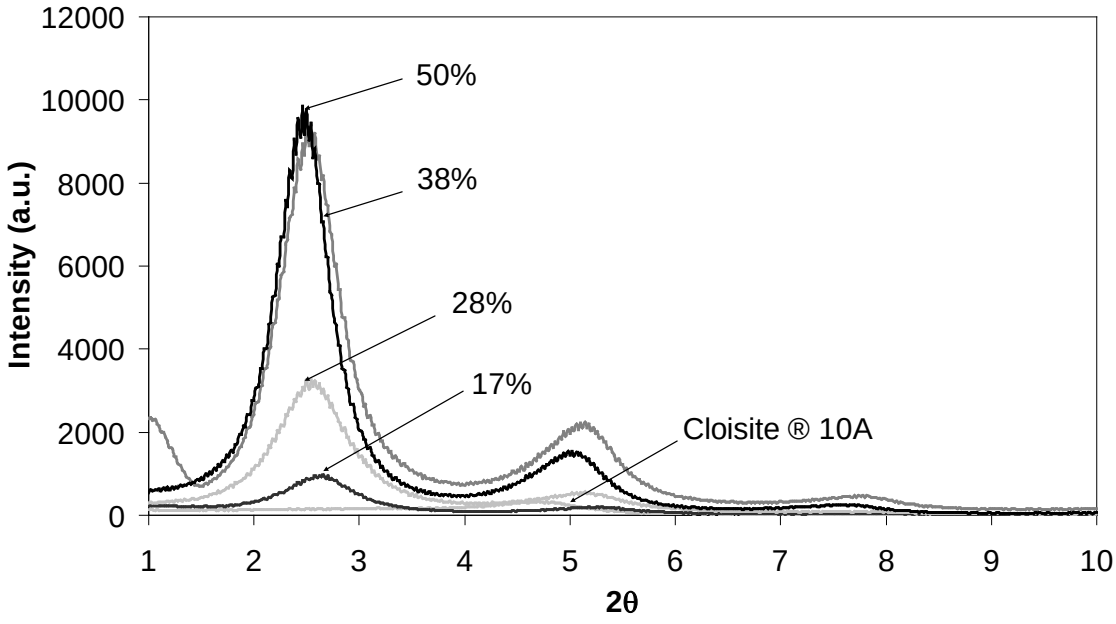

Figure 3.1. XRD diffractograms for C10A sonicated nanocomponent series.

Figure 3.2 and 3.3 are the corresponding diffractograms for the C20A and C30B nanocomposite series. C20A series, presented the lowest increase of the d_{001} basal spacing. The small increase can be explained by the presence of two tallow groups within the organic modifier used in this nanoclay, which shield the surface of the silicate platelets [26-28] and prevent the polymer species from penetrating the gallery space [29, 30]. The XRD diffractograms of the C30B series provided similar results to those of the C10A series. The maximum observed increase in the d_{001} basal spacing in the C30B series was 94%. Both C10A and C30B clays have only one tallow group present in the alkylammonium organic modifier. The large expansion of the gallery space for the C30B

series can be attributed to hydrogen bonding between the two hydroxyethyl groups present in the organic modifier and the polar section of the polyurethane [3]. These results suggest that the polymer indeed intercalates the clay structure. However, because the structural registry is retained, the clays do not appear to be fully exfoliated.

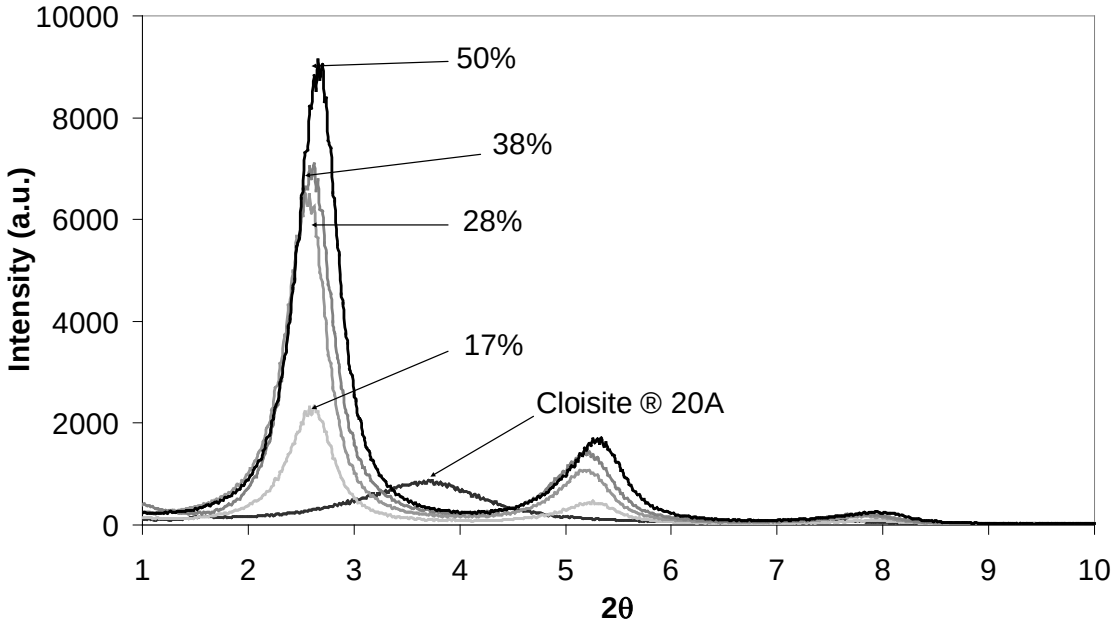

Figure 3.2. XRD diffractogram for C20A sonicated nanocomponent series

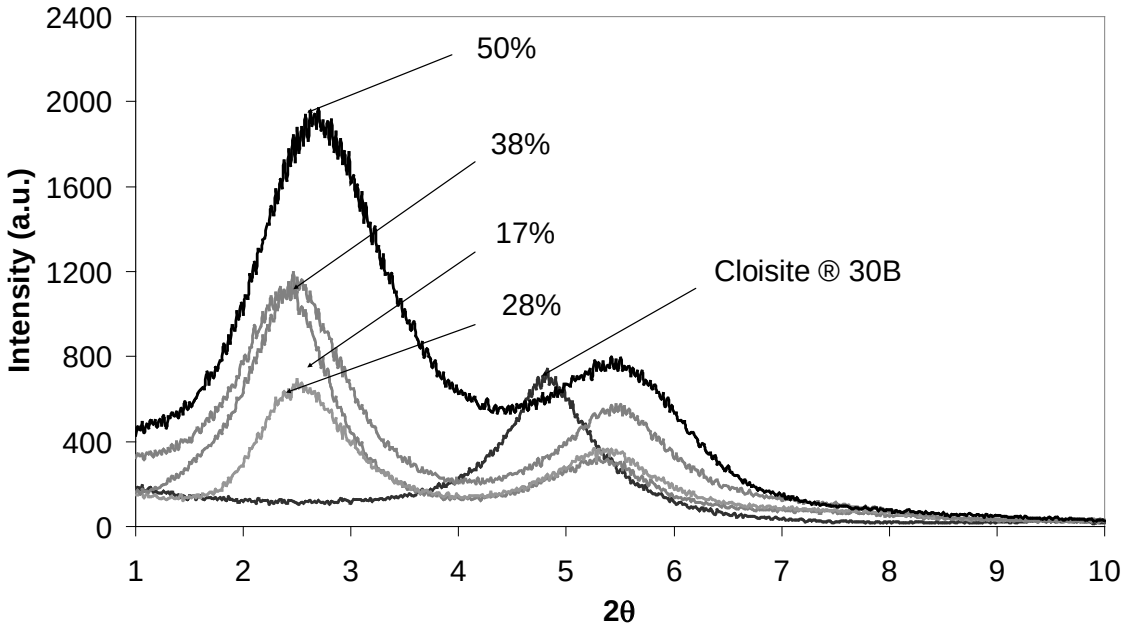

Figure 3.3. XRD diffractogram for C30B sonicated nanocomponent series.

The morphology of the polymer nanocomposites was observed by TEM images. Montmorillonite platelets have a higher electron density than the polyurethane, thus generating a higher resistance to electron transmission. This effect is seen with the TEM images as darker shapes. The TEM image in Figure 3.4 of the sonicated C30B polyurethane/clay nanocomposite suggests that the separation distance between the clay layers is on the order of 40 Å ± 20 Å, which is consistent with the XRD measurements. Comparing the TEM images corresponding to C30B series at 17% wt. (Figures 3.5 and 3.6) indicates that the samples processed by sonication generated a higher dispersion of the nanocomposite than the plain stirred samples [31].

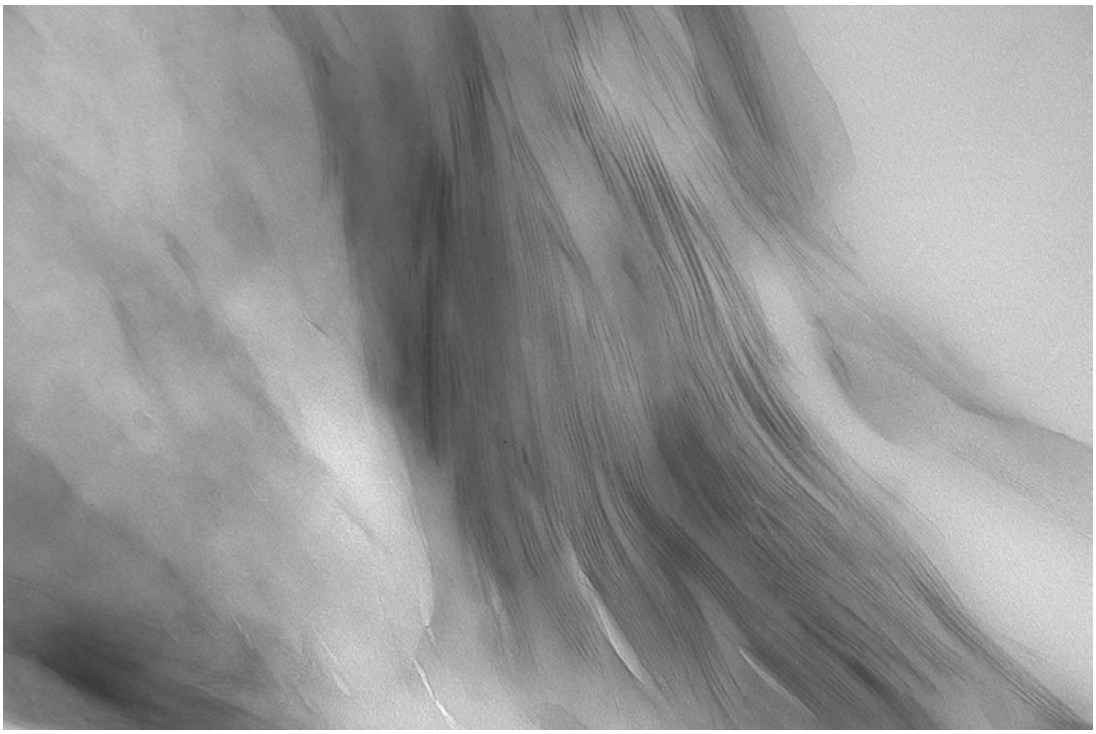

Figure 3.4. Transmission electron micrographs of the cross-section of 17 wt%., C30B sonicated.

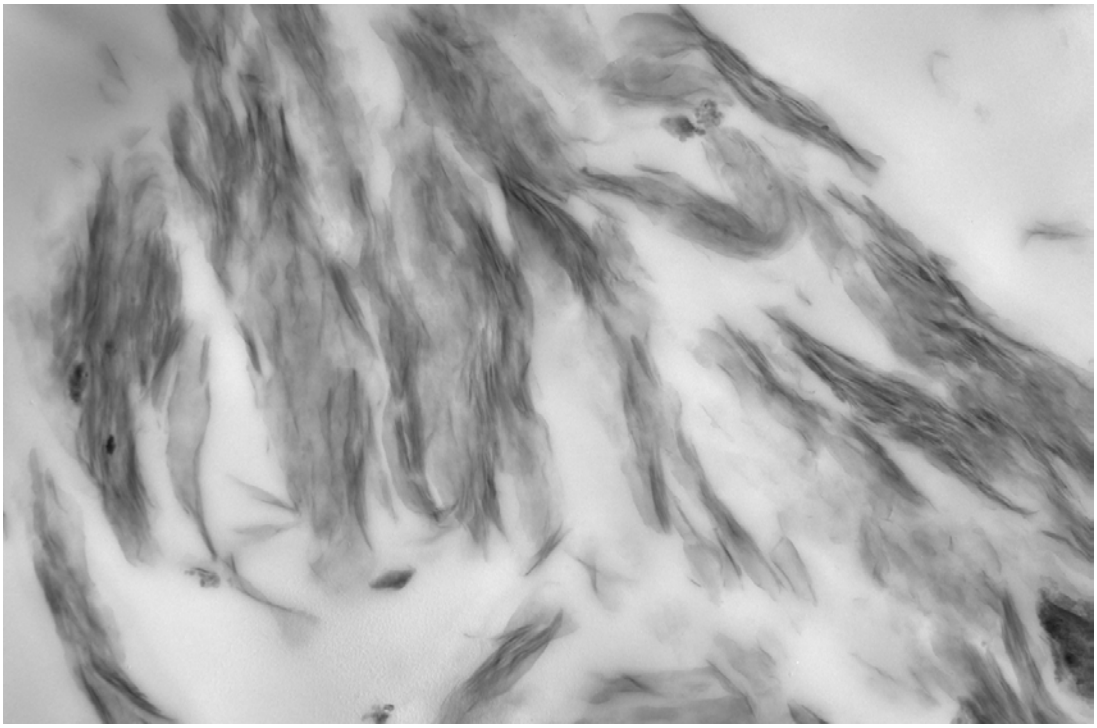

3.5. Transmission electron micrographs of the cross-section of 17 wt%., C30B stirred.

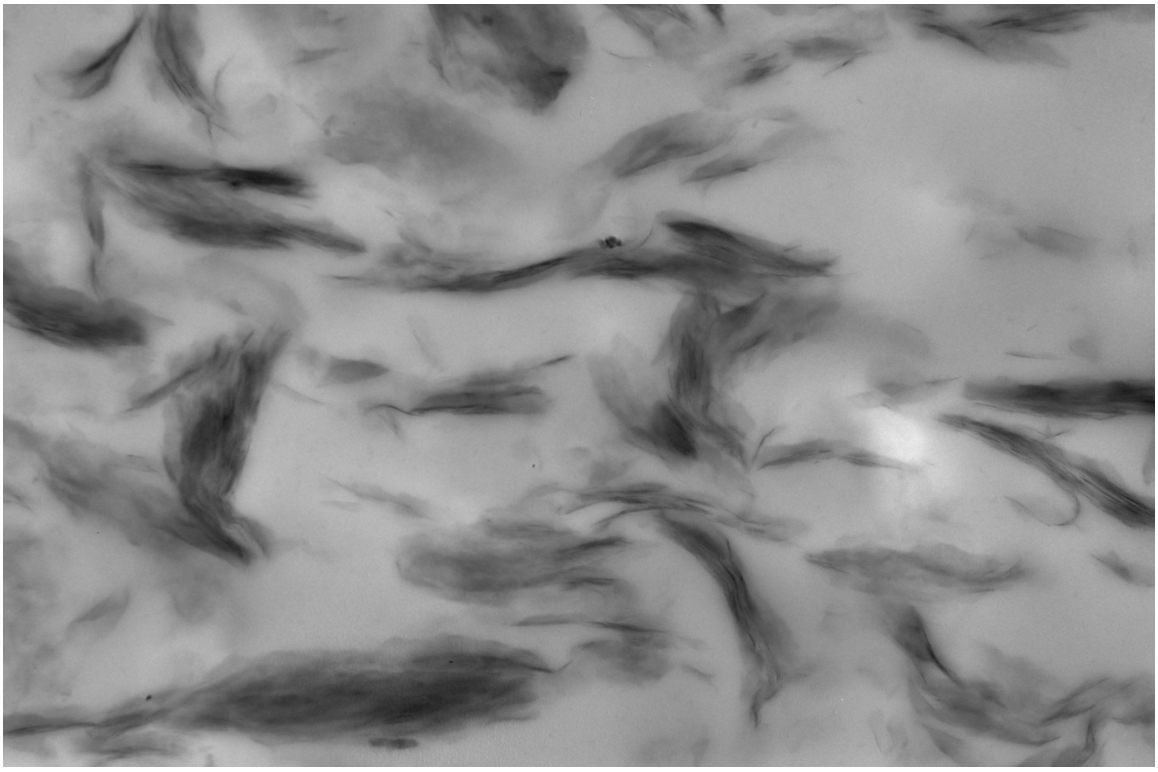

3.6. Transmission electron micrographs of the cross-section of 17 wt%., C30B sonicated.

TEM images also allowed for comparison between clay species, the micrographs for the sonicated C10A and the sonicated C20A at 28% wt., are seen in Figures 3.7 and 3.8. These TEM images confirm that the C10A series provides a better dispersion that the C20A series, which may suggest that the nanocomposites containing a one tail organic modifier disperses better than its counterpart C20A, containing a two tail organic modifier. The images related to the C20A nanocomposite series also indicate that this series contained the highest number of agglomerated clay layers and the highest stacking of the clay platelets. TEM images for all the nanocomposites indicated that the silicate platelets seen were arranged randomly throughout the barrier membrane. The aspect ratio of the clay layers appears to be greater than 100.

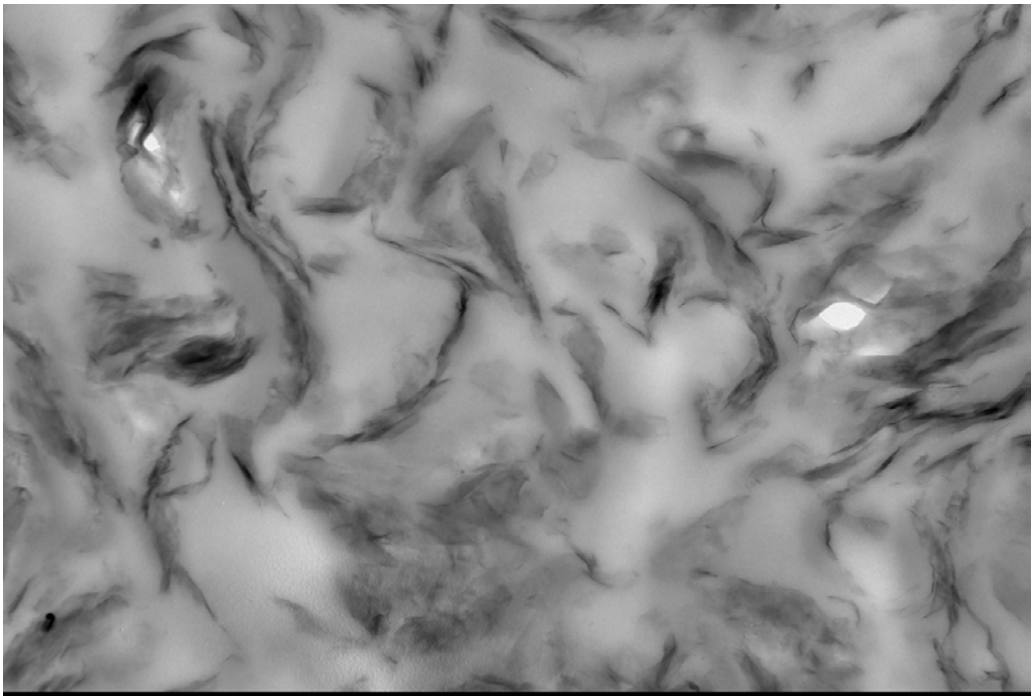

Figure 3.7. Transmission electron micrographs of the cross-section of 28 wt%., C10A sonicated.

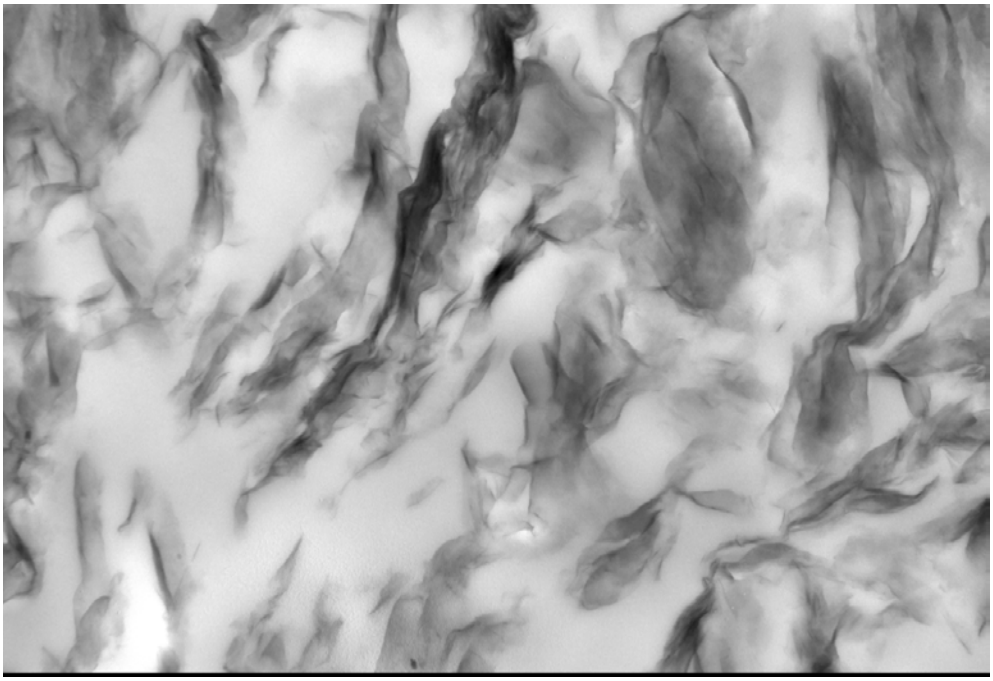

Figure 3.8. Transmission electron micrographs of the cross-section of 28 wt%., C20A sonicated.

3.5.2 DMTA Analysis

The dissipation factor (tan δ) is the ratio of the loss modulus and the stored modulus, and reflects the glass transition temperature T_g, when maximum. Table 3.3 summarizes the T_g values of the C10A, C20A and C30B stirred and sonicated nanocomposites as well as the pristine polymer.

Table 3.3 Measured T_g for stirred and sonicated polymer clay nanocomposites

		T_g (°C)	
Estane ® 58315		-44	
	wt%	**Stirred**	**Sonicated**
C10A			
	1	-31.5	-29.9
	2	-27.5	-26.8
	3	-24.7	-22
	5	-22.3	-18
C20A			
	1	-26.9	-26.5
	2	-27	-26.3
	3	-25	-20.9
	5	-23	-23.3
C30B			
	1	-37.1	-28.1
	2	-24.6	-25.9
	3	-23	-23.2
	5	-18.6	-19

This T_g corresponds to the micro-phase separated polyether segments in the polyurethane copolymer. The Tg increases with the addition of the clay in all the clay series as would be consistent with well-dispersed fillers with good interfacial contact [32]. For the C10A series, the Tg of the sonicated samples shifts to much higher temperatures compared to the stirred samples. This effect can be attributed to the processing method, which appears to generate a higher dispersion of the silicate platelets in the matrix [33]. The higher

surface area for the sonicated C10A series introduces a greater number of hydrogen bonding sites between the –OH groups, present on the silicate surface and the ether groups in the soft segment, as well as the isocyante groups in the hard phase of the polyurethane [34, 35]. Thus anchored, the clay platelets increase the glass transition temperature of the soft-phase by restricting segmental chain motion [36, 37], and generating an interphase region [38]. These restriction effects may also be responsible for broadening the tan δ peak, and the decrease in intensity of this peak [23], as well as the reduction of the damping capacity [31, 32, 39]. The small increase in T_g, for both sonicated and stirred C20A series, suggest a low degree of interaction between the polymer chains and the surface of the silicate platelets. Again, this effect may be related to the lower degree of exfoliation in this particular clay series, which can be attributed to the steric hindrance of the two tallow chains present in the alkylammonium organic modifier. These groups compete with the hard phase of the polyurethane, in interactions with the -OH species on the silicate surface [3, 40]. The changes in Tg in the C30 series at a given clay concentration are also insensitive to the processing method, although a significant increase in Tg is observed at 5 wt% C30A.

3.5.3 Permeation Data

3.5.3.1 Effect of Processing

Figures 3.9 and 3.10 compare the N_2 and CH_4 permeabilities in sonicated and stirred nanocomposites at 28% wt of clay. Clearly the addition of clay particles to a polymer matrix decreases the N_2 and CH_4 permeation when compared to that of the pristine polyurethane. The extent of this decrease is much higher when the clays are sonicated before being incorporated into the polyurethane matrix. For example, sonication in the C30B series decreased N_2 permeation by as much as 60% when compared with the stirred samples. While sonication does not affect the structure of the clay (as evidenced by the same basal spacing for sonicated and stirred samples), the permeation data coupled with the DMTA results, suggests that sonication may enhance dispersion. Intuitively, the permeation results do in fact imply that well dispersed clay particles create a more tortuous path for the penetrating gas molecules. Figures 3.6 and 3.7 also suggest that all the nanoclay series analyzed in this study are susceptible to the effect of processing via sonication. Statistical analysis of the permeation data indicates that the samples treated via sonication and plain stirring provide an error of less than 1%.

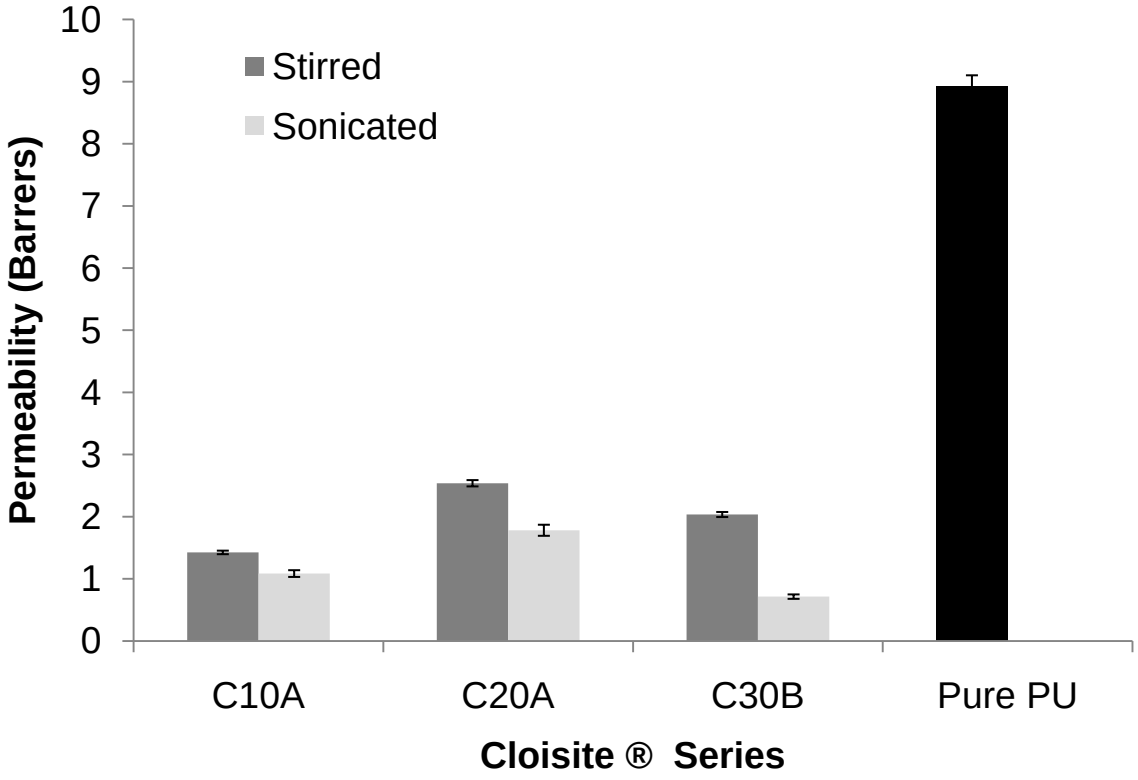

Figure 3.9 Comparison of O_2 permeation in nanocomposites, Sonication vs Stirrng Cloisite ® series with 28 wt%.

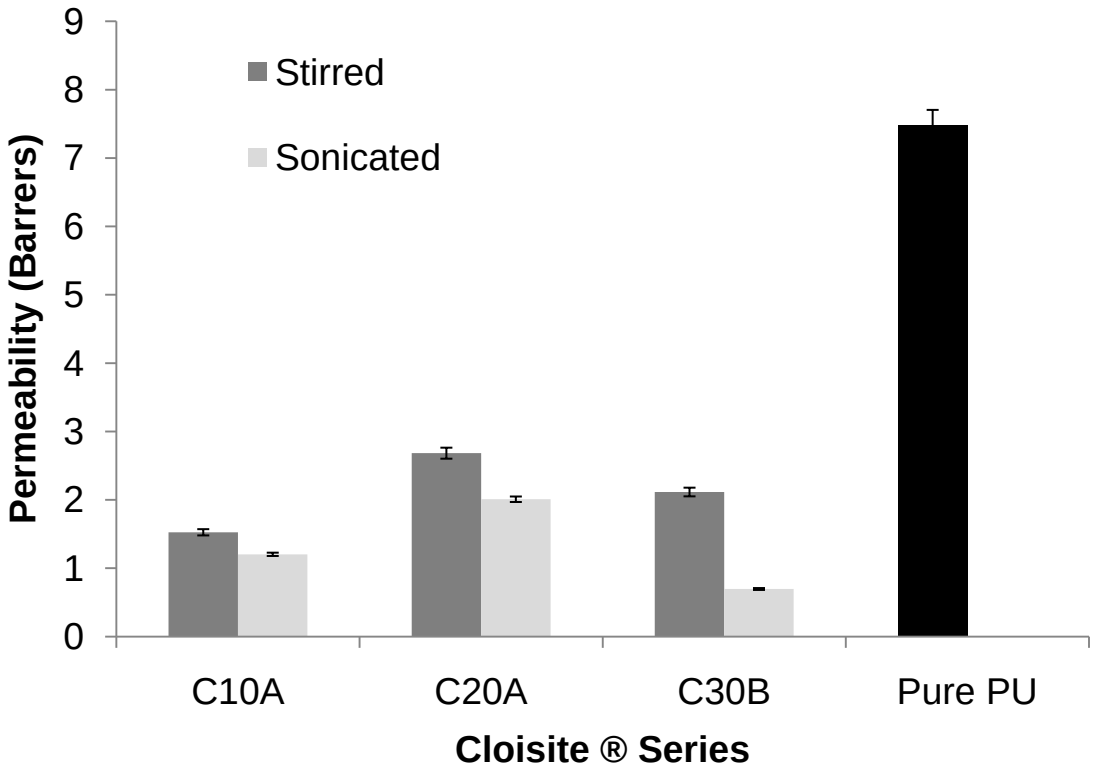

Figure 3.10 Comparison of CH_4 permeation in nanocomposites, Sonication vs Stirring Cloisite ® series with 28 wt%.

3.5.3.2 Effect of Clay Type

The CH_4 permeability data for the various nanocomposite clays are compared in Figure 3.11. These results indicate that the polymer/nanoclay composites using the C20A nanoclay series provided the poorest barrier properties compared to C10A and C30A clay nanocomposites. The poor performance of this series can be attributed to the increased difficulty of the polyurethane to penetrate the gallery space of the organically modified clay and thus preventing the generation of a more intercalated matrix. As expected, this clay series had the lowest d_{001} spacing as shown in Table 3.2. When comparing the He permeability in the various clay nanocomposites, as seen in Figures 3.12, results indicate

that in some cases the C10A series provided the best barrier properties per wt. % of clay. Gas permeation in the C10A nanocomposites dropped with the addition of the clay even without sonication, although sonication of the C10A clay particles decreased the permeation even further. Permeation results for the C30B indicated that these nanocomposites provided the best barrier properties when the clays were sonicated. At the highest clay concentration, 50% wt, the C30B nanocomposites have the lowest permeability.

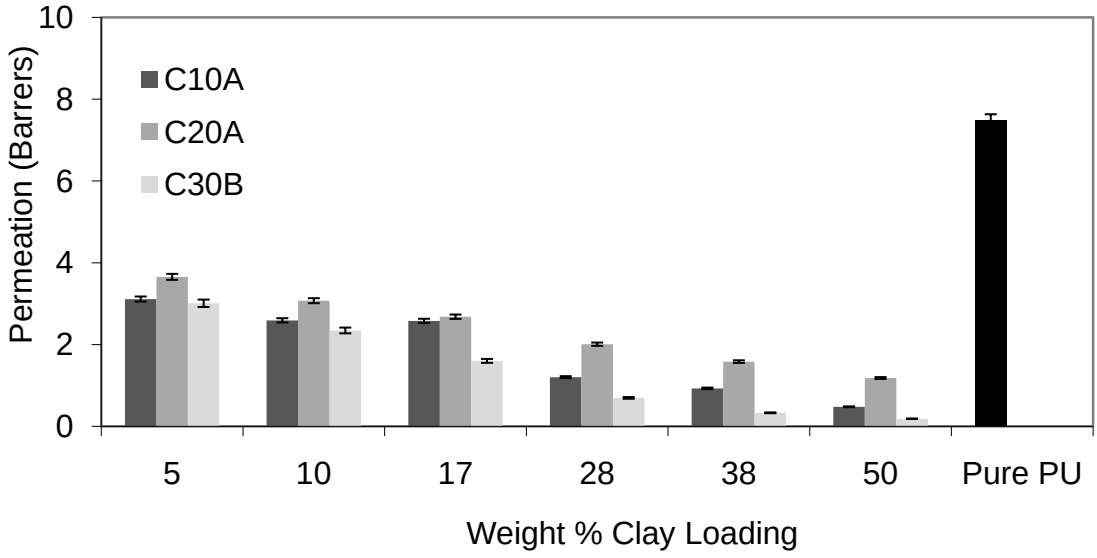

Figure 3.11 Comparison of CH_4 permeation in cancomposites fabricated by sonicating the clays of all Cloisite ® series samples.

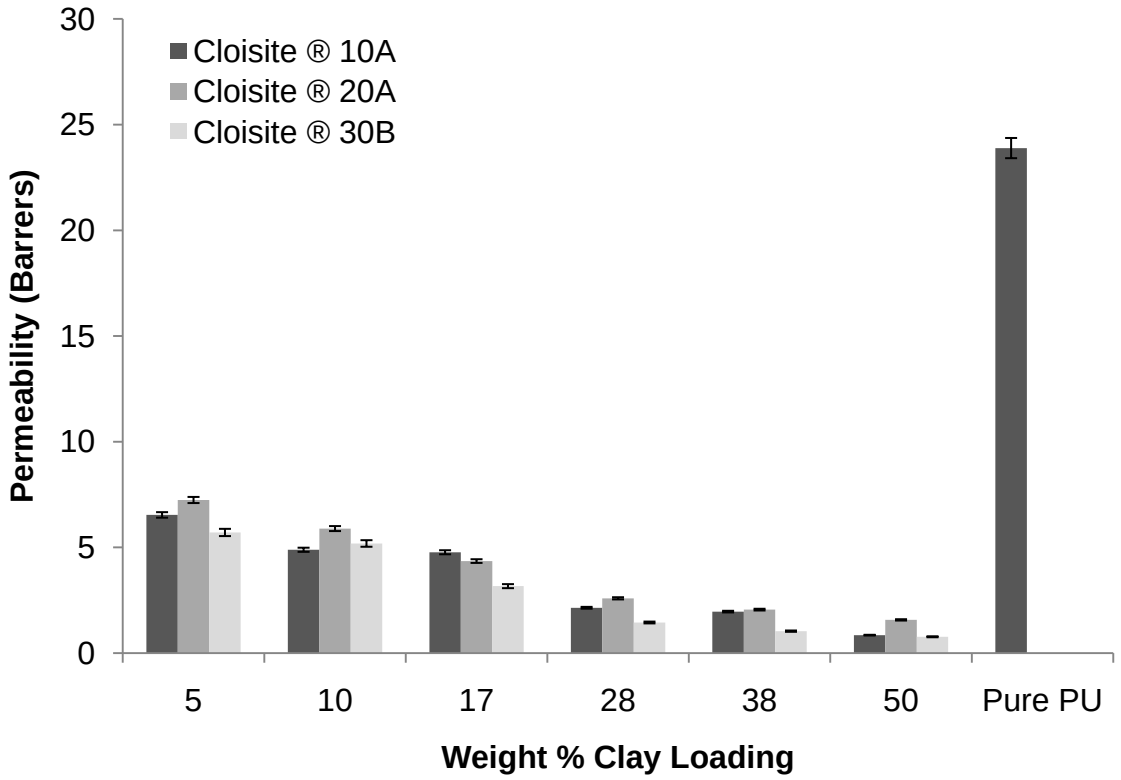

Figure 3.12 Comparison of He permeation in cancomposites fabricated by sonicating the clays of all Cloisite ® series samples.

3.5.3.3 Permeation Model

Numerous models have been proposed to predict the effective permeability through nanocomposite membranes [6, 41-44]. Nielsen's model [45], introduced the basic concept of tortuosity factor to predict the effective permeability as a function of the volume fraction for clay/polymer systems. This model is based on the idea the aligned impermeable flakes, acting as barriers increase the tortuosity of the diffusion path and decrease gas permeation through the polymer membrane. Lan et al. [46], used Nielsen's equation in order to calculate the aspect ratio of polyimide/clay nanocomposites.

Nielsen's equation can be modified using Cussler's [41] definitions of aspect ratio α, and volume fraction ϕ, thus rendering equation 3.1:

$$\frac{P}{P_0} = \frac{1-\phi}{1+\left(\frac{\alpha}{2}\right)\phi} \qquad \text{Eq. 3.1}$$

where, P and P_0 are the permeability of the composite film and that of the pristine polymer, respectively, ϕ is the volume fraction of the filler and α is the aspect ratio, defined as the ratio of the width-to-thickness of the impermeable flakes. The volume fraction of the flakes in the polymer matrix can be calculated using the equation 3.2 proposed by Chen et al. [47]:

$$\phi = \frac{1}{1+\frac{\rho_C(1-M_C)}{\rho_P M_C}} \qquad \text{Eq. 3.2}$$

where ϕ, is the volume fraction, ρ_C and ρ_p are the density of the nanoclay and the polymer, and M_c is the mass fraction. A calculated aspect ratio was obtained by fitting the permeation data obtained experimentally to Nielsen's model as seen in Figures 3.13 through 3.15. This theoretical model explains the consistent decrease in steady-state permeability with increasing nanoclay concentration. The trend is seen in all the nanocomposite membranes. The fitted aspect ratio for all the clay series falls somewhere between 10 and 40, which is much lower than the estimated aspect ratio reported in previous studies on montmorillonite clay particles [46, 48-50], and lower than the aspect ratio seen in the TEM micrographs, which appear to be greater than 100.

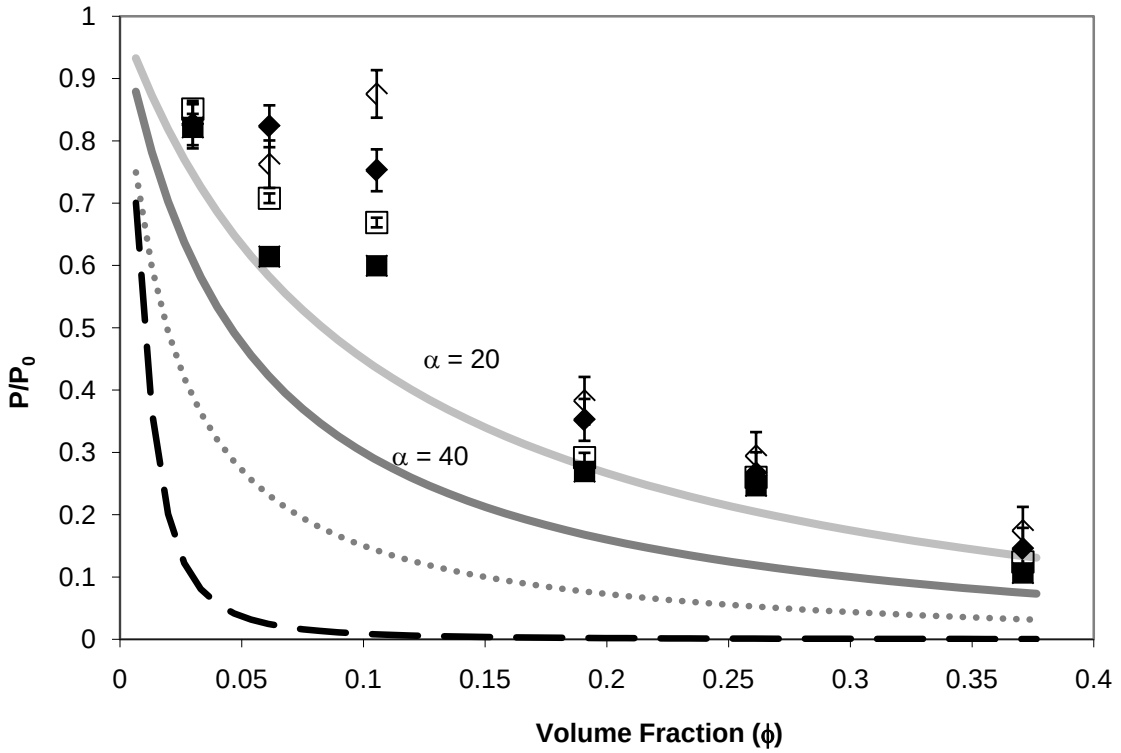

Figure 3.13 He and O_2 permeability in nanocomposites C10A prepared by sonication and stirring, ♦ He Stirred Samples, ◊ O_2 Stirred Samples, ■ He Sonicated Samples, □ O_2 Sonicated Samples ****** Nielsen α = 100, ----- Cussler α = 100.

In addition to Nielsen's model, the data for the polyurethane/clay nanocomposites was fitted to Cussler's model [41-44]. This model is a mathematical model for gaseous diffusion in polymer membranes containing impermeable flakes, based on the idealization of geometries that include pores, slits and random shaped flakes. The equation 3.3, derived by Cussler is:

$$\frac{P_0}{P} = 1 + \frac{\alpha^2 \phi^2}{1 - \phi} \qquad \text{Eq. 3.3}$$

When the experimental permeabilities of the clay nanocomposites were fitted to Cussler's model, the calculated aspect ratio was not within the observed range of lengths corresponding to montmorillonite platelets, and provided ever smaller values (<1) than Nielsen's model. Although none of the theoretical curves predicted by Nielsen's model exactly fit the experimental data, there is nevertheless, a clear trend when comparing the three different nanocomposite clay series. In the C30B series, Figure 3.14 indicates that sonication provides the highest increase in the calculated aspect ratio, when fitted by the Nielsen's equation. For example, sonicated C30B clay nanocomposites demonstrated an increase of 54 % in calculated aspect ratio for O_2 as well as 40% increase for He, at the highest concentration of clay 50% wt. when compared to plain stirred samples. The C30B sonicated series provided an average increase in aspect ratio for all the gases of 67% due to sonication, which is superior to the 34% of the C10A series and the 49% of the C20A series. Nanocomposites employing the C20A clays demonstrated the lowest calculated aspect ratio of the three clay series, as seen in Figure 3.15. This can be attributed to the low dispersion of the C20A nanoclay platelets, as well as low expansion and/or exfoliation of the silicate platelets [51].

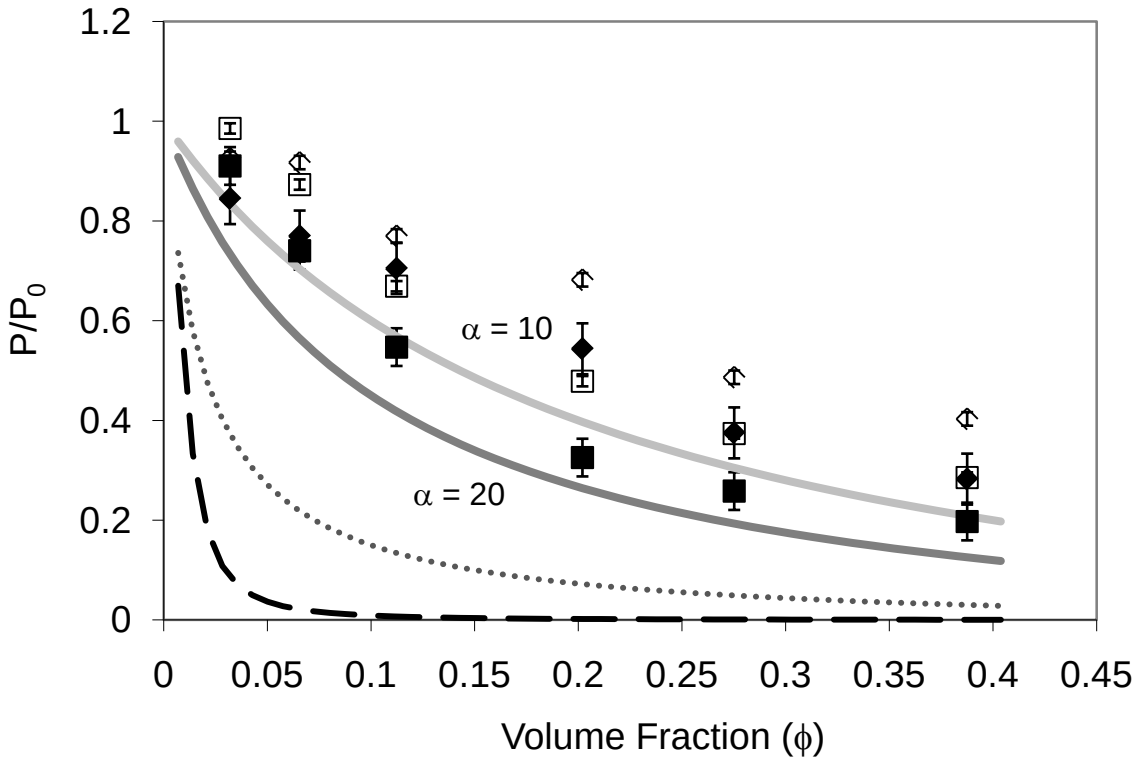

Figure 3.14 He and O_2 permeability in nanocomposites C20A prepared by sonication and stirring♦ He Stirred Samples, ◊ O_2 Stirred Samples, ■ He Sonicated Samples, □ O_2 Sonicated Samples, ****** Nielsen $\alpha = 100$, ----- Cussler $\alpha = 100$.

In general, clay structures in the sonicated nanocomposites provided much more tortuous diffusion pathways for the penetrating molecule then those in stirred nanocomposites. These results suggest that while the aspect ratio is an important variable in the design of barrier materials, the actual dispersion of the clay layers is critical if the clay is to act as a barrier. Because the phenomenological models employed in the permeation analysis implicitly considered the flakes to be perfectly randomly dispersed, the data fit was poor and the calculated aspect ratios were too small. These models may indeed be valid at low concentrations, but fail at high clay loadings.

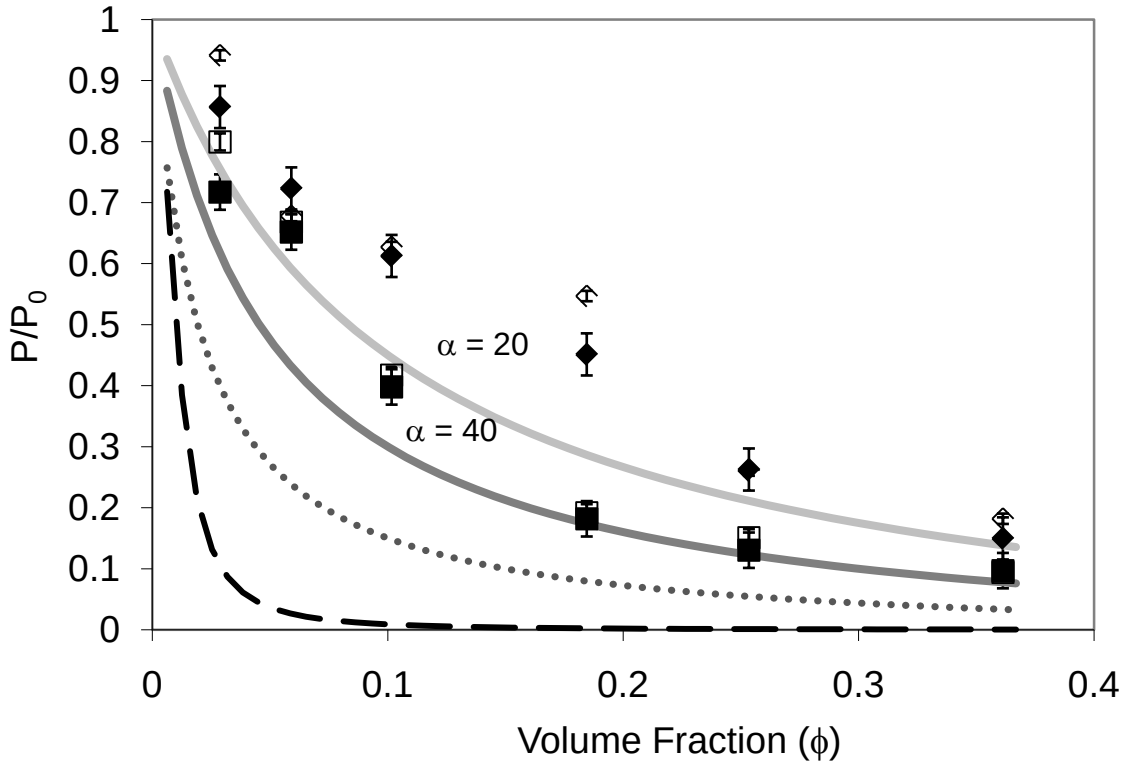

Figure 3.15 He and O_2 permeability in nanocomposites C30B prepared by sonication and stirring♦ He Stirred Samples, ◊ O_2 Stirred Samples, ■ He Sonicated Samples, □ O_2 Sonicated Samples, ****** Nielsen $\alpha = 100$, ----- Cussler $\alpha = 100$.

3.6 Conclusions

Polyurethane/clay nanocomposite films were evaluated as potential barrier membranes to gas permeation. The montmorrilonite clay was intercalated with different alkylammonium ion surfactants before being introduced into the polymer matrix. The XRD results suggest that the polymer achieved a better penetration within the gallery space of the montmorillonite nanoclays when these species were modified with alkylammonium groups with only one tallow group (C10A and C30B). Indexing of the

d_{001}, indicated that sonication does not alter the physical structure of the silica platelets, nor does it produce a completely exfoliated matrix.

On the other hand, permeation was highly sensitive to the pre-processing method. Membranes with sonicated particles in the polymer matrix had significantly lower permeation than membranes with stirred clay particles. This improvement in barrier properties was attributed to a better dispersion of the sonicated clays in the polymer matrix. Analysis of the permeation data with barrier models, which implicitly consider the flakes to be perfectly randomly dispersed, led to a poor fit and calculated aspect ratios that were too small.

References

1. Beyer, G., *Nanocomposites: a new class of flame retardants for polymers.* Plastics, Additives and Compounding, 2002. **4**(10): p. 22-28.
2. Zheng, X. and C.A. Wilkie, *Flame retardancy of polystyrene nanocomposites based on an oligomeric organically-modified clay containing phosphate.* Polymer Degradation and Stability, 2003. **81**(3): p. 539-550.
3. Chavarria, F. and D.R. Paul, *Morphology and properties of thermoplastic polyurethane nanocomposites: Effect of organoclay structure.* Polymer, 2006. **47**(22): p. 7760-7773.
4. Wang, Z. and T.J. Pinnavaia, *Nanolayer Reinforcement of Elastomeric Polyurethane.* Chemistry of Materials, 1998. **10**(12): p. 3769-3771.
5. Jeong, H.K., et al., *Fabrication of Polymer/Selective-Flake Nanocomposite Membranes and Their Use in Gas Separation.* Chemistry of Materials, 2004. **16**(20): p. 3838-3845.
6. Xu, B., et al., *Calculating barrier properties of polymer/clay nanocomposites: Effects of clay layers.* Polymer, 2006. **47**(8): p. 2904-2910.
7. Zhong, Y., et al., *Mechanical and oxygen barrier properties of organoclay-polyethylene nanocomposite films.* Polymer Engineering & Science, 2007. **47**(7): p. 1101 - 1107.
8. Ogasawara, T., et al., *Helium gas permeability of montmorillonite/epoxy nanocomposites.* Composites Part A: Applied Science and Manufacturing, 2006. **37**(12): p. 2236-2240.

9. Yoon, P.J., T.D. Fornes, and D.R. Paul, *Thermal expansion behavior of nylon 6 nanocomposites.* Polymer, 2002. **43**(25): p. 6727-6741.
10. Ray, S.S., K. Okamoto, and M. Okamoto, *Structure-Property Relationship in Biodegradable Poly(butylene succinate)/Layered Silicate Nanocomposites.* Macromolecules, 2003. **36**(7): p. 2355-2367.
11. Ray, S.S., et al., *Polylactide-Layered Silicate Nanocomposite: A Novel Biodegradable Material.* Nano Letters, 2002. **2**(10): p. 1093-1096.
12. Usuki, A., et al., *Synthesis of nylon 6-clay hybrid.* Journal of Materials Research, 1993. **8**(5): p. 1179-1184.
13. Kojima, Y., et al., *Sorption of water in nylon 6-clay hybrid.* Journal of Applied Polymer Science, 1993. **49**(7): p. 1259-1264.
14. Kojima, Y., et al., *Gas permeabilities in rubber-clay hybrid.* Journal of Materials Science Letters, 1993. **12**(12): p. 889-890.
15. Kim, J.K., et al., *Moisture barrier characteristics of organoclay-epoxy nanocomposites.* Composites Science and Technology, 2005. **65**(5): p. 805-813.
16. Gao, F., *Clay/polymer composites: the story.* Materials Today, 2004. **7**(11): p. 50-55.
17. Ryu, J.G., H. Kim, and J.W. Lee, *Characteristics of polystyrene/polyethylene/clay nanocomposites prepared by ultrasound-assisted mixing process.* Polymer Engineering & Science, 2004. **44**(7): p. 1198-1204.
18. Osman, M.A., et al., *Polyurethane Adhesive Nanocomposites as Gas Permeation Barrier.* Macromolecules, 2003. **36**(26): p. 9851-9858.
19. Xia, H., S.J. Shaw, and M. Song, *Relationship between mechanical properties and exfoliation degree of clay in polyurethane nanocomposites.* Polymer International, 2005. **54**(10): p. 1392 - 1400.
20. Madhavan, K. and B.S.R. Reddy, *Poly(dimethylsiloxane-urethane) membranes: Effect of hard segment in urethane on gas transport properties.* Journal of Membrane Science, 2006. **283**(1-2): p. 357-365.
21. Gomes, D., et al., *Gas transport properties of segmented poly(ether siloxane urethane urea) membranes.* Journal of Membrane Science, 2006. **281**(1-2): p. 747-753.
22. Chen-Yang, Y.W., et al., *Thermal and anticorrosive properties of polyurethane/clay nanocomposites.* Journal of Polymer Research, 2004. **11**: p. 275-283.
23. Sreedhar, B., D.K. Chattopadhyay, and V. Swapna, *Thermal and surface characterization of polyurethane-urea clay nanocomposites coatings.* Journal of Applied Polymer Science, 2006. **100**(3): p. 2393-2401.
24. Yuan, H., et al., *Using fugacity to predict volatile emissions from layered materials with a clay/polymer diffusion barrier.* Atmospheric Environment, 2007. **41**(40): p. 9300-9308.
25. *Diffusion in Polymers*, ed. J. Crank and G.S. Park. 1968, New York: Academic Press. 452.
26. Tjong, S.C. and Y.Z. Meng, *Impact-modified polypropylene/vermiculite nanocomposites.* Journal of Polymer Science, Part B: Polymer Physics, 2003. **41**(19): p. 2332-2341.

27. Tanaka, G. and L.A. Goettler, *Predicting the binding energy for nylon 6,6/clay nanocomposites by molecular modeling.* Polymer, 2002. **42**(2): p. 541-553.
28. Fornes, T.D., et al., *Effect of organoclay structure on nylon 6 nanocomposite morphology and properties.* Polymer, 2002. **43**(22): p. 5915-5933.
29. Fornes, T.D., P.J. Yoon, and D.R. Paul, *Polymer matrix degradation and color formation in melt processed nylon 6/clay nanocomposites.* Polymer, 2004. **44**(24): p. 7545-7556.
30. Tjong, S.C., *Structural and mechanical properties of polymer nanocomposites.* Materials Science and Engineering: R: Reports, 2006. **53**(3-4): p. 73-197.
31. Finnigan, B., et al., *Morphology and properties of thermoplastic polyurethane nanocomposites incorporating hydrophilic layered silicates.* Polymer, 2004. **45**(7): p. 2249-2260.
32. Gorrasi, G., M. Tortora, and V. Vittoria, *Synthesis and physical properties of layered silicates/polyurethane nanocomposites.* Journal of Polymer Science, Part B: Polymer Physics, 2005. **43**(18): p. 2454-2467.
33. Jin, J., et al., *An analysis on the enhancement of the fatigue durability of polyurethane by incorporating organoclay nanofillers.* Molecular Materials and Engineering, 2006. **291**(11): p. 1414-1421.
34. Lu, H. and S. Nutt, *Restricited relaxation in polymer nanocomposites near the glass transition.* Macromolecules, 2003. **36**(11): p. 4010-1016.
35. Zhang, X., et al., *The synthesis and characterization of polyurethane/clay nanocomposites.* Polymer International, 2003. **52**(5): p. 790-794.
36. Mondal, S. and J.L. Hu, *Structural characterization and mass transfer properties of nonporous segmented polyurethane membrane: Influence of hydrophilic and carboxylic group.* Journal of Membrane Science, 2006. **274**(1-2): p. 219-226.
37. Finnigan, B., et al., *Effect of the average soft-segment length on the morphology and properties of segmented polyurethane nanocomposites.* Journal of Applied Polymer Science, 2006. **102**(1): p. 128-139.
38. James Korley, L.T., et al., *Preferential assotiation of the segment blacks in polyurethane nanocomposites.* Macromolecules, 2006. **39**(20): p. 7030-7036.
39. Jin, J., et al., *A study on viscoelasticity of polyurethane-organoclay nanocomposites.* Journal of Applied Polymer Science, 2006. **99**(6): p. 3677-3683.
40. Choi, S., K.M. Lee, and C.D. Han, *Effects of Triblock Copolymer Architecture and the Degree of Functionalization on the Organoclay Dispersion and Rheology of Nanocomposites* Macromolecules, 2004. **37**(20): p. 7649 -7662.
41. Cussler, E.L., et al., *Barrier Membranes.* Journal of Membrane Science, 1988. **38**(2): p. 275-288.
42. Falla, W.R., M. Mulski, and E.L. Cussler, *Estimating diffusion through flake-filler membranes.* Journal of Membrane Science, 1996. **119**(1): p. 129-138.
43. Lape, N.K., E.E. Nuxoll, and E.L. Cussler, *Polydisperse flakes in barrier films.* Journal of Membrane Science, 2004. **236**(1-2): p. 29-37.
44. Yang, C., W.H. Smyrl, and E.L. Cussler, *Flake alignment in composite coatings.* Journal of Membrane Science, 2004. **231**(1-2): p. 1-12.
45. Nielsen, L.E., *Models for the permeability of filler polymer systems.* Journal of Macromolecular Science Chemistry, 1967. **A1**: p. 929-942.

46. Lan, T., P.D. Kaviratna, and T.J. Pinnavaia, *On the nature of polyamide-clay hybrid composites.* Chemistry of Materials, 1994. **6**(5): p. 573-575.
47. Chen, B. and J.R.G. Evans, *Nominal and effective volume fraction in polymer-clay nanocomposites.* Macromolecules, 2006. **39**(5): p. 1790-1796.
48. Lu, C. and Y.W. Mai, *Influence of aspect ratio on barrier properties of polymer-clay nanocomposites.* Physical Review Letters, 2005. **95**: p. 0883031-0883034.
49. Yano, K., et al., *Synthesis and properties of polyimide-clay hybrid.* Journal of Polymer Science Part A: Polymer Chemistry, 1993. **31**(10): p. 2493-2498.
50. Bharadwaj, R.K., et al., *Structure–property relationships in cross-linked polyester–clay nanocomposites.* Polymer, 2002. **43**(13): p. 3699-3705.
51. Bharadwaj, R.K., *Modeling the barrier properties of polymer-layered silicate nanocomposites.* Macromolecules, 2001. **34**(26): p. 9189-9192.

Chapter 4 Polymer/clay nanocomposites as VOC Barrier Materials and Coatings

4.1 Abstract

Polyurethane/clay nanocomposites barrier membranes were fabricated by two processing methods involving stirring and sonication of the clay particles. The concentration of Cloisite ® 30B in the nanocomposite was varied from 0 to 50 wt%. Characterization of membrane transport properties was achieved via a gravimetric sorption method. Material-phase diffusivity coefficients (D) decreased with increasing Cloisite ® concentration, while changes in the material/VOC partition coefficients (K) depended on the molecular interactions of the VOCs with the membrane material.

4.2 Introduction

New building materials such as structural insulating panels or SIPS have helped revolutionize the construction industry, providing improved durability, quality, high energy efficiency and affordability of housing. SIPS also make good environmental sense limiting job site waste, reducing landfill use and helping to preserve old-growth forests by using fast-growth farmed trees [1]. However SIP's ratio of cost/advantages may present certain drawbacks in other areas. Due to the manufacturing process, two outer layers and the inner core of the SIP's may contain volatile organic compounds, VOCs, such as pentene, toluene, formaldehyde, hexanal and styrene [1, 2]. New houses utilizing SIPs have odor thresholds for hexanal and other aldehydes that often exceed safe limits and may remain elevated for months after construction [2, 3]. The presence of VOCs in

indoor air and the combined effect of tight envelope buildings prevents proper ventilation, thus, leading to degradation of indoor air quality [4]. Polymer/clay nanocomposites have been known to improve gas barrier properties [5-8], mechanical [9, 10] and thermal properties [11], biodegradability [12, 13], and enhance flame retardancy [14, 15]. The addition of clay nanocomposites to pristine polymers has helped improve physical properties of polymers, as was seen by the Toyota group [16-18]. We propose that the addition of clay particles to SIPs, particularly near the surface, can help reduce VOC emissions. In order to enhance these overall properties and generate improved gas barriers, dispersion and/or exfoliation of the individual silicate platelets must be achieved within the polymer matrix. Proper selection of the polymer/clay matrix is also necessary to improve the synergy between the species. The objective of this study is to develop and test nanocomposite barrier materials that substantially reduce volatile emissions to indoor air. This is achieved by evaluating the transport properties of polyurethane/clay nanocomposite membranes as a function of clay content.

4.3 Materials

Decane, toluene and butanol were purchased from Sigma Aldrich and were used as received. The thermoplastic polyurethane used in this study was polyether-based TPU Estane® 58315 supplied by Estane®, unit of Noveon Inc. The commercially available nanoclays were purchased from Southern Clay Products. Cloisite ® 30B was used as the nanoclay for this study. This nanoclay was modified via ion-exchange with a quaternary ammomium salt that contains two hydroxyethyl groups, a methyl group and tallow group. According to the manufacturer the average concentration of the tallow (T) is as follows:

~65% C18; ~30% C16: ~5% C14, where the number following C refers to the number of carbon atoms in the tallow group. The fabrication of the barrier membranes can be found in a previous publication [19]. High resolution dynamic microbalance, 0.1-0.5 μg, model D200-02 Cahn equipped with a PC-based data acquisition system was used to measure and record changes in polyurethane/clay nanocomposite sample weight during sorption/desorption cycles. Temperature within the microbalance enclosure was maintained at 25.7 ± 0.3 °C using a Fisher Scientific Isotemp model 1038D temperature circulator connected to a heat exchanger in the enclosure. Temperature within the sample chamber was monitored with an Omega RTD model 2Pt100G3050, temperature transducer. For sorption testing, VOC's were supplied to the microbalance at constant temperature with a diffusion cell VICI Metrometrics, Inc, Dynacalibrator Model 190. Air flow rate was controlled with mass flow controllers Tylan-General MFC model FC-280S. Rectangular shaped barrier membranes of 3.81 cm x 2.54 cm were initially dried in a vacuum oven at 100 °C for 24 hours before being used in the microbalance. Calculation procedures of diffusivity coefficient, and partition coefficient can be found elsewhere [20].

4.4 Results and Discussion

4.4.1 Diffusivity Coefficient

The method for calculating diffusion coefficient D, of a liquid in a membrane was based on Fickian diffusion in a slab [21]. Figures 4.1 and 4.2 depict the experimental data as well as the predicted model profile obtained from Crank's [21] time-dependent equation seen in equation 4.1.

$$\frac{M_t}{M_\infty} = 1 - \frac{8}{\pi^2}\sum_{n=0}^{n=\infty}\frac{1}{(2n-1)^2}\,exp\left\{\frac{-D(2n-1)^2\pi^2 t}{l^2}\right\} \qquad \text{Eq.4.1}$$

The profile seen in Figure 4.1 shows the sorption-desorption cycle for a barrier membrane containing 50 wt% of Cloisite ® 30B. Figure 4.2 shows the approximation of Crank's equation to the experimental data and suggests that increasing the clay content within the polymer matrix will increase the sorption equilibrium time.

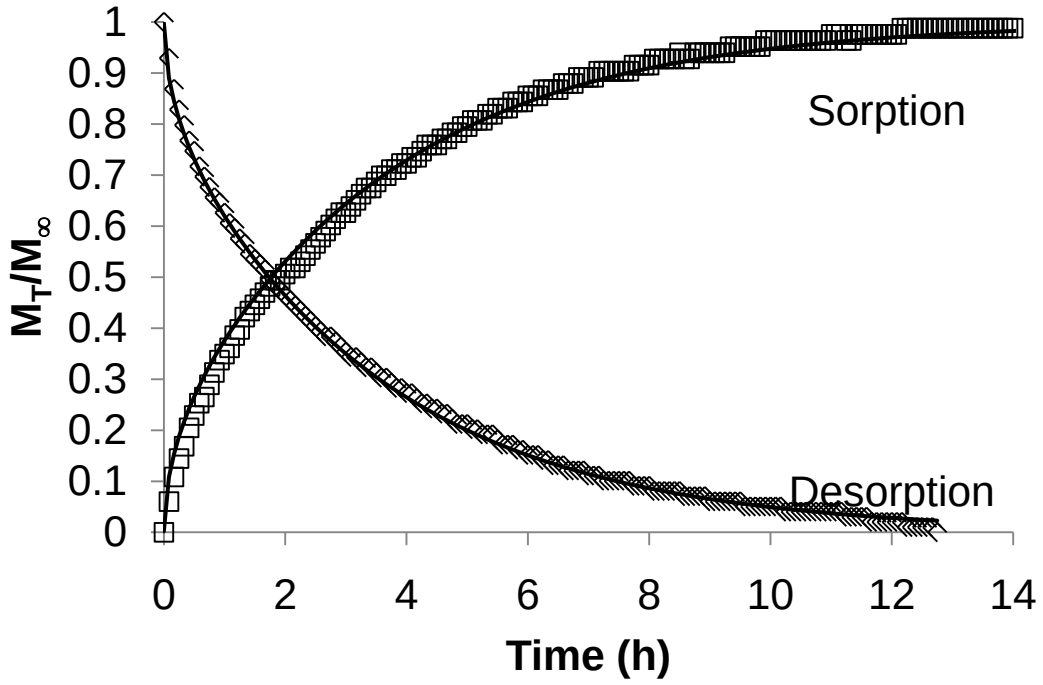

Figure 4.1 1. Fitting of toluene transient sorption/desorption data to diffusion model of sonicated 50% wt Cloisite 30B. (◊) Desorption, (□) Sorption data, ─ Model

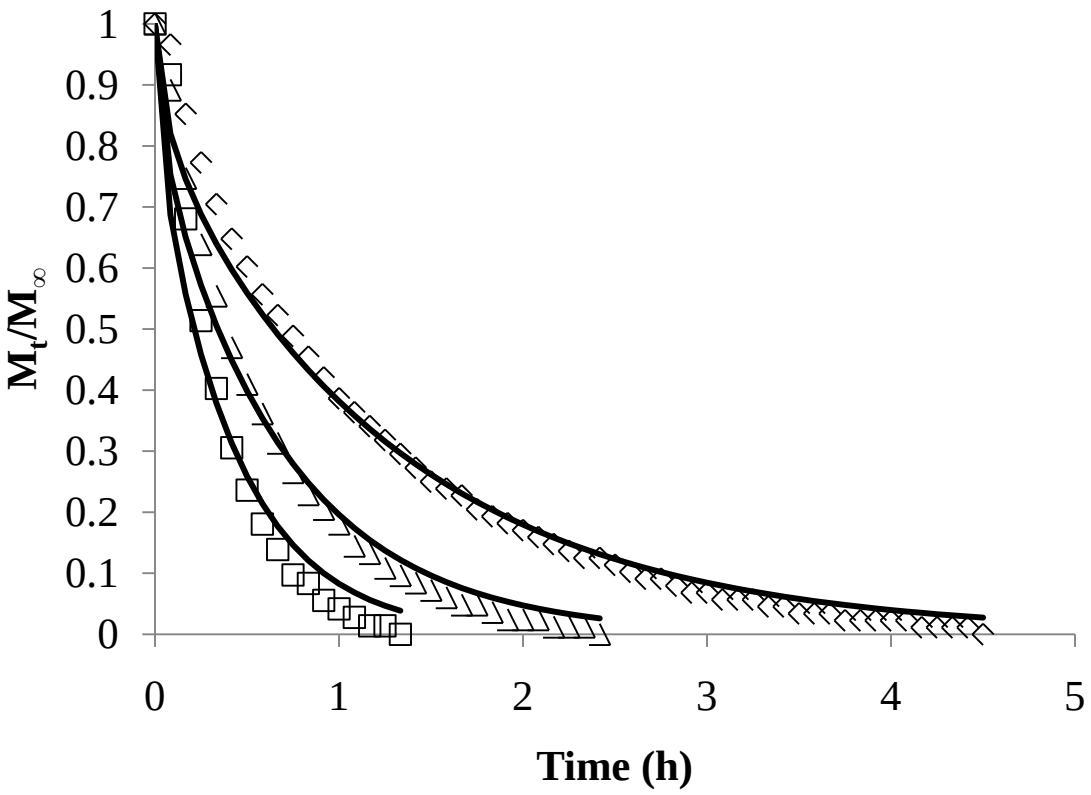

Figure 4.2. Transient mass loss of (□) 17% wt Cloisite 30B, (Δ)29% wt Cloisite 30B, (◊)38% wt Cloisite 30B, ─ Model, of polyurethane/clay nanocomposite during desorption of toluene.

Due to the symmetry of the profiles the data suggests that the sorption-desorption process for all the VOC's is reversible and that D is independent of concentration. The diffusivity, D, for the VOC's in the nanocomposites as a function of clay content and processing conditions are summarized in Table 4.1. N-decane demonstrates the lowest diffusivity coefficient at all clay concentrations analyzed, while toluene has the highest value of D. This is consistent with the work of Ghosal and Freeman et al. [22], who demonstrate that the diffusion coefficients tend to increase with decreasing size of the penetrant VOC molecule.

Table 4.1. Values of diffusivity coefficient (D) for different wt% of Cloisite ® 30B series sorption.

Diffusivity Coefficient (m^2/s)						
wt % Clay	Toluene		Decane		Butanol	
	Stirred	Sonicated	Stirred	Sonicated	Stirred	Sonicated
0	7.2 E-13	7.2 E-13	4.7 E-13	4.7 E-13	5.2 E-13	5.2 E-13
10	6.1 E-13	5.6 E-13	4.4 E-13	4.3 E-13	4.9 E-13	3.8 E-13
17	4.9 E-13	4.6 E-13	4.2 E-13	3.2 E-13	3.2 E-13	2.1 E-13
29	3.7 E-13	3.6 E-13	3.1 E-13	2.4 E-13	2.4 E-13	1.1 E-13
38	3.5 E-13	2.5 E-13	2.5 E-13	2.0 E-13	2.0 E-13	9.7 E-14
50	1.9 E-13	9.2 E-14	1.4 E-13	1.5 E-13	1.1 E-13	6.3 E-14

Table 4.1 also shows that increasing the nanoclay content within the polymer matrix leads to a decrease in the diffusivity for all the VOC's. Barrier membranes containing up to 50% wt. of nanoclay demonstrate a decrease in diffusivity coefficient of 87% for toluene, and butanol compared to the neat polymer. The nature of this progressive decrease can be seen in Figure 4.3 in the case of toluene. The decline in the diffusivity is also relatively high for decane, which had a maximum decrease of 70% at 50 wt% concentration of Cloisite ® 30B in the polyurethane compared to the neat polymer. The overall decrease in the diffusivity coefficient for the VOCs in nanocomposite films with increasing clay content may be attributed to enhanced tortuosity of the diffusion path in the matrix [23-25]. There also may be the possibility of enhanced restricted segmental motion of the polymer chains within the clay gallery space and at the interface with the clay layers [26, 27].

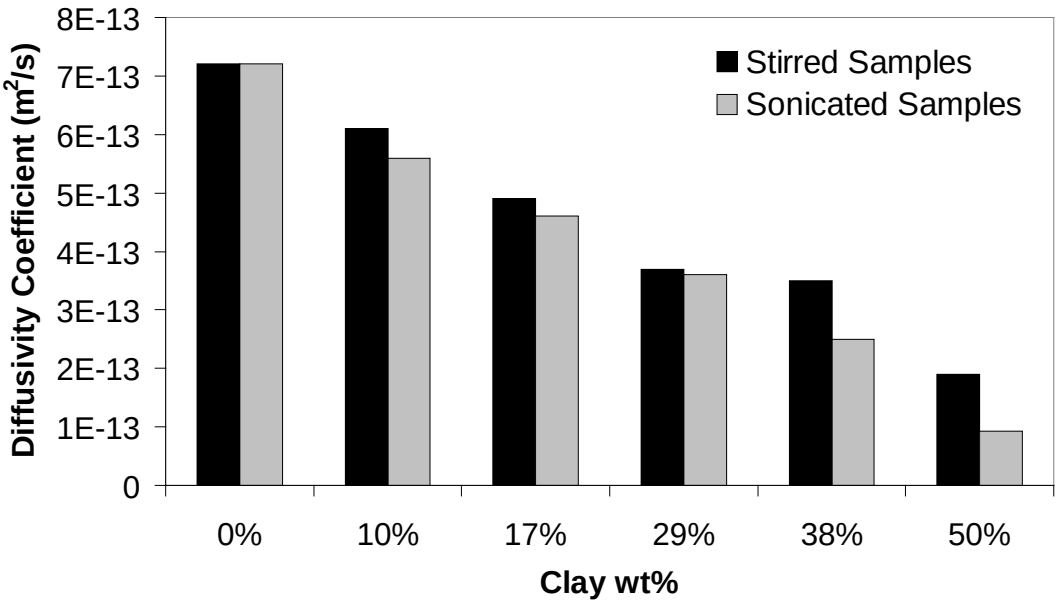

Figure 4.3. Comparison of Toluene diffusivity coefficient in nanocomposites, Sonication vs Stirring Cloisite ® 30B.

The processing effect of sonication is also demonstrated in Figure 4.3 and also in Table 4.1. The data suggests that sonication leads to a greater decrease in diffusivity coefficient when compared to samples only treated with stirring. This result may reflect a higher dispersion of clay layers achieved by sonication. This effect would further support the claim that the use of nanoclays in the polymer matrix generates more tortuous pathways for the penetrating VOC molecules [23-25].

4.4.2 Partition Coefficient

The sorption equilibrium, described by the partition coefficient, K, was obtained for toluene, decane and butanol as a function of clay content in the nanocomposites. This data is shown in Table 4.2. Toluene has the lowest K value in the series, while butanol has the highest. The partition coefficient for toluene decreases with increasing clay content, with the highest concentration of clay at 50 wt% decreasing the partition coefficient by 20% compared to the pristine polymer film.

Table 2. Values of partition coefficient (K) for different wt% of Cloisite ® 30B series sorption.

Partition Coefficient (K)						
wt % Clay	Toluene		Decane		Butanol	
	Stirred	Sonicated	Stirred	Sonicated	Stirred	Sonicated
0	1808	1808	3871	3871	4358	4358
10	1781	1712	4331	4727	4450	4022
17	1748	1687	4747	4271	4180	4106
29	1571	1602	4570	4314	4607	4160
38	1493	1550	4901	4014	4309	4218
50	1268	1460	4832	5137	3921	4127

By contrast, the partition coefficient of decane increases with clay content, while that of butanol does not show any clear trends. Furthermore, the effect of processing, i.e. sonication vs. stirring does not influence the partition coefficient to a significant degree. These results can be attributed to differences in molecular interactions between the VOCs and the polymer matrix [28]. Chemical and surface modifications were made to the clay in order to improve the synergy of the natural montmorillonite with different polymers. The Na^+ group attached to the natural montmorillonite was substituted via ion exchange

with an alkyl ammonium group, which renders a more hydrophobic surface and improves compatibility with the polyether based polyurethane. For example, the inverse relationship between the wt% of the clay in the matrix and the sorption values for toluene suggests that there is a repulsive interaction of toluene with the clay surface. As documented in Table 4.3, toluene is slightly polar, while the modified nanoclay surface is non-polar, thus prompting a decrease in K with increasing clay content. The opposite trend is seen with n-decane, whose K values increase with increasing clay concentration in the matrix. This suggests that there is an affinity between non-polar n-decane and the hydrogenated tallow tail of the alkyl ammonium group present on the nanoclay surface. As documented in Table 4.3, 1-butanol is highly polar and hence one would expect repulsive interactions between 1-butanol and the non-polar alkyl ammonium group. However, the data can more likely be explained by competing repulsive and attractive interactions, the latter arising from the interaction of the non-polar butane component with the alkyl group on the clay surface. In summary, the value of the partition coefficient is dominated by thermodynamic interactions and not by the morphology of the nanocomposite. This also helps explain why pre-manufacturing conditions, such as sonication, do not affect the value of K.

Table 4.3 Solubility parameters of the VOCs used in this study. The units of δ are $(MPa)^{1/2}$ [29]. The molar volume is expressed in cm^3/mol, and density g/ml.

VOC	δ_d Dispersion	δ_p Polarity	δ_h Hydrogen Bonding	δ_s Solvent	Molar Volume	Density
Toluene	18.0	1.4	2.0	18.1	106.8	0.86
1-Butanol	16.0	5.7	15.8	15.7	91.5	0.81
n-Decane	15.7	0	0	23.2	195.9	0.73

4.4.3. Nanocomposites/Solvent Interaction Parameter

To better understand the polymer-VOC interaction, we have used the sorption data to calculate the Flory-Huggins interaction parameter, χ, of the system [28, 29]. This parameter estimates the interaction energy between the penetrant VOC species and the polymer segments [30]. The interaction parameter can be calculated from Equation 4.2:

$$\ln a = \ln \phi + (1 - \phi) + x(1 - \phi)^2 \qquad \text{Eq. 4.2}$$

Where *a* is the activity of the penetrant vapor phase, ϕ the penetrant volume fraction and χ the polymer-penetrant interaction parameter. The activity coefficient for all the VOCs was determined from the experimental conditions by the ratio of the VOC partial pressure and the saturation vapor pressure. For the purpose of this study the specific activity of the organic vapor was maintained constant at P = 1 atm. The volume fraction of the penetrant VOC target molecule was determined with Equation 4.3:

$$\phi = \frac{C\left(\frac{V_1}{22{,}414}\right)}{1 + C\left(\frac{V_1}{22{,}414}\right)} \qquad \text{Eq. 4.3}$$

Where V is the molar volume of the penetrant VOC and C is the measured concentration of the penetrant in the polymer (ratio of cm^3 of penetrant sorbed per cm^3 of polymer) at P = 1 atm. As can be seen in Figure 4.4, with increasing clay concentration the interaction parameter of n-decane decreases, from 2.5 for the pristine polyurethane to 2.27 in samples having the highest clay concentration of 50 wt%.

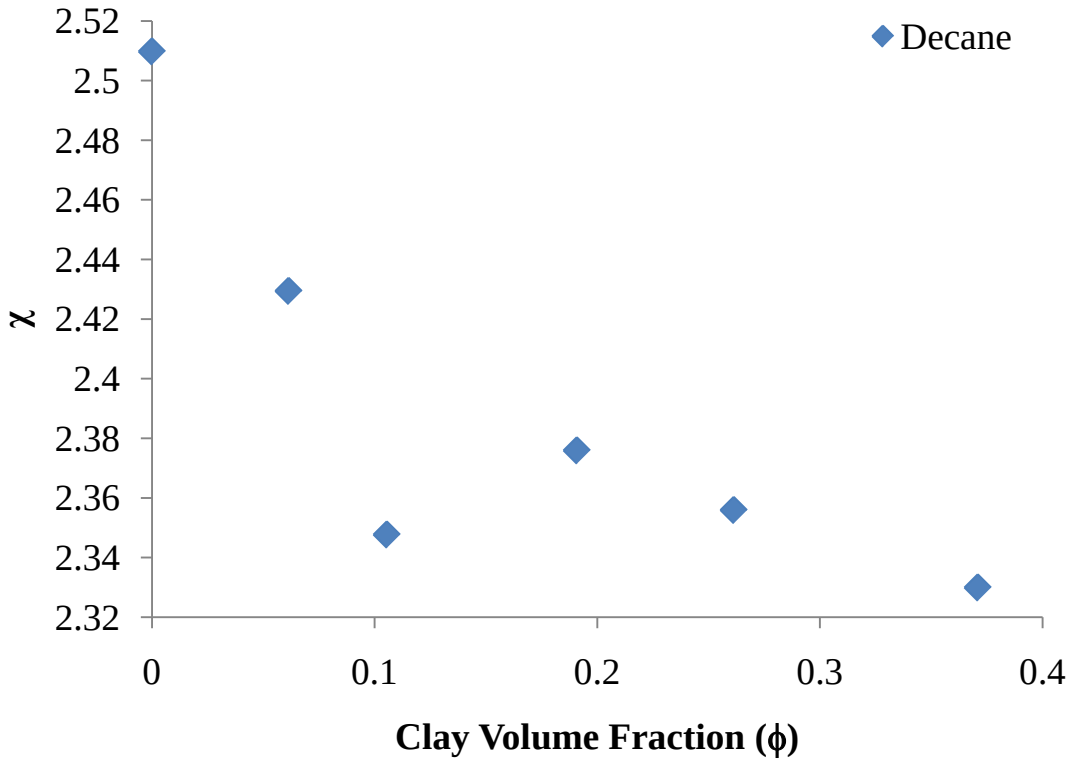

Figure 4.4 Polymer/clay-VOC interaction parameter at different clay volume fraction for decane at 25 °C.

Table 4.4 summarizes the χ interaction parameters for toluene, n-decane and 1-butanol as a function of the wt% clay in the nancomposite. In the case of toluene, the interaction parameter, χ, is negative, suggesting high solubility in the neat polymer matrix. However, the miscibility of toluene in the system decreases with the addition of

clay particles modified with a hydrophobic surfactant. The opposite trend is seen with n-decane, whose interaction parameter decreases with wt% clay, reflecting more favorable molecular interactions. Finally, the χ for 1-butanol does not follow a distinct trend.

Table 4.4 Experimental interaction parameter χ, for sonicated polyurethane/clay nancomposite sonicated series

Wt % Clay	$\chi_{n\text{-decane}}$	$\chi_{toluene}$	$\chi_{1\text{-butanol}}$
0	2.51	-0.59	0.032
10	2.36	-0.54	0.112
17	2.46	-0.52	0.092
29	2.45	-0.48	0.079
38	2.52	-0.44	0.065
50	2.28	-0.38	0.087

These experimental results can be compared with theoretical χ values calculated from Equation 4 [28, 29].

$$\chi = \beta + \frac{V_1(\delta_1 - \delta_2)^2}{RT} \qquad \text{Eq. 4.4}$$

Where β is a constant equal to 0.34, V_1 is the molar volume of the penetrant, δ_1 and δ_2 are the solubility parameters of the penetrant and the polymer respectively. In order to calculate the χ interaction parameter of the membranes, the solubility coefficient δ for the polyurethane Estane ® 58315 must first be determined. Different research groups evaluated this parameter via swelling measurements [31-34]. Within these groups Kim et al. [31], determined the solubility coefficient δ for a polyether based polyurethane network based on Gee's theory [35]. This theory states that in order to attain a good solubility of the polymer in the solvent, the square of the difference between the

solubility parameters of the polymer and the solvent must be kept to a minimum. Gee's theory is represented by Equation 4.5.

$$\frac{Q}{Q_{max}} = exp^{[-\alpha Q(\delta_1-\delta_2)^2]} \quad \text{Eq. 4.5}$$

Where Q is the swelling ratio, Q_{max} is the maximum swelling ratio, α is a constant and δ_1 and δ_2 are the solubility parameters of the solvent and the polymer. The swelling ratio Q, of the polyurethane/clay nanocomposite membranes was determined by utilizing Equation 4.6.

$$Q = 1 + \left(\frac{w_2}{w_1} - 1\right)\left(\frac{\rho_2}{\rho_1}\right) \quad \text{Eq. 4.6}$$

Where w_2 is the weight of the network at equilibrium, w_1 is the weight of the network before swelling, ρ_2 and ρ_1 are the density of the network and the density of the solvent respectively [36]. In our case the density of the polyurethane is ρ_p=1.12 g/cm^3, the density of Cloisite ® 30B is ρ_c = 1.98 and the density of the solvents are listed in Table 4.3. After the swelling ratio Q, is determined for each VOC, the Q values are plotted versus the solubility parameter δ of the corresponding VOCs. The maxium swelling Q_{max}, observed for this series was seen with n-butanol. Once Q_{max} of the system is established and the swelling ratio Q for each VOC is also established, the solubility parameter of the polyurethane Estane ® 58315 can be determined. Gee's Equation 4.4 can be rearranged as follows:

$$\left[\frac{1}{Q} ln\left(\frac{Q_{max}}{Q}\right)\right]^{0.5} = |\alpha^{0.5}(\delta_1 - \delta_2)| \quad \text{Eq 4.7}$$

The unknown parameters of the system α and δ_2, were determined by plotting the $[(1/Q)\ln(Q_{max}/Q)]^{0.5}$ vs the solubility parameters δ of the VOCs. The linearization of the

data via the plotting scheme yields the parameter, $\alpha^{0.5}$, and the solubility parameter of the polyurethane, δ_2, as the slope and the intercept in the horizontal axis, respectively. The value for the calculated solubility parameter of the pure Estane ® 58315 is 23.6 $(MPA)^{1/2}$, which is consistent with typical values reported for polyurethanes [37, 38].

Previous studies of the nanoclays determined that the silica-alumina structure has a hydrophilic nature and the addition of the alkyl ammine group via ion exchange provides a hydrophobic property to the clay. In order determine the solubility parameter of the modified clay surface, Jang et al. [39], modeled the entire clay structure based on the longest chain of the surfactant. According to the manufacturer, Southern Clay Products, Cloisite 30B longest group is a hydrogenated tallow group. Thus it can be simplified by considering a linear aliphatic chain. This aliphatic chain adds a third component to the polymer-sorbent system. This additional term yields a modification in the corresponding solubility parameter of the polymer, δ_2 term of equation 4.3. This new solubility parameter is modeled via equation 4.8, as follows:

$$\bar{\delta} = \sum_i \phi_i \delta_i = \phi_1 \delta_1 + \phi_2 \delta_2 \qquad \text{Eq. 4.8}$$

Where ϕ_1 and ϕ_2, are the volume fraction of the nanoclay and of the polymer in the composite membrane. The use of equation 4.7, results in the modification of equation 4.3 as follows:

$$\chi = \beta + \frac{V_1(\delta_1 - \bar{\delta})^2}{RT} \qquad \text{Eq.4.9}$$

The results for the calculated χ interaction parameter of the sonicated polyurethane/clay nanocomposite membranes can be seen in Table 4.5. These values are similar and within the observed range found in the literature [40]. These calculated results suggest that the presence of nanoclay in the matrix leads to an increase in the miscibility of the polymer/clay composite when exposed to n-decane and toluene and a decrease in miscibility when exposed to 1-butanol. The decrease of the interaction parameter χ suggests that the surfactant aliphatic chain has a similar solubility parameter as n-decane. This is consistent with the χ interaction parameters obtained by experimental means shown in Table 4.4. However, experimental χ interaction parameters for toluene and 1-butanol do not follow the calculated trends. Clearly, using a mean-field model, such as equation 4.3, may be too simplistic in modeling the χ interaction parameter of polar molecules, such as 1-butanol or toluene, which have specific (directional) interactions.

Table 4.5 Calculated χ interaction parameters for pristine polyurethane Estane ® 58315, and the subsequent polyurethane/clay nancomposite sonicated series.

Wt % Clay	$\chi_{\text{n-decane}}$	χ_{toluene}	$\chi_{\text{1-butanol}}$
0	3.06	1.45	0.36
10	2.78	1.28	0.34
17	2.58	1.17	0.35
29	2.22	0.97	0.40
38	1.95	0.83	0.49
50	1.56	0.64	0.71

4.5 Conclusions

Polyurethane/clay nanocomposites used as barrier membranes provide a noticeable decrease in VOC diffusivity. However, when compared to the neat polymer this decrease becomes important only at high clay content in the nano-composite. Processing methods of the barrier membranes do, in fact, influence the diffusivity, rendering better barrier properties when the clays are dispersed with sonication. Material/VOC partition coefficients, depend on the molecular interactions of the VOC with the membrane material. Thus, χ for non-polar VOC such as n-decane decreased with increasing clay concentration of organically modified clay in the matrix, due to favorable thermodynamic interactions. On the other hand, although the interaction parameter for toluene in the nano-composite is negative, suggesting high solubility in the polymer matrix, the addition of clay particles modified with hydrophobic alkyl groups increased the value of χ with wt% clay.

References

1. Morley, M., *Building with structural insulated panels (SIPs) strength and energy efficiency through structural panel construction*. 2000, Newtown, CT: Taunton Press.
2. Hodgson, A.T., D. Beal, and J.E.R. McIlvaine, *Sources of formaldehyde, other aldehydes and terpenes in a new manufactured house.* Indoor Air, 2000. **12**(4): p. 235–242.
3. Hodgson, A.T., et al., *Volatile Organic Compound Concentrations and Emission Rates in New Manufactured and Site-Built Houses.* Indoor Air, 2000. **10**(3): p. 178-192.
4. Liddament, M.W., *A review of ventilation and the quality of ventilation air*. Indoor Air, 2000. **10**(3): p. 193-199.
5. Jeong, H.K., et al., *Fabrication of Polymer/Selective-Flake Nanocomposite Membranes and Their Use in Gas Separation.* Chemistry of Materials, 2004. **16**(20): p. 3838-3845.
6. Xu, B., et al., *Calculating barrier properties of polymer/clay nanocomposites: Effects of clay layers.* Polymer, 2006. **47**(8): p. 2904-2910.

7. Zhong, Y., et al., *Mechanical and oxygen barrier properties of organoclay-polyethylene nanocomposite films.* Polymer Engineering & Science, 2007. **47**(7): p. 1101 - 1107.
8. Gain, O., et al., *Gas Barrier Properties of Poly(ε-caprolactone)/Clay Nanocomposites: Influence of the Morphology and Polymer/Clay Interactions.* Journal of Polymer Science Part B: Polymer Physics, 2004. **43**(2): p. 205-214.
9. Chavarria, F. and D.R. Paul, *Morphology and properties of thermoplastic polyurethane nanocomposites: Effect of organoclay structure.* Polymer, 2006. **47**(22): p. 7760-7773.
10. Wang, Z. and T.J. Pinnavaia, *Nanolayer Reinforcement of Elastomeric Polyurethane.* Chemistry of Materials, 1998. **10**(12): p. 3769-3771.
11. Yoon, P.J., T.D. Fornes, and D.R. Paul, *Thermal expansion behavior of nylon 6 nanocomposites.* Polymer, 2002. **43**(25): p. 6727-6741.
12. Ray, S.S., K. Okamoto, and M. Okamoto, *Structure-Property Relationship in Biodegradable Poly(butylene succinate)/Layered Silicate Nanocomposites.* Macromolecules, 2003. **36**(7): p. 2355-2367.
13. Ray, S.S., et al., *Polylactide-Layered Silicate Nanocomposite: A Novel Biodegradable Material.* Nano Letters, 2002. **2**(10): p. 1093-1096.
14. Beyer, G., *Nanocomposites: a new class of flame retardants for polymers.* Plastics, Additives and Compounding, 2002. **4**(10): p. 22-28.
15. Zheng, X. and C.A. Wilkie, *Flame retardancy of polystyrene nanocomposites based on an oligomeric organically-modified clay containing phosphate.* Polymer Degradation and Stability, 2003. **81**(3): p. 539-550.
16. Kojima, Y., et al., *Gas permeabilities in rubber-clay hybrid.* Journal of Materials Science Letters, 1993. **12**(12): p. 889-890.
17. Kojima, Y., et al., *Sorption of water in nylon 6-clay hybrid.* Journal of Applied Polymer Science, 1993. **49**(7): p. 1259-1264.
18. Usuki, A., et al., *Synthesis of nylon 6-clay hybrid.* Journal of Materials Research, 1993. **8**(5): p. 1179-1184.
19. Herrera-Alonso, J.M., et al., *Transport properties in polyurethane/clay nanocomposites as barrier materials: Effect of processing conditions.* Journal of Membrane Science, 2009. **doi:10.1016/j.memsci.2009.03.045**.
20. Cox, S.S., D. Zhao, and J.C. Little, *Measuring partition and diffusion coefficients for volatile organic compounds in vinyl flooring.* Atmospheric Environment, 2001. **35**(22): p. 3823-3830.
21. Crank, J., *The Mathematics of Diffusion*. Oxford Science Publications. 1979, New York: Oxford University Press.
22. Ghosal, K. and B.D. Freeman, *Gas separation using polymer membranes: An overview.* Polymers for Advanced Technologies, 1994. **5**(11): p. 673-697.
23. Eitzman, D.M., R.R. Melkote, and E.L. Cussler, *Barrier membranes with tipped impermeable flakes.* AIChE Journal, 1996. **42**(1): p. 2-9.
24. Nielsen, L.E., *Models for the permeability of filler polymer systems.* Journal of Macromolecular Science Chemistry, 1967. **A1**: p. 929-942.
25. Perry, D., W.J. Ward, and E.L. Cussler, *Unsteady diffusion in barrier membranes.* Journal of Membrane Science, 1989. **44**(2-3): p. 305-311.

26. Finnigan, B., et al., *Effect of the average soft-segment length on the morphology and properties of segmented polyurethane nanocomposites.* Journal of Applied Polymer Science, 2006. **102**(1): p. 128-139.
27. Mondal, S. and J.L. Hu, *Structural characterization and mass transfer properties of nonporous segmented polyurethane membrane: Influence of hydrophilic and carboxylic group.* Journal of Membrane Science, 2006. **274**(1-2): p. 219-226.
28. Prausnitz, J.M., R.N. Lichtenthaler, and E. Gomes de Azevedo, *Molecular Thermodynamics of Fluid-Phase Equilibria*. 3rd ed. 1999, Upper Saddle River, New Jersey: Prentice Hall PTR.
29. Hansen, C.M., *Hansen solubility parameters: a user's handbook*. 2nd ed, ed. C.M. Hansen. 2007, Boca Raton, FL: CRC Press.
30. Merkel, T.C., et al., *Gas sorption, diffusion, and permeation in poly(dimethylsiloxane).* Journal of Polymer Science: Part B: Polymer Physics, 2000. **38**(3): p. 415-434.
31. Kim, C.K., et al., *Structure-property relationships of hydroxy-terminated polyether based polyurethane network.* Polymer Bulletin, 2008. **61**: p. 225-233.
32. Roşu, D., C. Ciobanu, and C.N. Caşcaval, *Synthesis and properties of graft copolymer derived from polyurethane and dihydroxylate of bisphenol A.* Journal of Applied Polymer Science, 2001. **80**: p. 1802-1813.
33. Ajithkumar, S., N.K. Patel, and S.S. Kansara, *Sorption and diffusion of organic solvents through interpenetrating polymer networks (IPNs) based on polyurethane and unsaturated polyester.* European Polymer Journal, 2000. **36**: p. 2387-2393.
34. Gopakumar, S. and M.R. Gopinathan Nair, *Determination of molecular parameters of NR/PU block copolymers by transport studies.* European Polymer Journal, 2005. **41**: p. 2002-2009.
35. Gee, G., *Interaction between rubber and liquids. IV. Factors governing the absorption of oil by rubber.* Transactions, Institution of the Rubber Industry, 1943. **18**: p. 266-281.
36. Rabek, J.F., *Experimental Methods in Polymer Chemistry*. 1980, New York: John Wiley & Sons, Inc.
37. Ebdon, J.R., D.J. Hourston, and P.G. Klein, *Polyurethane-polysiloxane interpenetrating polymer networks: 1. A polyether urethanepoly(dimethylsiloxane) system.* Polymer, 1984. **25**: p. 1633-1639.
38. Mieczkowski, R., *Solubility parameter components of some polyurethanes.* European Polymer Journal, 1992. **28**(1): p. 53-55.
39. Jang, B.N., D. Wang, and C.A. Wilkie, *Relationship between the solubility parameter of polymers and the clay dispersion in the polymer/clay nanocomposites and the role of the surfactant.* Macromolecules, 2005. **38**(15): p. 6533-6543.
40. Wolińska-Grabczyk, A., *Transport of liquid hydrocarbons in the polyurethane-based membranes.* Journal of Membrane Science, 2007. **302**(1-2): p. 59-69.

Chapter 5 Gas Barrier Properties of Nanocomposites Based on *In situ* Polymerized Poly(n-butyl methacrylate) in the Presence of Surface Modified Montmorillonite

5.1 Abstract

Barrier membranes of poly(*n*-butylacrylate) were produced by the *in-situ* polymerization of *n*-butylacrylate in the presence of surface modified natural montmorillonite. This two-stage process allowed control over the extent of intercalation, ultimately leading to exfoliated nanostructures. The first stage of the process consisted of the organic modification of montmorillonite *via* ion-exchange reactions with (acryloyloxy) ethyl alkylammonium cations. This process anchored chemically-reactive species on the surface of natural clay and improved the mixing between the clay and the monomer. The second stage of the process comprised of the *in-situ* polymerization of *n*-butyl methacrylate and the unsaturated acryloxy ethyl groups anchored on the surface of the clay. Resulting membranes were characterized in terms of their microstructure and diffraction (XRD), their thermal properties (TGA and DSC), and gas-permeation properties. The resulting exfoliated morphology led to a decrease in gas permeability. Phenomenological models of gas barrier properties such as those of Cussler and Nielsen were used to determine the approach to ideal clay dispersions.

5.2 Introduction

Over the past two decades polymer/clay nanocomposites have drawn increasing interest due to the significant improvement of optical [1], mechanical [2, 3], flame

resistant [4-7], and barrier properties [8-10] in comparison to the corresponding pristine polymers. Polymer/clay nanocomposites are usually obtained via three mayor processes, which include melt intercalation, solution blending and in-situ polymerization [11, 12]. The subsequent morphology of the nanocomposites depends on the molecular interactions between the polymer and clay particles. The three possible morphologies for these nanocomposites include immiscible, intercalated and exfoliated structures [11, 13]. In the immiscible phase, also known as phase separated morphology, the polymer does not penetrate in between the clay platelets. Intercalation is attained when polymer chains penetrate within the gallery space and induce expansion of the clay platelets. Exfoliation is characterized by a random distribution of the clay platelets due to extensive penetration of the polymer chains, resulting in the delamination of the clay platelets and the loss of the crystalline structure of the clay. Montmorillonite (MMT) clays, which pertain to the smectite family, are of special interest due to their high surface area and high aspect ratio [14, 15]. These two parameters are known to influence the barrier properties of the barrier membranes [16-18]. MMT crystal composition consists of two tetrahedrally coordinated sheets of silicon fused to an edge shared octahedral sheet of aluminum. This tetrahedral-octahedral-tetrahedral (TOT) conformation of MMT generates a stacking of platelets perpendicular to the direction of the sheets. The stacking of the TOT sheets leads to regular van der Waals gaps between the layers. The layered silicates have a negative charge due to the heterovalent substitution which resides in the octahedral layer [19]. The charge deficiency extends throughout the whole lattice, forcing the counter ions to distribute within the interior of the crystal. The counter ions, which are usually alkali and alkaline earth metals, such as Na^{+}, Li^{+} or Ca^{2+}, reside between the sheets, minimizing the

overall electrostatic energy. The cations in the interlayer occupy the basal spacing of the silicate sheets, whose distance is determined by the nature of the cation as well as the degree of hydration. Natural clays, such as MMT, may be organically modified to render the silicate sheets more organophilic and compatible with the penetrating polymer [20, 21]. Alkylphosphonium and alkylammonium cations are commonly used for this purpose to modify the surface of the clays [11, 22]. These surface modifiers decrease the surface energy [23] of the silicate platelets, and increase the basal spacing between the layers [24, 25]. According to Bergaya and Lagaly [26], the preferred method for synthesis of organically modified clays is via ion exchange reactions. Some surfactants added to the silicate platelets can also react with monomers and initialize polymerization reactions [27]. The reacting surfactant group anchored on the silicate surface may improve the dispersion of the silicate platelets in the polymer matrix, eventually leading to improved gas barrier properties and mechanical properties [28, 29]. This work focuses on the synthesis of intercalated/exfoliated poly (n-butylmethacrylate)/clay nanocomposites via in-situ polymerization. Furthermore it examines the effect of the processing method prior to surface modification of the silicate platelets on the mechanical, thermal and gas barrier properties of the nanocomposites.

5.3 Materials and Methods

Sodium montmorillonite, Cloisite ® Na^+ was purchased from Southern Clay Inc, and dried for 24 hours before use. 2,2'-azobisisobutyronitrile free radical initiator was purchased from Sigma-Aldrich and was purified in methanol and recrystalized. [2-(Acryloyloxy)ethyl]-trimethylammonium chloride, was purchased from Sigma-Aldrich

and used as received. Butyl methacrylate was purchased from Sigma-Aldrich and distilled at reduced pressure before use. 1-Methyl-2-pyrrolidinone was purchased from Sigma-Aldrich and used as received. Anhydrous chloroform, was purchased from Sigma-Aldrich and used as received

5.4 Preparation of Modified Clays

5.4.1 Clay Modification Method A (Stirring)

5g of Cloisite ® Na^+ was added to 330ml of deionized water and left to stir overnight. After the stirring the solution was heated in a water bath to 80°C and left for 1 hour. The solution was then cooled to room temperature. An excess of [2-(Acryloyloxy)ethyl]-trimethylammonium chloride was added to the solution and stirred vigorously overnight. The resulting suspension was filtered and the solids were washed with deionized water to remove the unreacted quaternary salt. After the solution was filtered, the solid was stored at 4 °C for two days. In order to remove all the quaternary salt, 200ml of deionized water was added to the clay and stirred vigorously for 8hr. The solution was filtered, and the resulting clay slurry was stored at 4 °C.

5.4.2 Clay Modification Method B (Sonication)

5g of Cloisite ® Na^+ was added to 330ml of deionized water, and set for 6 hours. The solution was then placed in a sonication bath for 1 hour and left to stir overnight. The solution was then heated in a water bath to 80°C, let sit for 1 hour, sonicated for 1 hour at 80°C, and then cooled to room temperature. An excess of [2-(Acryloyloxy)ethyl]-trimethylammonium chloride was added to the cooled solution and stirred vigorously

overnight. The resulting suspension was filtered and the solids were washed with deionized water to remove the unreacted quaternary salt. After the solution was filtered, the solid was stored at 4 °C for two days. In order to remove all the quaternary salt, 200ml of deionized water was added to the clay and stirred vigorously for 8hr. The solution was filtered, and the resulting clay slurry was stored at 4 °C.

5.4.3 Synthesis and fabrication of pristine poly(n-butyl methacrylate) and poly(n-butyl methacrylate)/clay composites membranes.

In-situ polymerization reaction of poly(n-butyl methacrylate)/clay composites was carried out with different amounts of modified nanoclay. Clay content in the membranes varied from 0 to 5 wt%. The nomenclature of the poly(n-butyl methacrylate)/clay composites membranes with different clay contents, as used in this study is summarized in Table 1. 10 g of 1-Methyl-2-pyrrolidinone (NMP) and the specific clay amount were placed in a glass vial and stirred for 2 hours at 25°C until the mixture became homogenous. After the stirring process, 5 g of monomer butyl methacrylate, and 0.0577g of AIBN were added to the vial and stirred vigorously for 15 min at 25°C. The final mixture was flushed with N_2 for 15 min and thermally sealed. Once sealed, the vial was placed in an oil bath at 65°C for 24 hours, with vigorous stirring. After the 24 hour reaction time, the polymer was precipitated in 100 ml ethanol and vigorously stirred for 4 hours. The white precipate was later filtered and left at room temperature for 24 hrs to dry. After the drying, the polymer was dissolved in chloroform for 2 hrs. 100ml of ethanol was again added to the solution to precipitate the polymer. This procedure insured the removal of unreacted monomer from the solution. The polymer was filtered,

dried at room temperature for 24 hrs, and dried under vacuum at 60°C for an additional 24 hours. 0.518 g of the dried composite was dissolved in 5 ml of chloroform and stirred vigorously for 8 hours. Once the solution was homogenous, it was cast on Teflon plates and the solvent was allowed to evaporate slowly at room temperature for 24hrs. The controlled drying process reduced the presence of pinholes in the membrane and prevented curling the membranes. After 24 hours the membrane was placed under vacuum at 60°C for 24 hours, to insure the removal of all the solvent.

Table 1. Nomenclature for sonicated and stirred polymer/clay nanocomposites used for this publication.

Clay Content wt %	Stirred	Sonicated
0	PBMA	
1	PBMA-1	SPBMA-1
3	PBMA-3	SPBMA-3
5	PBMA-5	SPBMA-5

5.5 Characterization

Gas permeabilities in the pure polymer, stirred poly(n-butyl methacrylate)/clay and sonicated poly(n-butyl methacrylate)/clay membranes were measured in a constant volume-variable pressure system [30]. The membranes were placed in a stainless steel cell with chambers of known volume on each side. The upstream side of the membrane was pressurized to 4 atm at 25 °C with the penetrating gas species. The downstream side was initially evacuated to $P < 0.001$ atm. The variation in downstream pressure was monitored in real time and was analyzed only after steady state is achieved. All gases employed (He, O_2, N_2, CO_2 and CH_4) were ultra-high purity gases (minimum purity

99.999%) and were obtained from Airgas, Inc. Permeation of each gas through every barrier membrane was carried out 3 times in order to establish a statistically consistent result. Some nanocomposites systems where tested for permeability using more than one sample to confirm the reproducibility of the data. Permeability is reported in the units of barrer (1 barrer = $1*10^{-10}$ (cm^3(STP)*cm)/(cm^2*sec*cmHg)) with 2% error. X-Ray diffractometry, XRD, was used to determine the interspacial distance within the clay platelets. The system used was a Sintag XDS 2000 powder diffractometer using Ni filtered Cu KαX-ray radiation (λ=1.54Å) at voltage of 45KV, 40mA current, and filament current of 3.30A. The scanning rate for the low angle samples was done at 0.25°/min over a range of 2θ = 1-10°. The XRD measurements were conducted on the membrane samples, while the clay was analyzed in the powder form. Dynamic mechanical thermal analysis (DMTA) was performed on a Rheometric Scientific DMTA IV with a ramp rate of 2°C/min and a frequency of 1 Hz. Thermogravimetric Analysis (TGA) was performed on a TA Instruments Thermogravimetric analyzer model Q5000 IR. Measurements were carried out under a nitrogen flow. The analysis was done from room temperature to 600°C, with a heating rate of 10°C/min. Dynamic Scanning Calorimetry (DSC) measurements were carried out in a TA Instruments Differential Scanning Calorimeter Q2000, from -20°C to 150°C, with a heating rate of 10°C/min.

5.6 Results and Discussion

5.6.1 XRD Characterization

The XRD diffractograms for powder Cloisite Na^+, and organically modified Cloisite Na^+ processed via sonication and stirring can be seen in Figure 1. Bragg's equation, $2d \sin\theta = n\lambda$, was used to calculate the basal spacing of the modified clay as well as of the pristine clay. The characteristic d_{001} diffraction peak for Cloisite Na^+ in the 2θ region is located at 7.5°, d_{001} = 1.15 nm. The modification of the clays with (acryloyloxy) ethyl alkyl ammonium shifts the d_{001} peak to lower values in the 2θ region, rendering sonicated clay's d_{001} = 1.43nm, and stirred clay's d_{001} = 1.42 nm. This shift suggests an increase in the basal spacing of the silicate platelets. The increase of the basal spacing is due to the penetration and grafting of the quaternary salt via ion exchange to the clay platelets. The indexing of the d_{001} peak in the diffractograms of both sonicated and stirred modified clays also suggests that the morphology of the clays is intercalated.

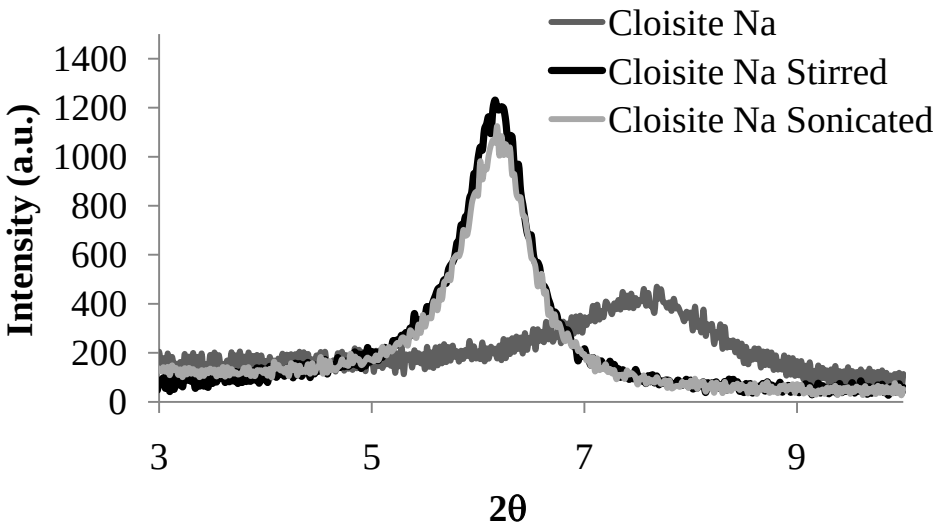

Figure 5.1 XRD Diffractograms of pristine Cloisite ® Na^+, and surface modified Cloisite ® Na^+ via sonication and stirring.

The XRD diffractogram for SPBMA-3 nanocomposite membrane can be seen in Figure 2. The d_{001} peak for the SPBMA-3 could not be indexed. This peak was also non-existant in the XRD diffractograms of all other nanocomposite membranes in the two series. This suggests that all of the polymer/clay nanocomposites have an exfoliated morphology. The expansion and further exfoliation of the montmorillonite clay can be represented by schemes 1 and 2 respectively, shown in Figure 3.

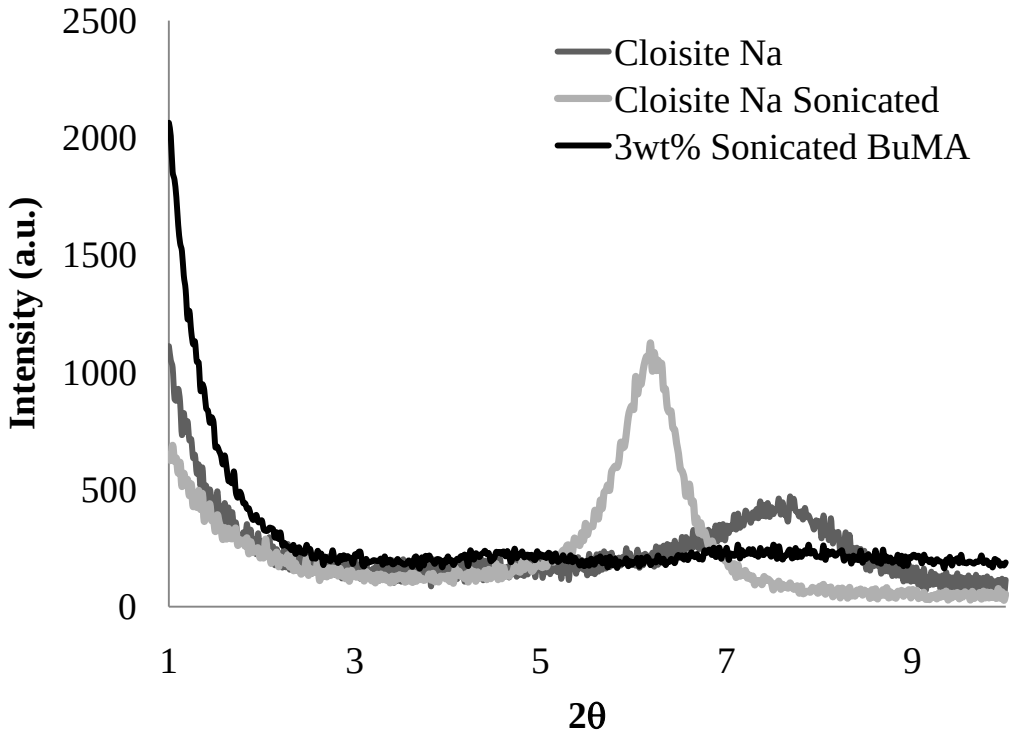

Figure 5.2 XRD Diffractograms of pristine Cloisite ® Na^+, surface modified Cloisite ® Na^+ via sonication and polymer/clay nanocomposite membrane SPBMA-3.

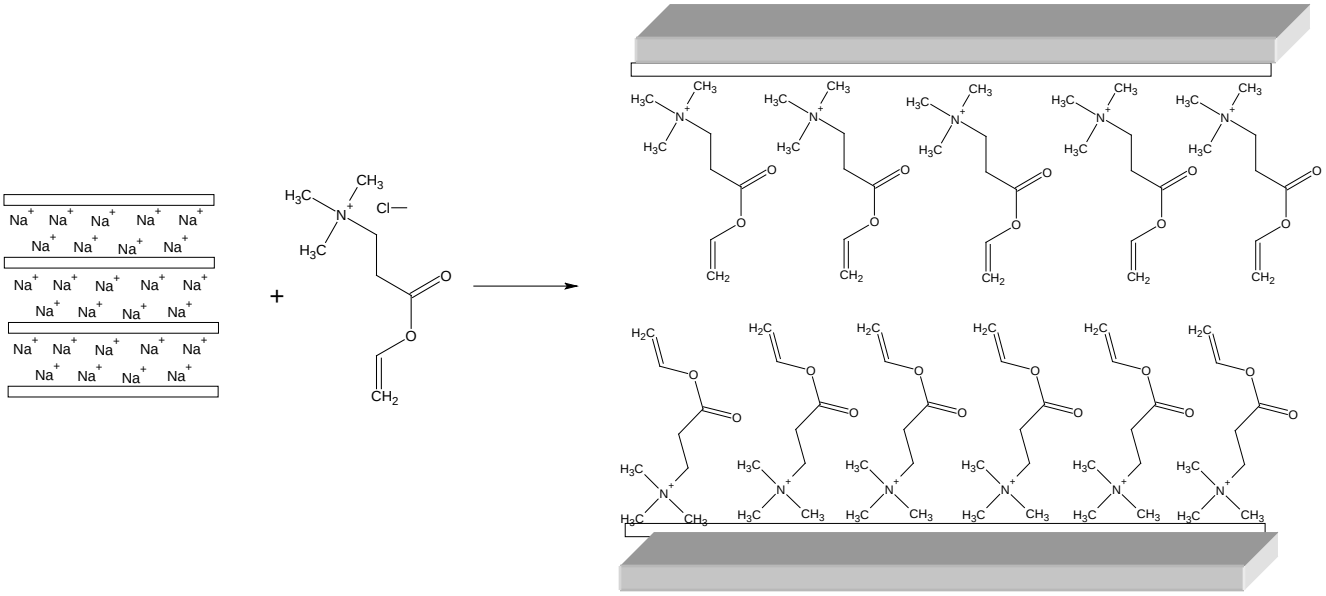

Figure 5.3 Schematic representation of surface modification of Cloisite ® Na+ via ion exchange.

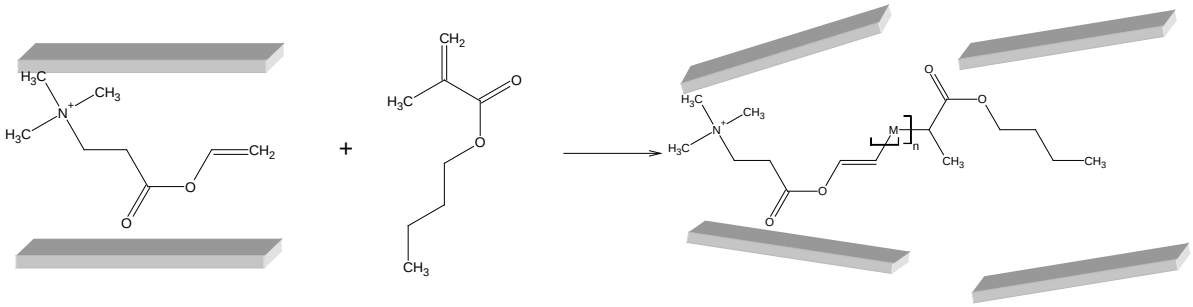

Figure 5.4 Schematic representation of *in situ* polymerization of poly(n-butyl methacrylate) with montmorillonite clay platelets as seed surface.

5.6.2. Size Exclusion Chromatography (SEC) Characterization

In order to obtain the molecular weight of the polymer, the polymer and clay in the nanocomposite were separated via centrifugation. The polymer/clay nanocomposite was dissolved in 10 ml of chloroform and centrifuged at 1500 rpm for 4h. After 4 hours the remaining solution was separated from the clay particles deposited in the bottom of the centrifuge tubes. The separated liquid or serum was placed in the centrifuge for another 4 h. After the solution was centrifuged the remaining liquid was cast on a Teflon pan and the chloroform was allowed to evaporate. This procedure insured the evaluation of the molecular weight of the isolated polymer without interference from the clay particles. All of the membranes analyzed in this study had a SEC elution patters characteristic of a monomodal distribution. The clay processing method affected the resulting molecular weight, M_n and M_w, of the poly (n-butyl methacrylate) as demonstrated in Table 2. Samples prepared with modified sonicated clays had a higher molecular weight than samples prepared via plain stirring. The higher molecular weight suggests an increase in penetration of the monomer within the basal spacing of the modified clay and an improved accessibility of the monomer to the surface reacting site.

Table 2. M_n and M_w values determined via SEC of polymer/clay composites membranes.

Composite	M_w	M_n	Polydispersity Index (M_w/M_n)
PBMA	141000	98800	1.43
PBMA-1	161000	99300	1.62
PBMA-3	170000	104000	1.64
PBMA-5	330000	179000	1.82
SPBMA-1	169000	104000	1.62
SPBMA-3	214000	116000	1.84
SPBMA-5	582000	353000	1.65

5.6.3 Differential Scanning Calorimetry (DSC)

Differential Scanning Calorimetry (DSC) was used to determine the glass transition temperature, T_g, of PBMA and polymer/clay nanocomposites barrier membranes. The glass transition temperature of the pristine PBMA, and the different composites membrane series, SPBMA-X and PBMA-X are summarized in Table 3. The polymer/clay nanocomposite membranes have a higher T_g than that of the pristine PBMA. This may be due to the increased restricted segmental chain mobility of the poly(n-butyl methacryalte) anchored to the silicate surface [1, 31-33]. The small temperature increase suggests that the overall relaxation behavior is dominated by the relaxation of the bulk polymer. The slightly higher T_g of the sonicated samples (as compared to the clays prepared by stirring) is likely due to the higher molecular weight of the polymer in the SPBMA samples.

Table 3. T_g of pristine PBMA and poly(n-butyl methacrylate)/clay nanocomposite membranes determined via dynamic scanning calorimentry (DSC), thermogravimetric analysis (TGA) parameters for thermal degradation profile.

	T_g	Onset Temperature (ºC)	Temperature at % weight loss (ºC)	
			10%	50%
PBMA	37.1	255	265	322
PBMA-1	38.6	259	272	345
PBMA-3	40.1	259	272	345
PBMA-5	40.9	259	271	344
SPBMA-1	40.6	256	269	340
SPBMA-3	40.9	260	274	350
SPBMA-5	41	260	275	355

5.6.4 Thermogravimetric Analysis (TGA)

The thermograms of the pristine poly(n-butyl methacrylate) and the subsequent polymer/clay nanocomposites have two stages of thermal decomposition. The first stage is located between the temperature region of 100°C to 225°C, and is associated with the volatilization of remnant chloroform solvent molecules encapsulated within the pure polymer and polymer/clay membranes. This stage also provides the removal of excess water molecules sorbed onto the surface of these membranes. The second thermal decomposition stage is located between 225°C and 450°C and presents a dramatic weight loss related to the thermal degradation by depolymerisation of the poly(n-butyl methacrylate) [34-37]. Table 3 summarizes the onset temperature and the temperatures at 10% and 50% weight loss for all the samples. The onset decomposition temperature of the poly(n-butyl methacrylate)/clay nanocomposites is slightly higher in comparison with the pristine poly(n-butyl methacrylate). This increase suggests that the addition of

modified natural montorillonite to the polymer matrix delays the thermal decomposition of the nanocomposite by providing a local heat sink in the matrix [7]. The effect is more pronounced in samples whose clay particles have been sonicated.

5.6.5 Permeation Data

As explained in the previous sections, the in-situ polymerization of poly(n-butyl methacrylate)/clay composites leads to an exfoliated morphology in case of all the nanocomposite membranes. The exfoliated morphology increases the effective surface area of the clay in the matrix, thus increasing the tortuous pathway for the permeating gas molecules. As seen in Figure 5.5 and 5.6 increasing the clay concentration in the polymer matrix leads to an expected decrease in permeation values.

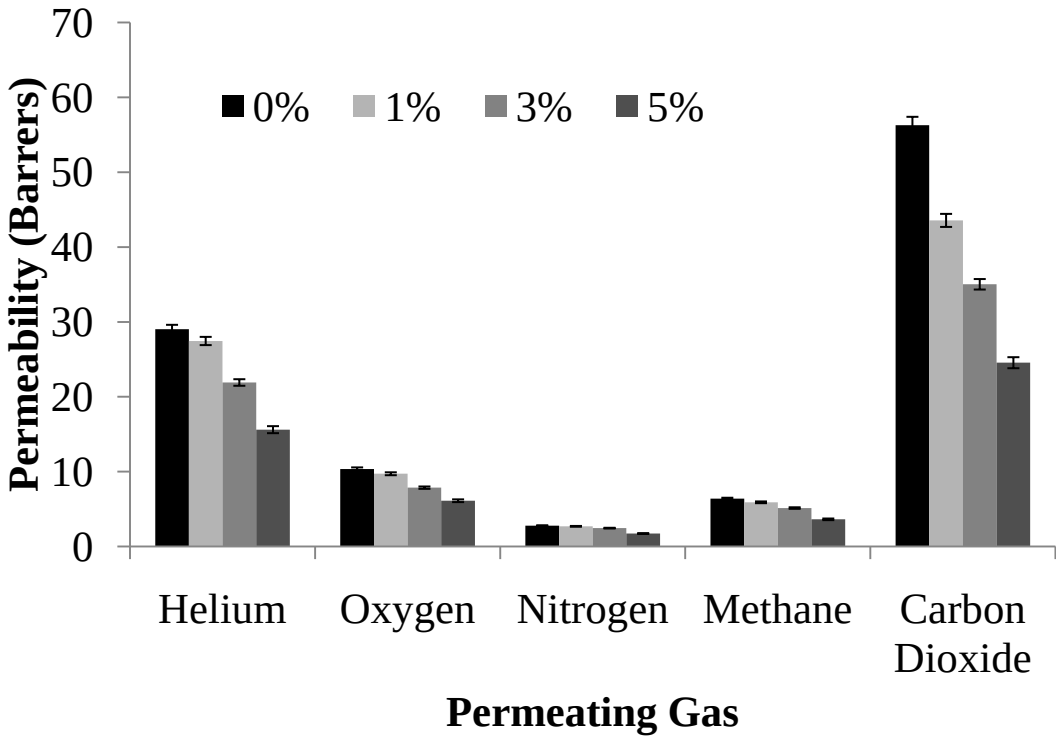

Figure 5.5 Effect of clay concentration in gas permeability of different gases. Sonicated series.

For example, the CO_2 permeation obtained for the pristine poly(n-butyl methacrylate) membrane is 56.3 ± 1.8 barrers. The addition of 5 wt% nanoclay in the matrix decreases the CO_2 permeability value of 24.6 ± 0.9 barrers. This represents a 56% decrease in permeability in comparison with the pristine polymer sample. Similar results are seen in the permeabilities of the other gases. Whether or not the clay particles are sonicated during surface modification also has an effect on the barrier properties of the polymer/clay nanocomposites. As can be seen in Figure 5.6, the effect of dispersing the nanoclay particles via sonication improves barrier properties of all samples, particularly of those having the highest clay content, 5 wt%. For example, the CO_2 permeability of SPBMA-5 is 25 barrer in comparison to 30 barrer of the PBMA-5. These results suggest that pre-treating the clays with sonication increases the dispersion of the clay particles

substantially. This in turn generates more tortuous pathways for permeating gas molecules [38].

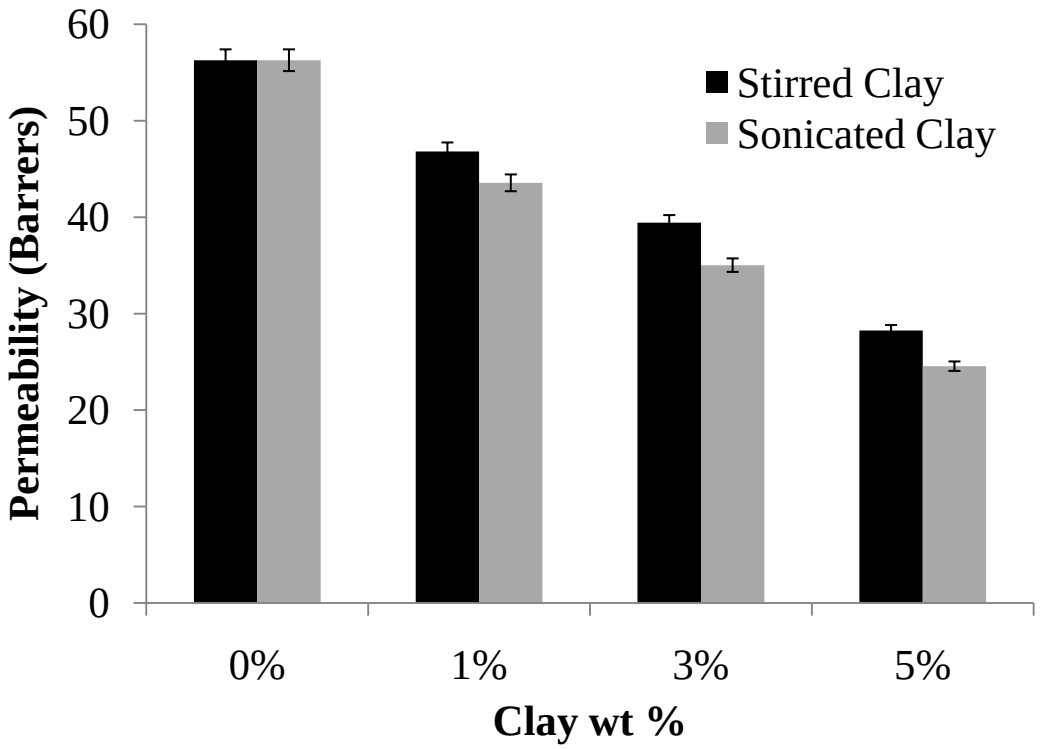

Figure 5.6 Comparison of the effect of sonication and stirring for gas permeation properties of CO_2 in a polymer/clay nanocomposite matrix.

5.6.6 Gas Permeation Models

Phenomenological models such as those of Cussler [39, 40], and Nielsen [41] have been used to predict the effective permeation properties of polymer/clay nanocomposites. These models are based on ideal conditions, such as complete exfoliation of the flake platelets, perfect alignment of the flakes in a perpendicular direction to the flow of the permeating molecules [42], and the assumption that the type

of polymer used as the matrix has no effect on the effective permeability. The mathematical representation of Nielsen's model is presented in equation 1.

$$\frac{P_0}{P} = \frac{1+\left(\frac{\alpha}{2}\right)\phi}{1-\phi} \quad \text{Eq.1}$$

Where, P and P_0 are the permeability of the composite film and that of the pristine polymer, respectively, ϕ is the volume fraction of the filler and α is the aspect ratio, defined as the ratio of half the width to thickness of the impermeable flakes. The volume fraction of the clay content in the matrix can be determined by the use of equation 2:

$$\phi = \frac{1}{1+\frac{\rho_C(1-M_C)}{\rho_P M_C}} \quad \text{Eq. 2}$$

where ϕ is the volume fraction, ρ_C and ρ_p are the density of the nanoclay and the polymer, and M_c is the mass fraction. In a similar model, Cussler et al [39], considered that the steady state flux in a composite membrane, is dominated by wiggles around the impermeable flakes. Thus the flux is dependent on the loading of the nanoclay in the matrix and the geometry of the flakes, which in this case is represented by the specific aspect ratio of the flakes [43]. Cussler's equation is as follows:

$$\frac{P_0}{P} = 1 + \frac{\alpha^2\phi^2}{1-\phi} \quad \text{Eq.3}$$

The parameters in equation 3 are the same as those in Nielsen's equation 1. These models can predict the ratio of the permeation of the pristine polymer to that of the nanocomposite membrane as a function of clay content and aspect ratio. The experimental gas permeation data was fitted to both models using the aspect ratio as an

adjustable parameter. The results can be seen in Figures 5.7 and 5.8. Figure 5.7 shows CO_2 and O_2 permeation data fitted with Nielsen's model. For examples, the adjusted aspect ratio, α, obtained by fitting CO_2 permeation of the SPBMA samples was between 100 and 150. The aspect ratio of the PBMA samples was slightly lower, falling between 100 and 120. When fitting the O_2 permeation data, the aspect ratio of the SPBMA series fell between 35 and 80, while that of the PBMA samples was between 20 and 50. The fact that there is a discrepancy between the adjusted aspect ratio of the CO_2 and the O_2 permeabilities reflects the idealized nature of the phenomenological models. However, the consistently higher aspect ratios of the samples, whose clay particles have been sonicated again suggests that these samples have better dispersion than those whose clay particles have been processed by stirring.

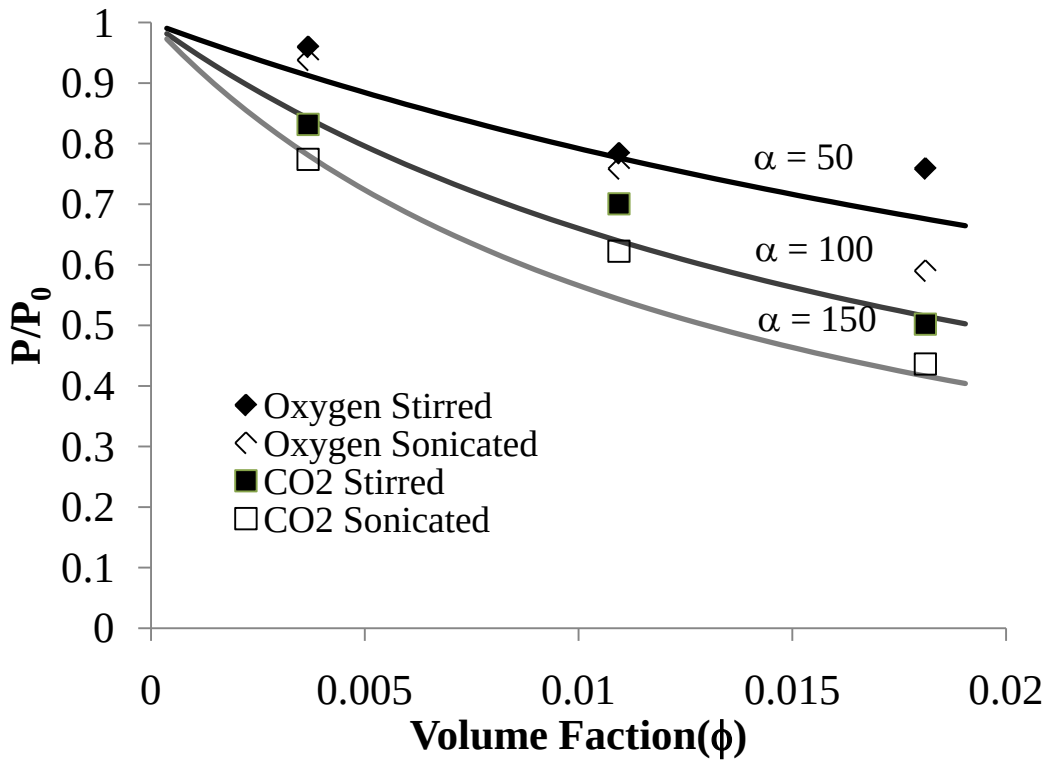

Figure 5.7 Nielsen phenomenological model plot of O_2 and CO_2 permeability in nanocomposites prepared by sonication and stirring, ♦ O_2 Stirred Sample, ◊ O_2 Sonicated Sample, ■ CO_2 Stirred Sample, □ CO_2 Sonicated Sample.

Figure 5.8 shows the fit of Cussler's model to the experimental permeation data. As is the case for Nielsen's model at the lowest clay loading of 1 wt%, the apparent aspect ratio seen by the permeating gas molecules is similar in the case of nanocomposites prepared with sonicated as well as with stirred clays. But as the clay loading increases to the highest amount of 5 wt% of clay, the differences in the aspect ratio between the stirred and sonicated series widen, especially in the case of O_2 permeability. Again, this is reflection of the deviation from the idealized structure of Cussler's model. Actually, Cussler et al., acknowledged that the model might present some variability [43], attributed to the random orientation of the flakes in the matrix [40].

Also, it should be pointed out that aspect ratios in the range of 50 to 100 are consistent with those observed by other groups using the same models [24, 38, 44]. Finally, in comparison to barrier properties achieved by preparing nanocomposites by simply mixing the clay particles in a polymer solution [45], the in-situ polymerization in the presence of exfoliated clay platelets provides a better fit to Cussler and Nielsen's idealized phenomenological model in predicting permeation values of polymer/clay nanocomposite systems.

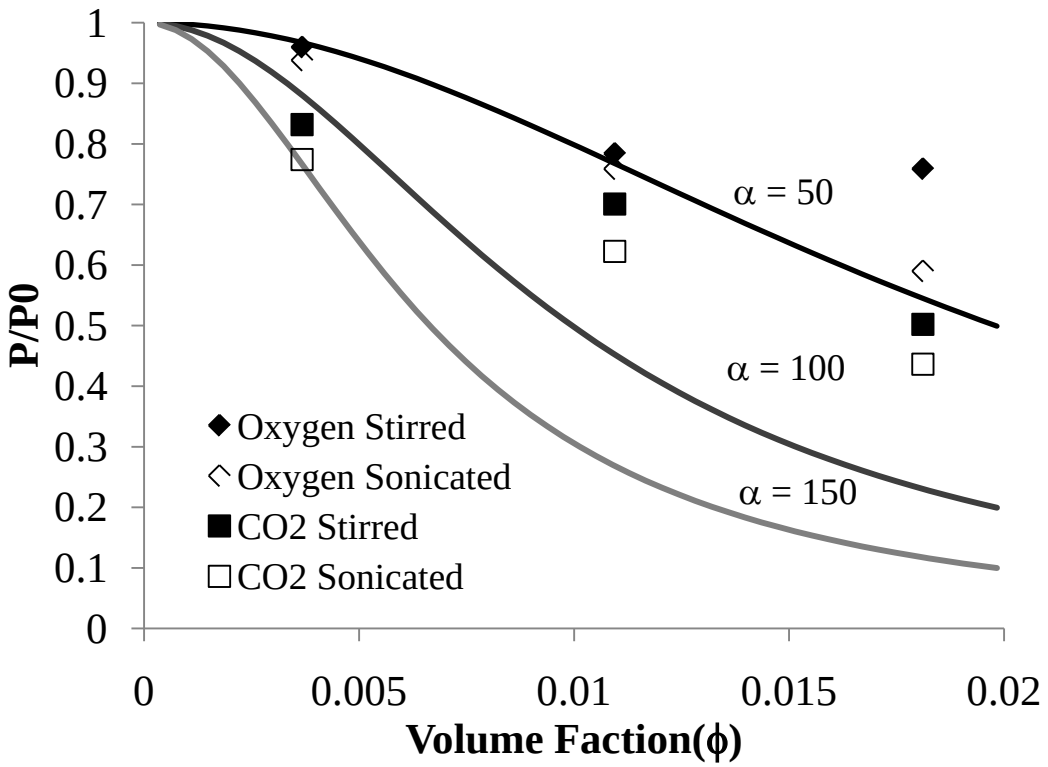

Figure 5.8 Cussler phenomenological model plot of O_2 and CO_2 permeability in nanocomposites prepared by sonication and stirring, ♦ O_2 Stirred Sample, ◊ O_2 Sonicated Sample, ■ CO_2 Stirred Sample, □ CO_2 Sonicated Sample.

5.7 Conclusion

The increasing basal spacing seen via XRD analysis of surface modified natural montmorillonite, Cloisite ® Na^+ suggested grafting of the quaternary salt on the clay surface. The grafting of alkylammine group allowed an anchoring site for the *In situ* polymerization poly (n-butyl methacrylate). The polymerization reaction produced barrier membranes with exfoliated morphologies, as determined via XRD analysis. Sonication of the clays before polymerization of the matrix lead to higher molecular weights than when the clays were stirred due to better particle dispersion and accessibility of the monomer to reaction sites. The addition of clay particles to the polymer matrix improved the mechanical properties of the polymer and also improved the thermal stability of the nanocomposites in comparison to the pristine polymer. The complete exfoliation of the clay platelets provided a decrease in gas permeability of up to 50% for certain gases. This effect was achieved at relatively low clay loadings of 1 to 5 wt%. Phenomenological models of effective gas permeabilities in nanocomposites, such as those of Nielsen and Cussler, although able to fit the experimental data are still too idealized to explain differences in effective permeabilities of different gases through the same nanocomposite.

Acknowledgments

We thank the National Science Foundation for support of this work via grant CMMI 0600090.

References

1. Cui, L., N.H. Tarte, and S.I. Woo, *Effects of modified clay on the morphology and properties of PMMA/Clay nanocomposites synthesized by in situ polymerization.* Macromolecules, 2008. **41**(12): p. 4268-4274.
2. Chavarria, F. and D.R. Paul, *Morphology and properties of thermoplastic polyurethane nanocomposites: Effect of organoclay structure.* Polymer, 2006. **47**(22): p. 7760-7773.
3. Wang, Z. and T.J. Pinnavaia, *Nanolayer Reinforcement of Elastomeric Polyurethane.* Chemistry of Materials, 1998. **10**(12): p. 3769-3771.
4. Beyer, G., *Nanocomposites: a new class of flame retardants for polymers.* Plastics, Additives and Compounding, 2002. **4**(10): p. 22-28.
5. Zheng, X. and C.A. Wilkie, *Flame retardancy of polystyrene nanocomposites based on an oligomeric organically-modified clay containing phosphate.* Polymer Degradation and Stability, 2003. **81**(3): p. 539-550.
6. Zheng, X., D.D. Jiang, and C.A. Wilkie, *Methyl methacrylate oligomerically-modified clay and its poly(methyl methacrylate) nanocomposite.* Thermochimica Acta, 2005. **435**(2): p. 202-208.
7. Si, M., et al., *Effect of clay type on structure and properties of poly(methyl methacrylate)/clay nanocomposites.* Macromolecular Materials and Engineering, 2006. **291**(6): p. 602-611.
8. Jeong, H.K., et al., *Fabrication of Polymer/Selective-Flake Nanocomposite Membranes and Their Use in Gas Separation.* Chemistry of Materials, 2004. **16**(20): p. 3838-3845.
9. Ogasawara, T., et al., *Helium gas permeability of montmorillonite/epoxy nanocomposites.* Composites Part A: Applied Science and Manufacturing, 2006. **37**(12): p. 2236-2240.
10. Xu, B., et al., *Calculating barrier properties of polymer/clay nanocomposites: Effects of clay layers.* Polymer, 2006. **47**(8): p. 2904-2910.
11. Ray, S.S. and K. Okamoto, *Polymer/layerd silicate nanocomposites: a review from preparation to processing.* Progress in Polymer Science, 2003. **28**(11): p. 1539-1641.
12. Gao, F., *Clay/polymer composites: the story.* Materials Today, 2004. **7**(11): p. 50-55.
13. Tjong, S.C., *Structural and mechanical properties of polymer nanocomposites.* Materials Science and Engineering: R: Reports, 2006. **53**(3-4): p. 73-197.
14. Giannelis, E.P., *Polymer layered silicate nanocomposites.* Advanced Materials, 1996. **8**(1): p. 29-35.
15. Gatos, K.G. and J. Karger-Kocsis, *Effect of the aspect ratio of silicate platelets on the mechanical and barrier properties of hydrogenated acrylonitrile butadiene rubber (HNBR)/layered silicate nanocomposites.* European Polymer Journal, 2007. **43**(4): p. 1097-1104.
16. Vermogen, A., et al., *Evaluation of structure and dispersion in polymer-layered silicate nanocomposites.* Macromolecules, 2005. **38**(23): p. 9661-9669.
17. Yang, C., W.H. Smyrl, and E.L. Cussler, *Flake alignment in composite coatings.* Journal of Membrane Science, 2004. **231**(1-2): p. 1-12.

18. Lan, T., P.D. Kaviratna, and T.J. Pinnavaia, *On the nature of polyamide-clay hybrid composites.* Chemistry of Materials, 1994. **6**(5): p. 573-575.
19. Brady, P.V. and J.L. Krumhansl, *Oxide Surface*. Surfactant Science Series, ed. J.A. Wingrave. Vol. 103. 2001, New York, N.Y.: Marcel Dekker, Inc.
20. Lagaly, G. and K. Beneke, *Intercalation and exchange reactions of clay minerals and non-clay layer compounds.* Colloid & Polymer Science, 1991. **269**(12): p. 1198-1211.
21. Pinnavaia, T.J. and G.W. Beall, eds. *Polymer-Clay Nanocomposites*. 2000, John Wiley & Sons Ltd.
22. Kurian, M., et al., *Investigation of the effects of silicate modification on polymer-layered silicate nanocomposite morphology.* Journal of Polymer Science Part B: Polymer Physics, 2004. **42**(22): p. 4075-4083.
23. Kornmann, X., et al., *Synthesis of amine-cured, epoxy-layered silicate nanocomposites: the influence of the silicate surface modification on the properties.* Journal of Applied Polymer Science, 2002. **86**(10): p. 2643 - 2652.
24. LeBaron, P.C., Z. Wang, and T.J. Pinnavaia, *Polymer-layered silicate nanocomposites: an overview.* Applied Clay Sciences, 1999. **15**(1-2): p. 11-29.
25. Fornes, T.D., et al., *Effect of organoclay structure on nylon 6 nanocomposite morphology and properties.* Polymer, 2002. **43**(22): p. 5915-5933.
26. Bergaya, F. and G. Lagaly, *Surface modification of clay minerals.* Applied Clay Sciences, 2001. **19**(1-6): p. 1-3.
27. Krishnamoorti, R., R.A. Vaia, and E.P. Giannelis, *Structure and dynamics os polymer-layered silicate nanocomposites.* Chem. Mater., 1996(8): p. 7.
28. Dan, C.H., et al., *Effect of clay modifiers on the morphology and physical properties of thermoplastic polyurethane/clay nanocomposites.* Polymer, 2006. **47**(19): p. 6718-6730.
29. Wang, D., et al., *A comparison of various methods for the preparation of polystyrene an poly(methyl methacrylate) clay nanocomposites.* Chemistry of Materials, 2002. **14**(9): p. 3837-3843.
30. *Diffusion in Polymers*, ed. J. Crank and G.S. Park. 1968, New York: Academic Press. 452.
31. Ingram, S., et al., *Influence of clay type on exfoliation, cure and physical properties of in situ polymerised poly(methyl methacrylate) nanocomposites.* Polymer International, 2008. **57**(10): p. 1118-1127.
32. Zhang, Z., et al., *Synthesis and characterization of poly(butyl acrylate-co-methyl methacrylate) clay nanocomposites via emulsion polymerization.* International Journal of Nanoscience, 2006. **5**(2&3): p. 291-297.
33. Patel, S., et al., *Effect of acrylic copolymer and terpolymer composition on the properties of in-situ polymer/silica hybrid nanocomposites.* Journal of Material Science, 2006. **41**(3): p. 927-936.
34. Novaković, K., L. Katsikas, and I.G. Popović, *The thermal degradation of poly(iso-butyl methacrylate) and polu (sec-butyl methacrylate).* Journal of Serbian Chemical Society, 2000. **65**(12): p. 867-875.
35. Milovanović, M., et al., *The thermal degradation of poly(diethyl fumarate).* Polymer Degradation and Stability, 2006. **91**(12): p. 3221-3229.

36. Demirelli, K., A. Kurt, and M. Coşkun, *Thermal degradation and synthesis of block copolymers of styrene and n-butyl methacrylate by atom transfer radical polymerization.* Polymer-Plastics Technology and Engineering, 2004. **43**(4): p. 1245-1263.
37. Daraboina, N. and G. Madras, *Thermal and photocatalytic degradation of poly(methyl methacrylate), poly(butyl methacrylate), and their copolymers.* Industrial & Engineering Chemistry Research, 2008. **47**(18): p. 6828-6834.
38. Yano, K., A. Usuki, and A. Okada, *Synthesis and properties of polyimide-clay hybrid films.* Journal of Polymer Science Part A: Polymer Chemistry, 2000. **35**(11): p. 2289 - 2294.
39. Cussler, E.L., et al., *Barrier Membranes.* Journal of Membrane Science, 1988. **38**(2): p. 161-174.
40. Eitzman, D.M., R.R. Melkote, and E.L. Cussler, *Barrier membranes with tipped impermeable flakes.* AIChE Journal, 1996. **42**(1): p. 2-9.
41. Nielsen, L.E., *Models for the permeability of filler polymer systems.* Journal of Macromolecular Science Chemistry, 1967. **A1**: p. 929-942.
42. Bharadwaj, R.K., et al., *Structure–property relationships in cross-linked polyester–clay nanocomposites.* Polymer, 2002. **43**(13): p. 3699-3705.
43. Perry, D., W.J. Ward, and E.L. Cussler, *Unsteady diffusion in barrier membranes.* Journal of Membrane Science, 1989. **44**(2-3): p. 305-311.
44. Ray, S.S., K. Okamoto, and M. Okamoto, *Structure-Property Relationship in Biodegradable Poly(butylene succinate)/Layered Silicate Nanocomposites.* Macromolecules, 2003. **36**(7): p. 2355-2367.
45. Herrera-Alonso, J.M., et al., *Transport properties in polyurethane/clay nanocomposites as barrier materials: Effect of processing conditions.* Journal of Membrane Science, 2009. **337**(1-2): p. 208-214.

Chapter 6 Gas Transport Properties of Poly Acrylate/Clay Nanocomposites Prepared Via Emulsion Polymerization

6.1 Abstract

Polymer/clay nanocomposites were synthesized via emulsion polymerization to act as barrier membranes. Cloisite ® Na^+ was modified via ion exchange to tether a reactive group on the surface of the silicate platelet in order to promote polymerization and exfoliation of the stacked platelets. Poly(n-butyl methacrylate)/clay and poly(n-butyl methacrylate-co-methyl methacrylate)/clay barrier membranes provided possible exfoliated morphologies in the matrix, as seen by X-ray diffraction analysis. The addition of organically modified clays in the matrix improved the thermal properties of the barrier membranes. Results from dynamic light scattering (DLS) suggest that the growth of particles in the emulsion may be restricted by the presence of montmorillonite clay platelets as well as copolymer composition.. Permeability data indicates that the use of a glassy co-polymer improves barrier properties of the membrane. Phenomenological models suggest an improved alignment and dispersion of the clay platelets in the matrix.

6.2 Introduction

Since the inception 20 years ago by the Toyota group [1, 2] the synthesis of polymer/clay nanocomposites has been of considerable interest to the packaging and automotive industries. Polymer/clay nanocomposites are attractive and offer potential growth because of their wide range applications over traditional polymers [3-5]. These nanocomposites have proven to increase the mechanical [6], chemical and thermal properties [7]. Therefore these

nanocomposites generate a higher resistance to gas permeability [8-11], flammability [12, 13]. The polymer/clay interactions within the matrix ultimately decide the morphology of the nancomposite. The morphologies of the clays in the nanocomposites have been cited as phase separated, intercalated or exfoliated [4, 14, 15]. Different synthesis procedures, in situ polymerization, solution blending and melt polymerization [16-20], have been used in order to obtain the different morphologies. The exfoliated or delaminated morphology is the preferred in order to maximize the effect of the clay in the matrix. The morphology of the nanocomposites has a direct effect on the mechanical, thermal and barrier properties [21, 22]. Recently, another method used to obtain polymer/clay nanocomposites has been emulsion polymerization [23-26]. Emulsion polymerization offers a cleaner and "greener" alternative to the solvents used in *in-situ* polymerization and furthermore limits to the thermal degradation of the clay platelets that occurs in melt processing. The use of colloidal dispersions offers another broad range of applications for nanocomposite technology within the realm of coatings and paints [27]. Different groups [28-34], have used solid particles or in this case clay nanoparticles as stabilizers in emulsions in order to substitute surfactants. This process is commonly known as "Pickering emulsions [35]." Nanoclay platelets act as surfactants and are located at the liquid-liquid interface [36], which causes a decrease in the interfacial energy. This interface is the ideal self-assembly point for the nanoparticles [37]. Improved emulsion stability is directly related to the decrease of interfacial tension between the particles and the liquids [32]. The success of the stabilization effect of these emulsions is now at the basis of many technological advances in the food industry, the cosmetics industry, pharmaceutical industry and the oil recovery industry.

The goal of this study was to use organically modified natural montmorillonite Cloisite Na+ and exfoliate/intercalate the silicate platelets via emulsion polymerization process. Silicate

platelets are used as seed surfaces for emulsion polymerization due to the tethering of the reactive group via ion-exchange reactions. The grafting of the subsequent polymer chains to the silicate surface ensures the intercalation/exfoliation of the platelets in the emulsion. This work also evaluates the thermal stability and transport properties of the nanocomposites as barrier membranes for gas separation processes. This study also evaluates the use of glassy copolymer PMMA as the matrix in the dispersion of clay platelets and the resulting transport properties of the nanocomposites.

6.3 Materials and Methods

Sodium montmorillonite, Cloisite ® Na+ was purchased from Southern Clay Inc, and dried for 24 hours before use. Sodium dodecylbenzenesulfonate (SDS) was purchased from Sigma-Aldrich and used as received. Ammonium persulfate was purchased from Sigma-Aldrich and used as received. Butyl methacrylate (BMA) and methy methacrylate (MMA) were purchased from Sigma-Aldrich and were distilled at reduced pressure before use. Anhydrous tetrahydrofuran (THF) was purchased from Sigma-Aldrich and used as received. Cloisite Na+ modification via sonication was carried out as previously reported [38]. This modification consists of the anchoring of the [2-(Acryloyloxy)ethyl]-trimethylammonium via ion exchange in order to establish a reactive group on the surface of the natural montmorillonite Cloisite ® Na+. The tethered group may react with the acrylate monomer in the emulsion. Nanocomposite synthesis was carried out using modified Cloisite Na+ as seed particles. All reactions were carried out in a 250 ml three neck round bottom flask equipped with a nitrogen inlet, a thermometer, and reflux condenser with an outlet to a bubble counter. Stirring in the reactor was kept at 500 rpm. Polymerization reactions were carried out at 70 ºC for 8 h. The polymerization procedure followed is as previously reported [39]. The procedure includes the initial dispersion

of the modified clay, and the surfactant SDS, in dionized water for 10 min. After the modified clay and the surfactant are dispersed in water the monomer, in this case butyl methacrylate is added to the solution and stirred for 10 min. A small amount of the clay/monomer solution is fed to the reactor with the addition of the initiator, ammonium persulfate, and left to react for 10 min. Further addition of the clay/monomer solution was carried out in nitrogen environment at a slow rate to generate monomer starved conditions. The specific amounts of monomer, modified clay, surfactant and initiator can be found in the reference [37]. The only departure from this procedure is the water to polymer ratio, which was kept at 10:1. The addition of modified Cloisite ® Na+ in the emulsion varied from 1 to 5 wt% as can be seen in Table 1. In the formation of the copolymer, the ratio of methyl methacrylate monomer to butyl methacrylate was varied in the The monomer weight ratio of butyl methacrylate: methyl methacrylate varied from 90:10 to 60:40. The nomenclature for these samplescan also be found in Table 1.

Table.1 Nomenclature used for the different polymer/clay and co-polymer/clay nanocomposite membranes used. Poly (n-butyl methacrylate) will be abbreviated as PBMA and the copolymer poly(n-butyl methacrylate-co-methyl methacrylate) will be abbreviated as CPBM. The number for the PBMA series represent the wt% of modified clay in the sample. The number for the CPBM series represent ratio of the butyl methacrylate: methyl methacrylate in the emulsion. All CPBM samples contained 5 wt% of modified clay.

Clay Content wt %	Nomenclature for this publication
0	PBMA
1	PBMA-1
3	PBMA-3
5	PBMA-5
5	CPBM/90-10
5	CPBM/80-20
5	CPBM/70-30
5	CPBM/60-40

Barrier membranes were prepared in a two step process. A 10:1 ratio of ethanol to emulsion was placed in a beaker in order to precipitate the polymer/clay composite. Vigorous stirring was applied to the solution for 2 hours. The solution was then filtered to remove the composite. Once filtered the product was left to dry in vacuum for 24h at 25ºC. Approximately, 0.7 to 0.8g of the dried nanocomposite was then dissolved in 5ml of THF with vigorous stirring for 8hrs at room temperature. The product was then cast in Teflon pans and the solvent was allowed to evaporate slowly at room temperature for 24hrs. The controlled evaporation process reduced the presence of pinholes in the membrane and prevented curling the membranes. After 24 hours the membrane was placed under vacuum at 60°C for 24 hours to insure the removal of all the solvent.

6.4 Characterization

X-Ray diffractometry, XRD, was used to determine the interspacial distance within the clay platelets. The system used was a Sintag XDS 2000 powder diffractometer using Ni filtered Cu KαX-ray radiation (λ=1.54Å) at voltage of 45KV, 40mA current, and filament current of 3.30A. The scanning rate for the low angle samples was done at 0.25°/min over a range of 2θ = 1-10°. The XRD measurements were conducted on the membrane samples in film form, while the clay was analyzed in the powder form. Dynamic light scattering (DLS) was preformed on Malvern Instruments Zetasizer nanoseries, Nano-ZS, at 25 ºC. Thermogravimetric Analysis (TGA) was performed on a TA Instruments Thermogravimetric analyzer model Q5000 IR. Measurements are carried out under a nitrogen flow. The analysis was done from room temperature to 600°C, with a heating rate of 10°C/min. Dynamic Scanning Calorimetry (DSC) measurements were carried out in a TA Instruments Differential Scanning Calorimeter Q2000, from -20°C to 150°C, with a heating rate of 10°C/min. Scanning electron microscopy (SEM) micrographs were taken using a LEO (Zeiss) 1550 high-performance Schottky field-emission SEM with an acceleration voltage of 5kV. Colloidal solutions were gold coated prior to scanning. Gas permeabilities of the pure polymer poly(n-butyl methacrylate), sonicated poly(n-butyl methacrylate)/clay membranes and co-polymer poly(n-butyl methacrylate) poly(methyl methacrylate)/clay membranes were measured in a constant volume-variable pressure system. The membranes were placed in a stainless steel cell with chambers of known volume on each side. The upstream side of the membrane was pressurized to 4 atm, maintained at 25 °C with the penetrating gas species. The downstream side was initially evacuated to $P < 0.001$ atm. The variation in downstream pressure was monitored in real time and the permeability was calculated only after steady state was achieved [40]. All gases employed (He, O_2, N_2, CO_2 and CH_4) were

ultra-high purity (minimum purity 99.999%) and were obtained from Airgas, Inc. For each gas analyzed every barrier membrane was tested 3 times in the permeation set-up in order to establish a statistically consistent result. Some nanocomposites systems where tested for permeability using more than one sample, to confirm the reproducibility of the data.

6.5 Results and Discussion

6.5.1XRD Characterization

X-ray diffraction (XRD) was used to study the morphology of the barrier membranes nanocomposites. Figure 6.1, shows the XRD diffraction patterns of the PBMA/clay barrier membrane series in comparison to the modified clay. The diffraction pattern for the surface modified clay shows a peak at ≈ 6.16 in the 2θ region, which corresponds to the d_{001} reflection. By using Braggs law, the gallery space between the platelets of the modified Cloisite ® Na+ was calculated to be approximately 14.3 Å. The diffractograms seen for the PBMA/clay nanocomposites series are very broad and have a very weak signal. These weak intensities have small peaks in between the values of 6.9 and 7.3, in the 2θ region, which corresponds to a interspacial distance of 12.5 to 12.7 Å.

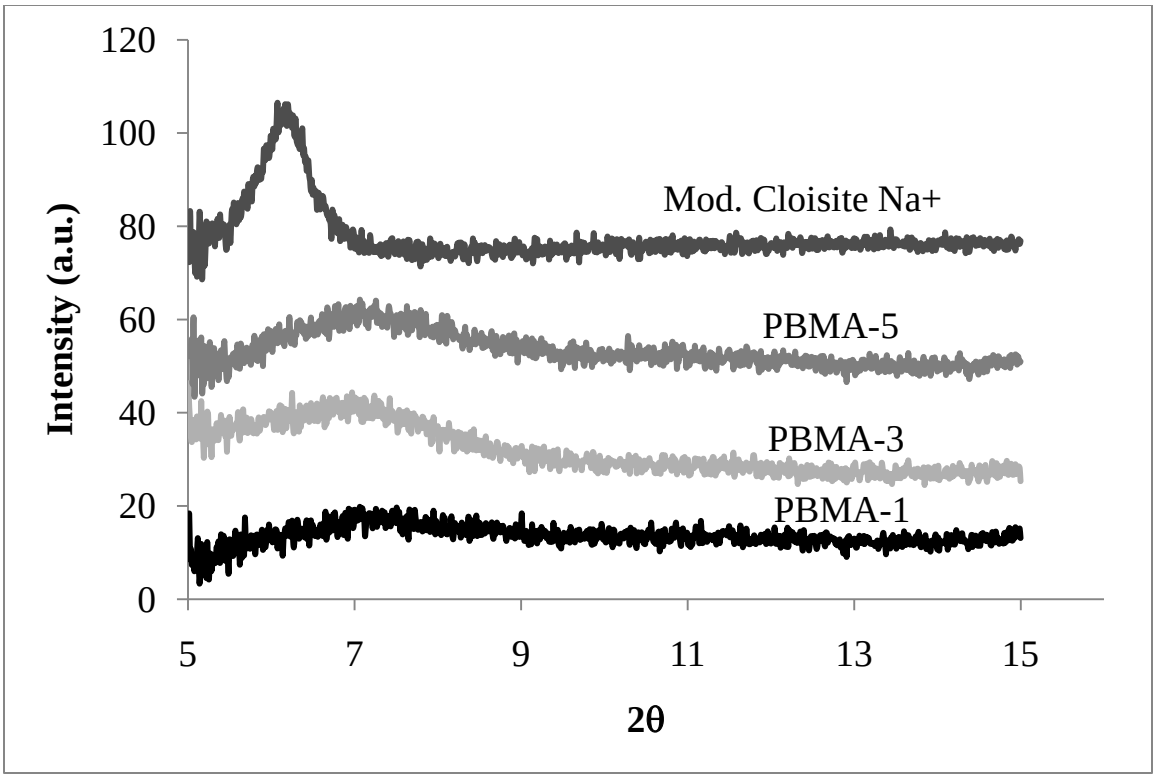

Figure 6.1. XRD diffraction patterns of modified Cloisite ® Na+ and PBMA/clay series.

Figure 6.2, shows the resulting diffractograms of the CPBM/clay copolymer barrier membrane series in comparison to the modified clay. The diffractograms from this series also are very broad and of a very low intensity in comparison to the signal seen for the modified Cloisite ® Na+. The probable peaks are related to the d_{001} reflection, seen for this series also are between the values of 7.2-7.3 in the 2θ region, which corresponds to a distances of 12.1 to 12.2 Å. The weak signals for all the nanocomposites may suggest a partial delamination/exfoliation of the clay platelets in the matrix.

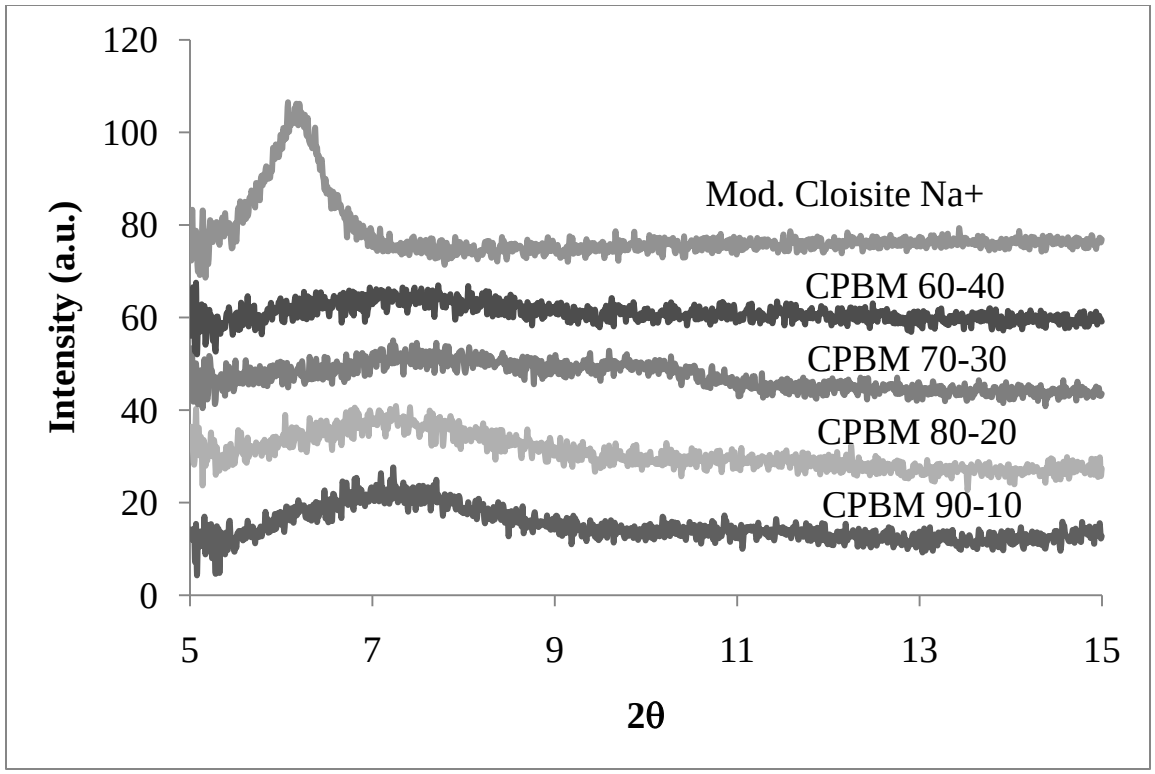

Figure 6.2. XRD diffraction patterns of modified Cloisite ® Na+ and CPBM/clay series.

6.5.2 Scanning Electron Microscopy (SEM)

SEM micrographs for the PBMA/clay series are presented in Figures 6.3 and 6.4. As can be seen from these micrographs the clay platelets are located at the surface of the PBMA emulsion particles and provide armored-like colloidal particles [28, 29, 32, 34]. These micrographs suggest that more than one silicate platelet maybe attached to the PBMA emulsion particles.

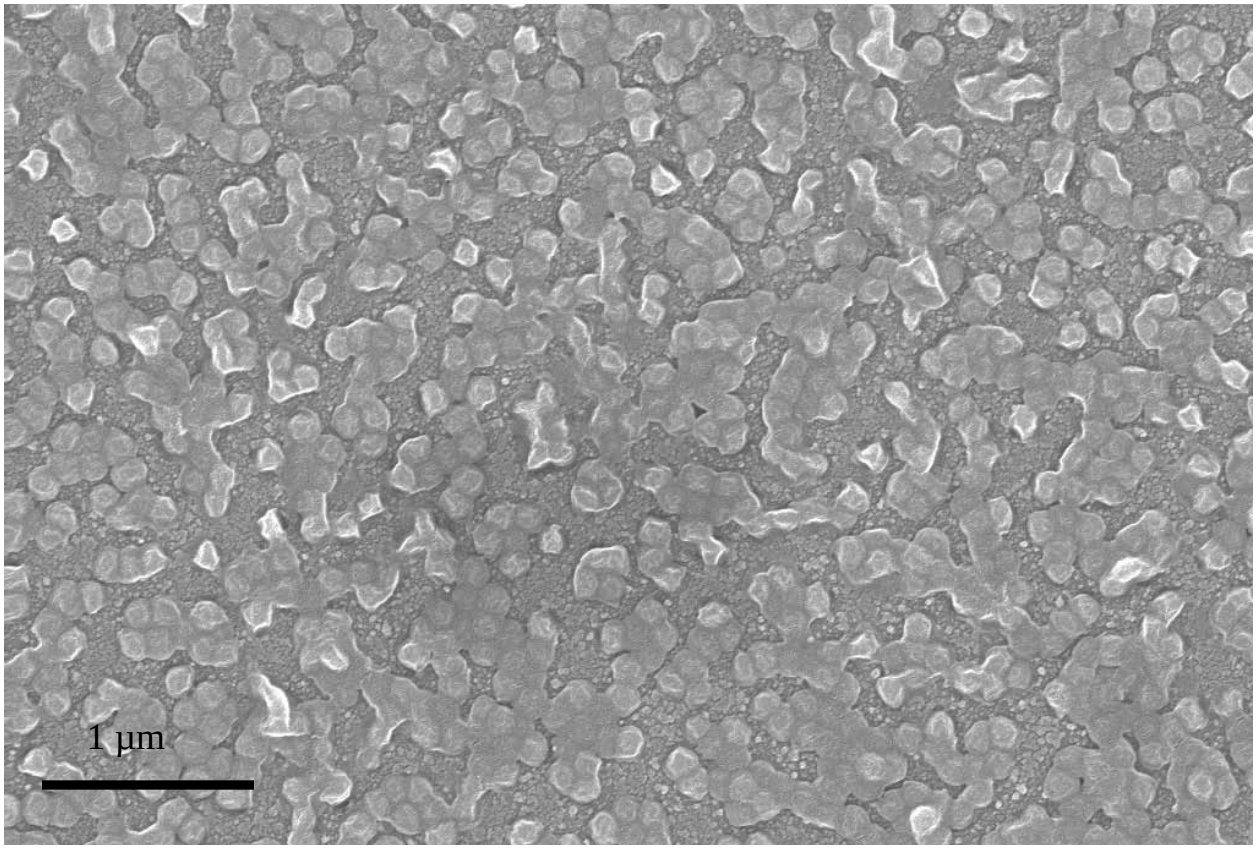

Figure 6.3. SEM micrograph of nanocomposites latex PBMA/5 particles

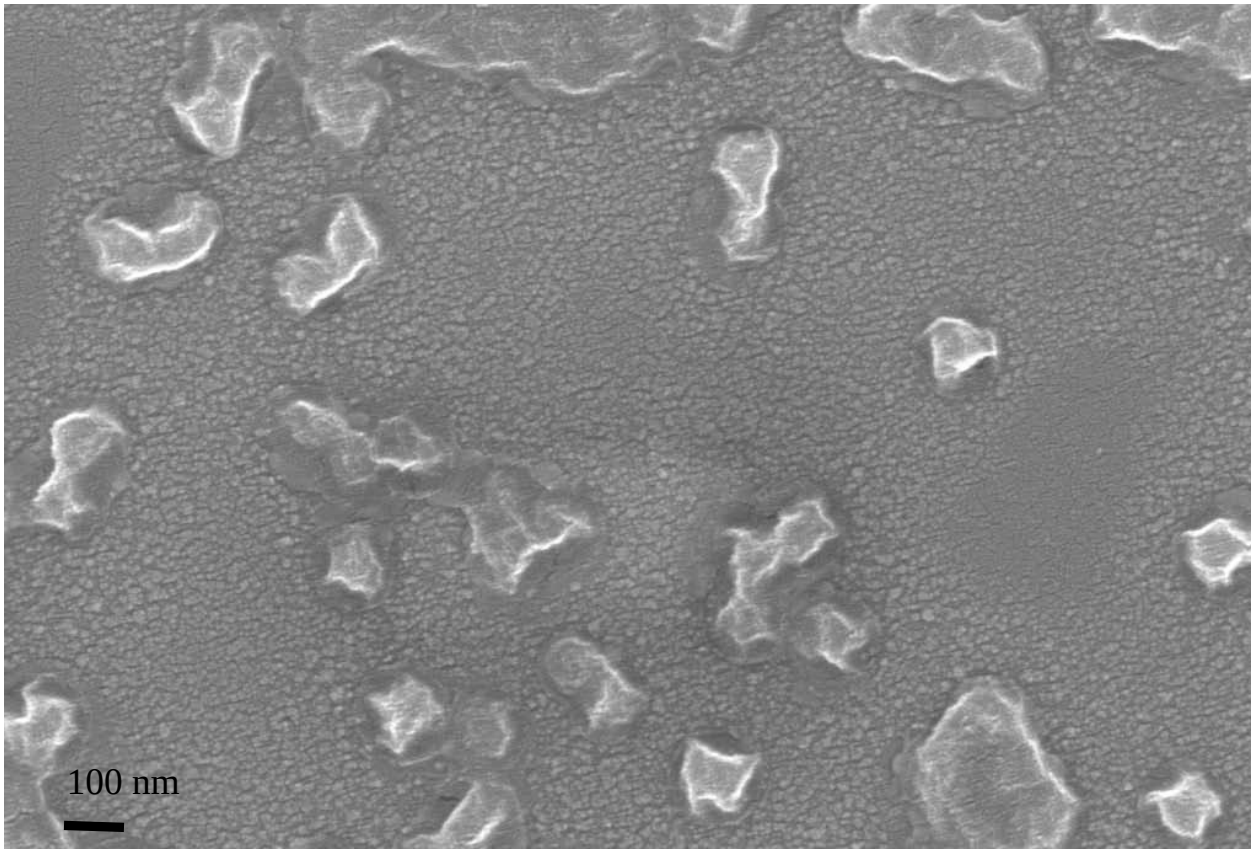

The micrographs for the copolymer CPBM/clay series can be seen in Figures 6.5 through 6.7. These micrographs also suggest that more than one CPBM particle can be attached to the silicate platelets, thus forming a dumbbell like morphology and also a snowman like morphology. These morphologies were proposed by Voorn et al. [41], but for encapsulation of clay platelets. The irregular non-spherical particle morphology of the CPBM/clay series was caused by the silicate platelets in the colloidal solution [42].

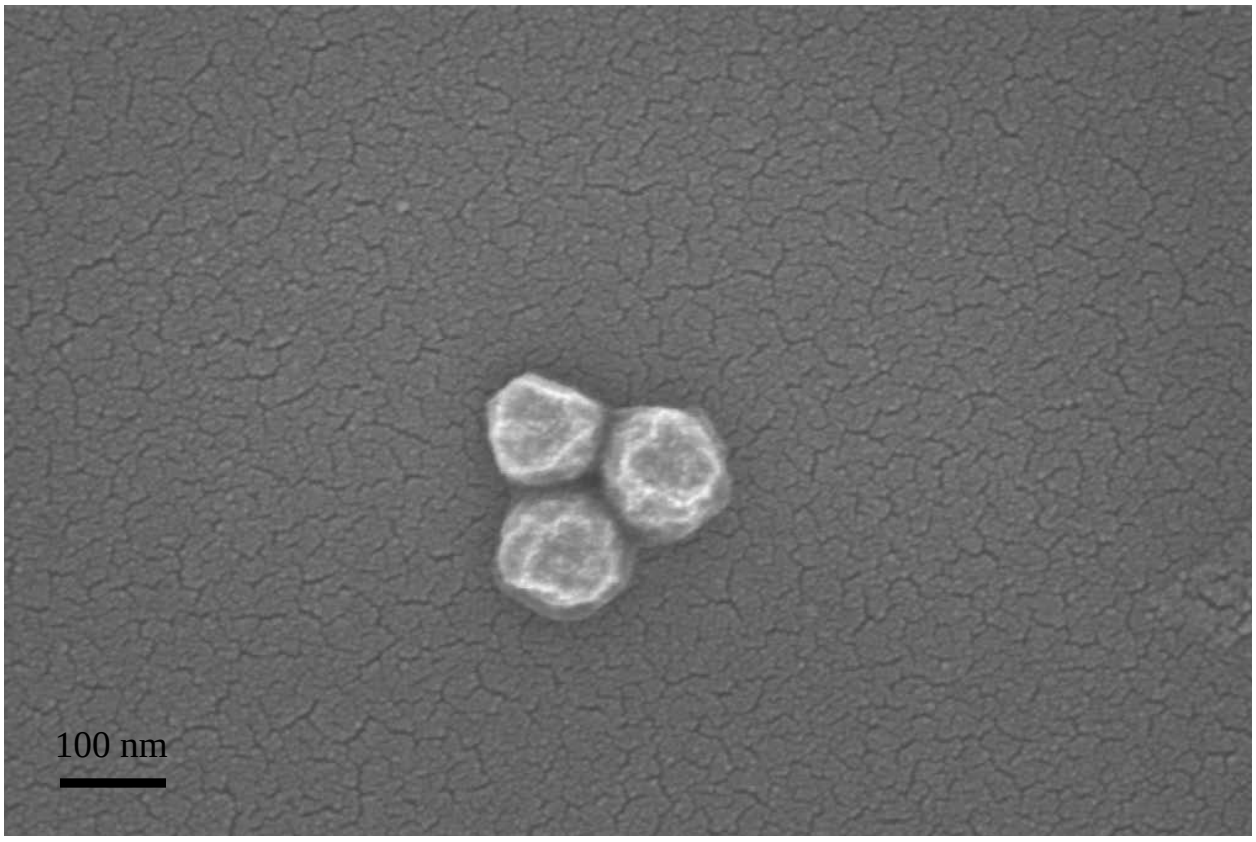

Figures 6.5 SEM micrograph of nanocomposites latex CPBM/80-20

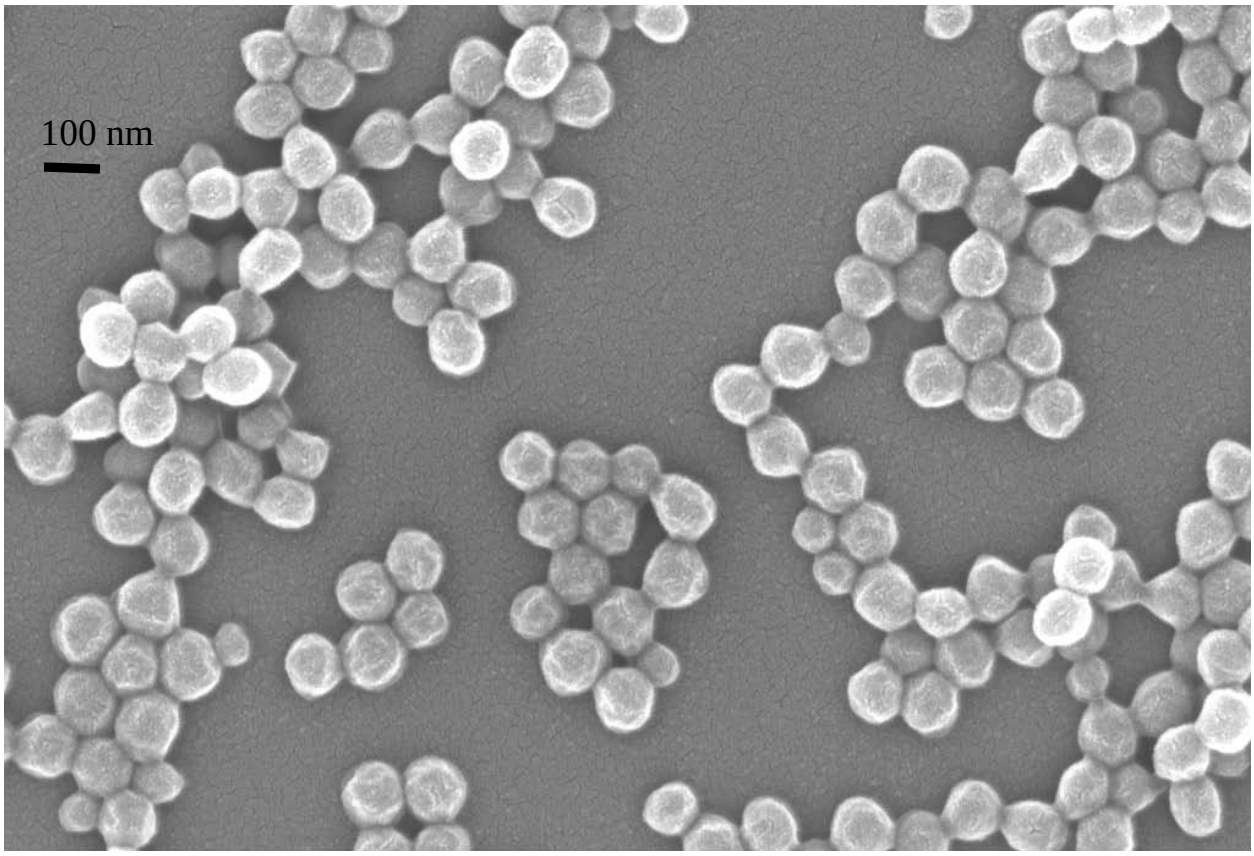

Figures 6.6 SEM micrograph of nanocomposites latex CPBM/80-20 distribution of particles

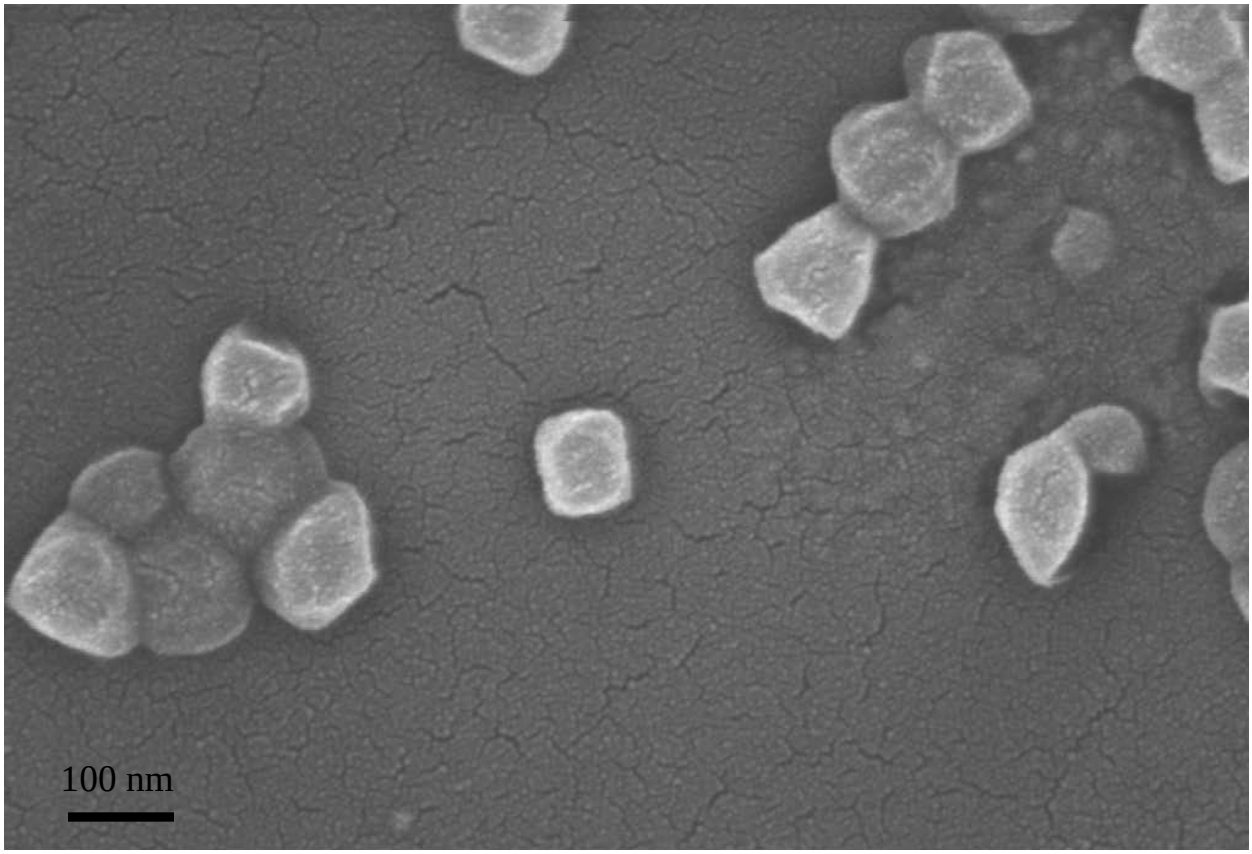

Figures 6.7 SEM micrograph of nanocomposites latex CPBM/60-40 single particles and agglomerate particles in emulsion.

6.5.3 Dynamic Scanning Calorimetry (DSC)

Glass transition temperature, T_g, was determined via dynamic scanning calorimentry (DSC) for the PBMA/clay series, and the CPBM/clay series of barrier membranes. A summary of the glass transition temperatures for the barrier membranes can be found in Table 6.2. As expected pure PBMA provided the lowest glass transition temperature at 36.1 °C. Increasing clay concentration in the colloidal systems led to an increased glass transition temperature for the barrier membranes in the PBMA/clay series. PBMA/5 provided a glass transition temperature of 47.5 °C. The increase is related to a higher restricted segmental chain motion of the polymer chains due to interfacial interactions with the nanoclay [43]. CPBM/clay nanocomposite

membranes provided a higher glass transition temperature than PBMA/clay nanocomposites due to the addition of the PMMA. The higher semi-crystalline structure of the PMMA copolymer further restricts the segmental chain motion, thus increasing the glass transition temperature of the copolymer. The increase in carbon atoms in the side chain decreases T_g due to a higher molecular mobility [44]. As expected the highest weight ratio of PMMA in the colloidal system, CPBM/60-40 led to the highest T_g 61 °C for the PBMA/PMMA/clay series.

Table 2. Glass transition temperature (T_g) of the different series evaluated via dynamic scanning calorimentry (DSC). Decomposition temperatures of the barrier membranes set at 10wt% and 50 wt%. Decomposition peaks seen in the differential thermograms for all the nanocomposites.

	Tg (ºC)	Temperature Loss (ºC)		DTG Decomposition Temperature (ºC)	
		10%	50%	Region 1	Region 2
PBMA	36.1	222	265	230	264
PBMA/1	45.9	257	310	273	317
PBMA/3	45.6	252	306	276	317
PBMA/5	47.5	260	311	278	320
CPBM/90-10	48.3	265	317	280	322
CPBM/80-20	55.5	266	316	278	321
CPBM/70-30	59.4	264	319	280	325
CPBM/60-40	60.1	268	324	280	333

6.5.4 Thermogravimetric Analysis (TGA)

The thermogravimetric analysis (TGA) and differential thermogravimetric (DTG) results for the PBMA/clay series and for the CPBM series are presented in Table 6.2. Typical decomposition curves the PBMA/clay series and the CPBM/clay series can be seen in Figures 6.8 and 6.9. The differential thermogravimetric curves suggest that there are two important thermal stages. The first stage can be seen in the region of 100-300 ºC as a small shoulder on the

main decomposition peak, and the second stage is located in the 300-400 ºC region [45]. The first stage may be related to the decomposition of the head-to-head linkages, and the second is related to the unzipping of the polymer via random scission of the polymer chains [46-51]. The addition of the modified clay to the pure PBMA shifted the onset temperature, which in this case is the temperature corresponding to the loss at 10 wt%, to higher values form 222 ºC to 250-260 ºC for the PBMA/clay series. This shift to a higher temperature was also seen for the CPBM/clay series. For this series the onset temperature for the CPBM/60-40 was shifted to 276 ºC, which represents an increase of 50 ºC with respect to the pristine PBMA polymer. These results indicate that the thermal stability of the pure polymer is increased by the addition of clay nanocomposites. During thermal decomposition layered materials such as montmorillonite, generate a protective layer at the surface of the polymer. The charred layered material produces a thermal insulating layer, which reduces the concentration of the polymer at the surface and ultimately leads to a less flammable material [13, 52-54]. The insulating layer produced by the layered material hinders the diffusion of volatile compounds produced during the decomposition stages of the polymer. The characterization also suggests that the thermal stability of the barrier membranes also increased by the addition of the methyl methacrylate content in the copolymer composition. The improved thermal stability of PMMA/clay systems was previously reported by Giannelis et al.[55]. This group reported that PMMA/montmorillonite nanocomposites had improved thermal stability due to a higher amount of aluminosilicates in the montmorillonite.

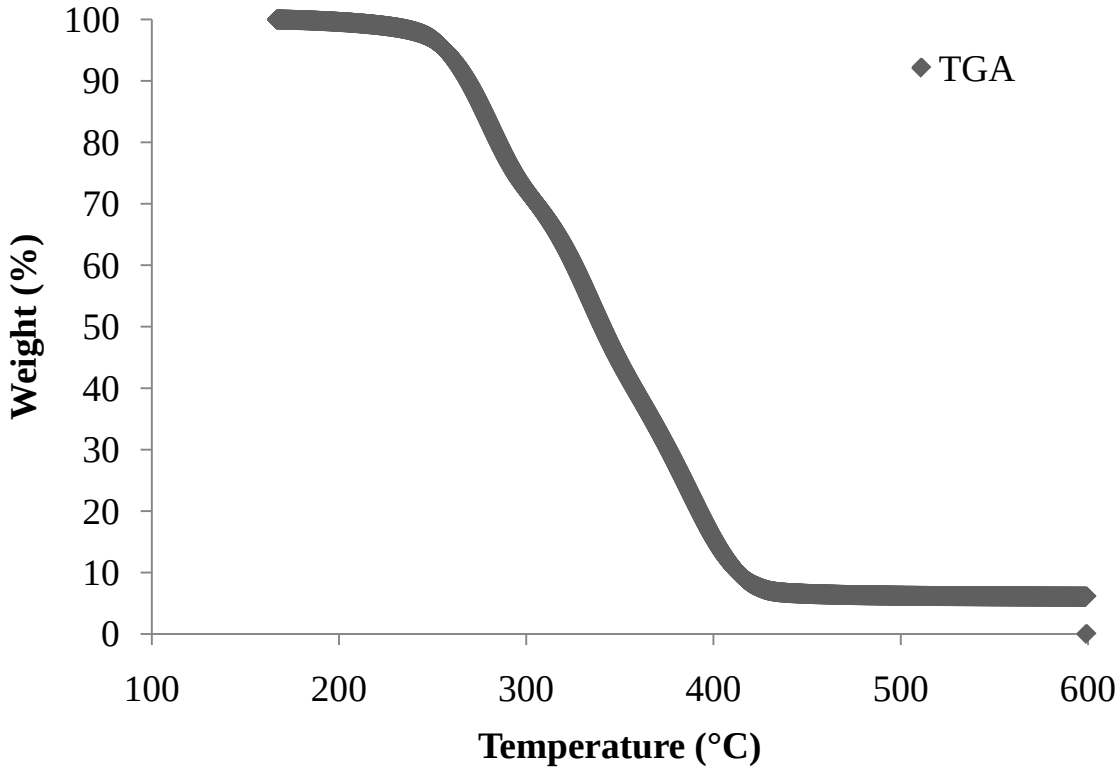

Figure 6.8. TGA and DTG of CPBM/70-30

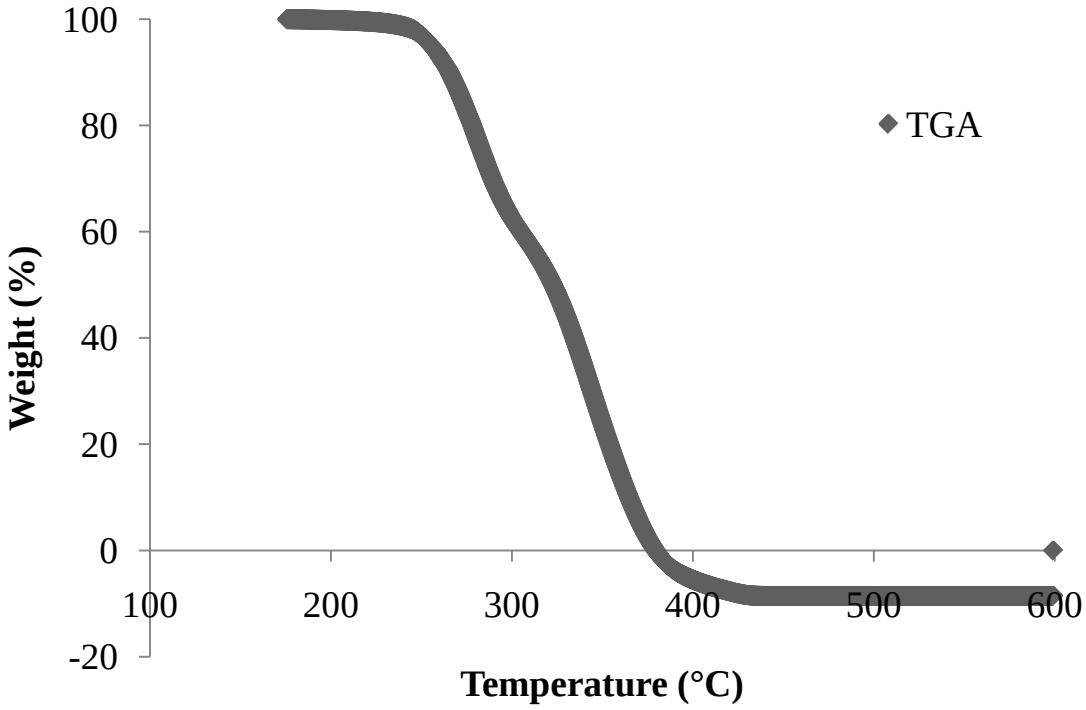

Figure 6.9. TGA and DTG of PBMA/5.

6.5.5 DLS Characterization of Emulsions

The morphology of the PBMA/clay and CPBM/clay colloidal systems were characterized via dynamic light scattering (DLS). The particle size distribution of the composites emulsion of PBMA/5 can be seen in Figure 6.10. Results from this figure suggest that emulsion particles have a monomodal distribution and also provide a narrow particle distribution size. The trends seen in this figure were the same for the whole PBMA/clay series.

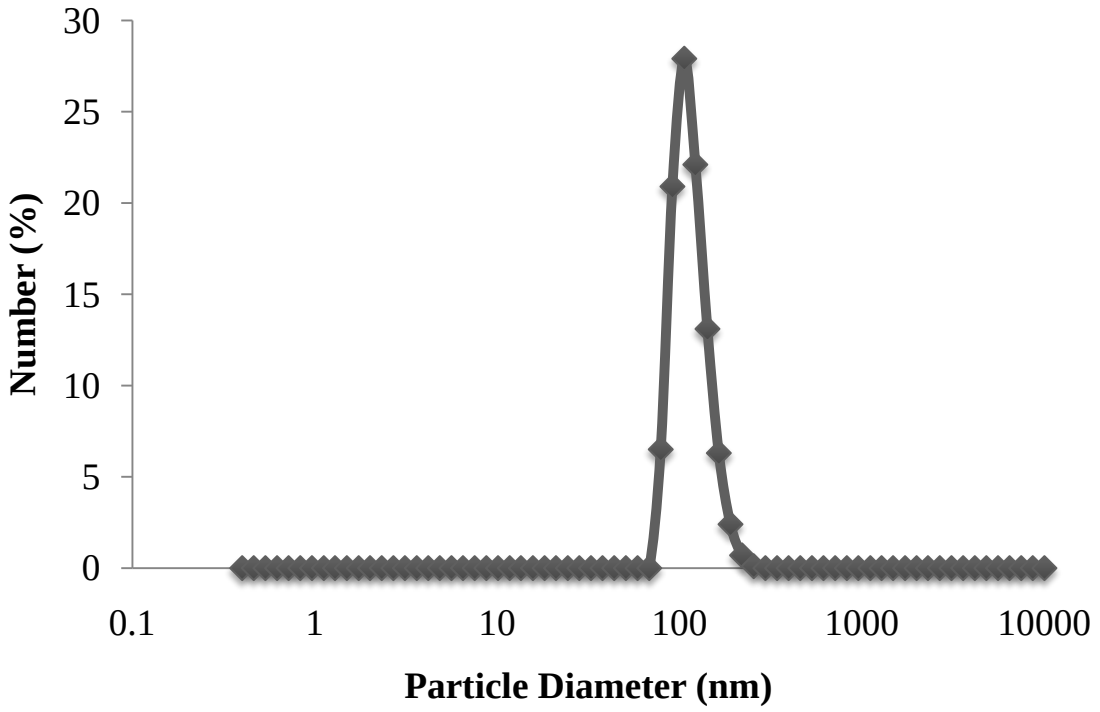

Figure 6.10 Particle size distribution of PBMA/5.

The average diameter for the PBMA/clay nanocomposite series peaked in the PBMA-1 emulsion, with an average particle size of 155.5 ± 2.12 nm. Increasing the clay concentration in PBMA/clay colloidal system lead to a decrease in particle size as can be seen in Table 6.3. This same trend was also reported by Negrete-Herrera et al [42]. PBMA/5 showed the lowest particle size in the PBMA/clay series, the value for this emulsion was 134.1 ± 2.34 nm, which suggests

that size distribution varies with clay concentration. This effect may be related to the findings of Voorn et al. [31]. This group found that the montmorillonite nanoclay platelets were located on the surface of the latex particles and their presence constrained particle growth [30, 31]. Thus, higher clay concentration led to lower particle sizes [23]. The characterization of the particle size for the CPBM/clay colloidal systems series is also summarized in Table 3.

Table 3. Average particle diameter obtained via dynamic light scattering (DLS), the effect of increasing clay concentration in the matrix decreased the particle diameter in the PBMA series. The same trend is seen with increasing methyl methacrylate concentration.

	Average particle diameter (nm)
PBMA	146.05 ± 1.61
PBMA-1	155.48 ± 2.12
PBMA-3	136.72 ± 2.23
PBMA-5	134.18 ± 1.41
CPBM/90-10	145.51 ± 2.54
CPBM/80-20	137.30 ± 4.19
CPBM/70-30	126.75 ± 1.73
CPBM/60-40	116.65 ± 1.27

The monomodal, and narrow particles size distribution plots seen in the PBMA/clay series were also seen in the CPBM/clay series. At the lowest PMMA weight ratio, 90/10, the average diameter was 145.5 ± 2.54 nm. CPBM/60-40 colloidal system provided the lowest particle size in the CPBM/clay series, with an average size of 116 ± 1.2 nm. The addition of PMMA to the colloidal system further decreased the average diameter of the particles. According to He et al. and Riess [56, 57], the decrease in particle size of the copolymer particle is due to the polarity of the methyl methacylate monomer. The polarity of the MMA monomer, 0.149, is higher than that of the butyl methacrylate monomer, 0.096. The increase in hydrophobicity of the monomer leads to a decrease in particle size, as reported by Zhang et al [58], thus indicating that

the composition of the copolymer played an important role in the particle size of the CPBM/clay series.

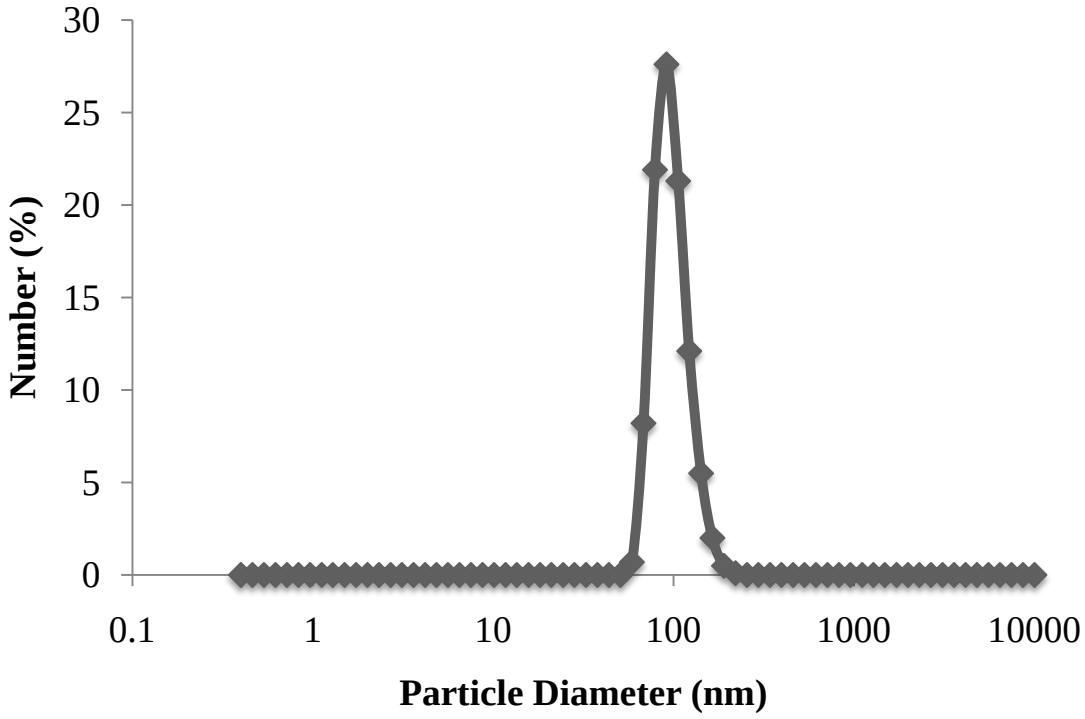

Figure 6.11 Particle size distribution of CPBM/60-40.

6.5.6 Permeation Data

Gas permeation results for the PBMA/clay series can be seen in Figure 6.9. As seen in Figure 6.12, permeability decreased with increasing modified clay concentration in the matrix, as expected. The decrease in gas permeation in composites with the initial modified clay concentration 1 wt%, was on the average of 10% compared to the pristine PBMA. At the highest clay concentration of 5 wt% in the matrix, gas permeation in the nanocomposites decreased by 28%. Results of these gas permeation measurements suggest that emulsified barrier nanocomposites have decreased barrier properties compared to barrier nanocomposites synthesized via *in situ* polymerization [38].

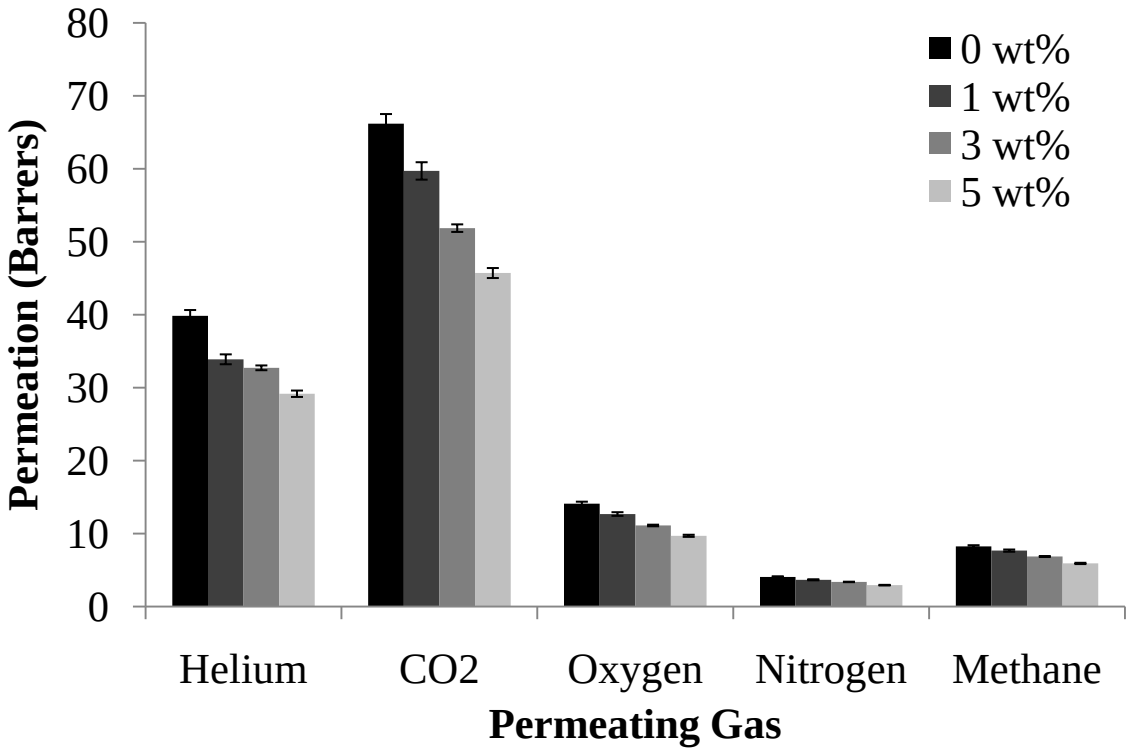

Figure 6.12. Permeation values for PBMA/clay series. Increasing clay concentration lead to decrease in permeability values for all gases tested.

The use of a glassy co-polymer such as PBMA-PMMA, improved the overall thermal properties, and the mechanical properties of the nanocomposites, but also decreased gas permeability due to more restricted segmental chain motion and decreased free volume in the matrix [59, 60]. Gas permeation data from the PBMA-PMMA/clay nanocomposites series can be seen in Figure 6.10. This figure compares the permeation values of the pristine PBMA and the co-polymers of PBMA-PMMA nanocomposites. Data from Figure 6.13 suggests that as the weight ratio of PMMA to PBMA increases, from 10-90 up to 40-60, the gas permeation values for the penetrant gases decrease, thus generating improved barrier properties. At the 40:60 weight ratio of PMMA-PBMA, permeation values for CH_4 and CO_2 decreased by 85% and 83% respectively, when compared to the pristine PBMA barrier membrane. The decrease in

permeability due to the addition of the PMMA component, may be due to a denser packed polymer chain in the matrix [61]. The packing density increase may also lead to a decrease of the voids in the vicinity of the chains [62], thus hampering the overall gas permeation.

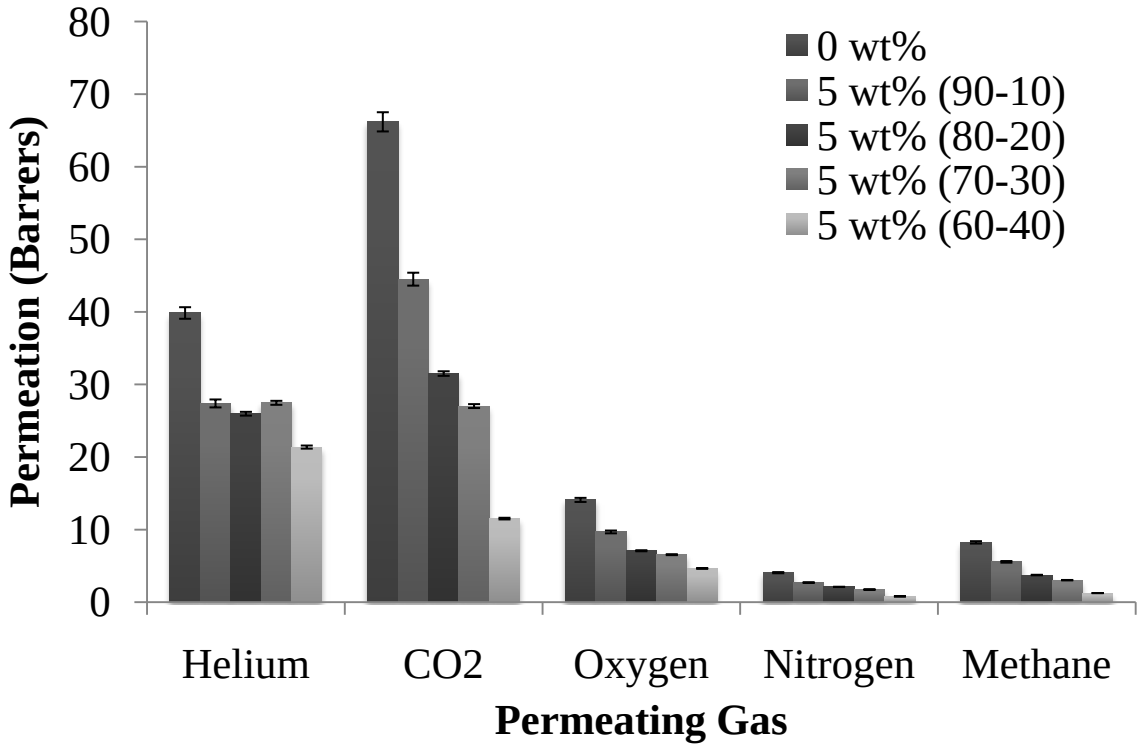

Figure 6.13. Comparision of pristine PBMA and co-polymer CPBM/clay series. Increasing weight ratio of MMA monomer decrease permeation values.

6.5.7 Gas Permeation Models

Different phenomenological models have been used to predict gas permeation properties of polymer/clay nanocomposites [63-70]. One of the first models was Nielsen's model [68]. This model was based on certain geometric assumptions corresponding to the ribbons contained within the polymer matrix. Nielsen defined the ribbons as of a width *w*, thickness *t*, and infinite length. This model also assumes a perfect dispersion and alignment of the ribbons in the polymer matrix. Cussler's initial model [64, 65] was also based on perpendicular alignment of the ribbons

to the direction of the permeating molecules, and even distribution of the flake like platelets. Yang and Cussler's [69] modified the initial mode, which considered monodispersity of the flakes, to account for random spacing of the flakes in the matrix. Lape and Cussler [67] also accounted for the polydispersity effect in the matrix, thus prompting a further modification of the original equation. Lape's modification considers the random arrangement of the flake like structures in the matrix, and also suggests that the flakes may vary with respect to the width *w*, but considers the thickness of the flakes as a constant *t* value. The permeability data obtained for the different barrier membrane nanocomposites, PBMA/clay and for PBMA-PMMA/clay were fitted to the models cited above. In order to compare the experimental data obtained via permeation measurements, the properties of the clay composite must be known. According to provider of Cloisite ® Na+, Southern Clay Products, the natural montmorillonite has an aspect ratio α, between 50-100. The data points for the permeating gases can be seen in this Figure 6.14. This figure indicates that the relative permeability decreases with increasing clay loading. The smooth lines in Figure 6.14 are the profiles obtained from the different permeation models when fixing the aspect ratio at 50. These results suggest that the PBMA/clay barrier membranes have an adequate and even dispersion of the clay platelets in the matrix. These results also suggest that the barrier membranes approach the ideal behavior. This figure also indicates that the PBMA/clay series provides a constant aspect ratio value throughout.

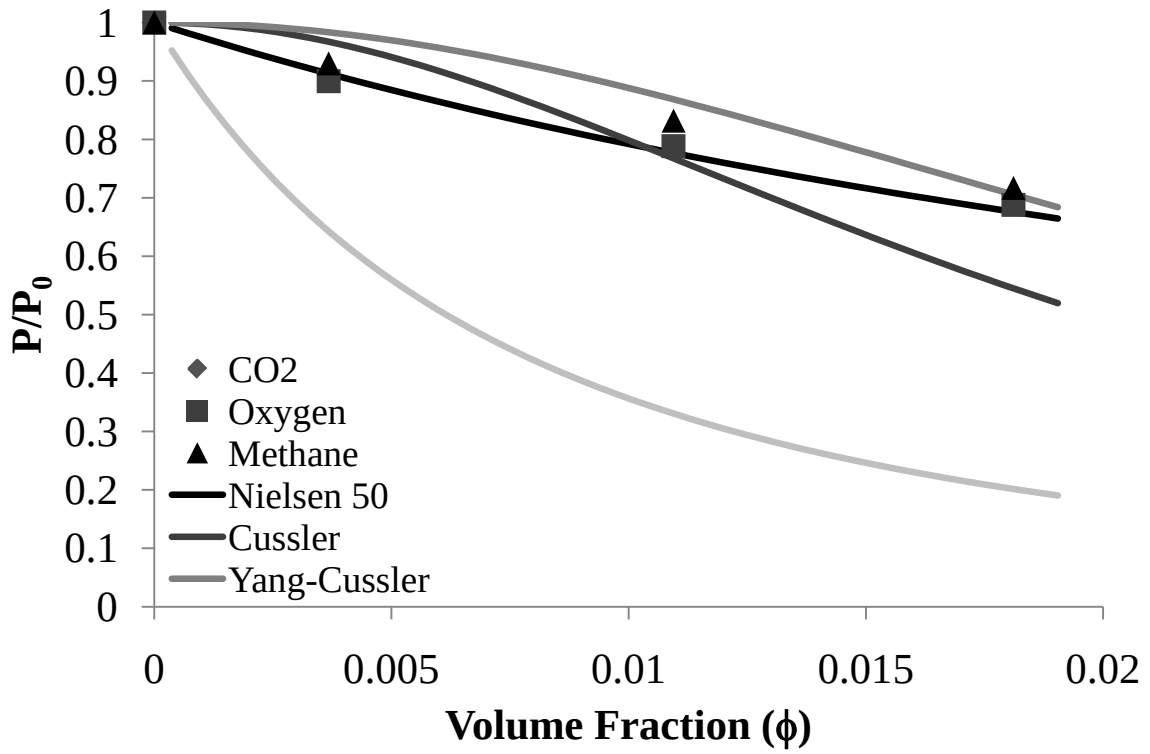

Figure 6.14. Phenomenological models used to predict permeation values for barrier membrane nanocomposites. Aspect ratio used in this plot was $\alpha = 50$ for all the models. ♦CO_2, ■O_2, ▲CH_4.

6.6 Conclusions

Polymer/clay nanocomposites prepared by emulsion polymerization demonstrated possible exfoliation of the clay platelets in the polymer matrix. The combination of SEM micrographs and DLS measurements suggest that clay exfoliation in the colloidal solution restricts the size of the polymer particles. SEM micrographs also suggest the presence of more than one polymer particle attached to delaminated clay platelets in the matrix. The composition of the PBMA-PMMA copolymer also modified the average diameter of the polymer/clay particles in the emulsion. Thermogravimetric analysis indicated improved thermal decomposition properties with increasing clay concentration. Gas permeation characterization pointed out that the combined effect of a more glassy polymer in the matrix and the modified clay helped yield

better barrier properties for the polymer/clay nanocomposites. The restricted segmental chain motion in of the polymer chains due to presence of exfoliated clay layers helped generate a more tortuous pathway for permeating gas molecules. According to the phenomenological models used to predict relative permeation ratios for nanocomposites, the more glassy polymer in this case PMMA, helped improved dispersion properties of the individual platelets.

Acknowledgments

We thank the National Science Foundation for support of this work via grant CMMI 0600090, and the Nanoscale Characterization and Fabrication Laboratory, a Virginia Tech facility operated by the Institute for Critical Technology and Applied Science for the help on the SEM micrographs.

References

1. Usuki, A., et al., *Synthesis of nylon 6-clay hybrid.* Journal of Materials Research, 1993. **8**(5): p. 1179-1184.
2. Kojima, Y., et al., *Mechanical properties of nylon 6-clay hybrid.* Journal of Materials Research, 1993. **8**(5): p. 1185-1189.
3. Gao, F., *Clay/polymer composites: the story.* Materials Today, 2004. **7**(11): p. 50-55.
4. Tjong, S.C., *Structural and mechanical properties of polymer nanocomposites.* Material Science and Engineering R, 2006(53): p. 124.
5. Sinha Ray, S. and M. Okamoto, *Polymer/layered silicate nanocomposites: a review from preparation to processing.* Progress in Polymer Science, 2003. **28**(11): p. 1539-1641.
6. Wang, Z. and T.J. Pinnavaia, *Nanolayer Reinforcement of Elastomeric Polyurethane.* Chemistry of Materials, 1998. **10**(12): p. 3769-3771.
7. Yoon, P.J., T.D. Fornes, and D.R. Paul, *Thermal expansion behavior of nylon 6 nanocomposites.* Polymer, 2002. **43**(25): p. 6727-6741.
8. Beyer, G., *Nanocomposites: a new class of flame retardants for polymers.* Plastics, Additives and Compounding, 2002. **4**(10): p. 22-28.
9. Jeong, H.K., et al., *Fabrication of Polymer/Selective-Flake Nanocomposite Membranes and Their Use in Gas Separation.* Chemistry of Materials, 2004. **16**(20): p. 3838-3845.
10. Ogasawara, T., et al., *Helium gas permeability of montmorillonite/epoxy nanocomposites.* Composites Part A: Applied Science and Manufacturing, 2006. **37**(12): p. 2236-2240.

11. Xu, B., et al., *Calculating barrier properties of polymer/clay nanocomposites: Effects of clay layers.* Polymer, 2006. **47**(8): p. 2904-2910.
12. Cárdenas, M.A., et al., *Mechanical and fire retardant properties of EVA/clay/ATH nanocomposites – Effect of particle size and surface treatment of ATH filler.* Polymer Degradation and Stability, 2008. **93**(11): p. 2032–2037.
13. Du, B., et al., *Flame retardant mechanism of organo-bentonite in polypropylene.* Applied Clay Science, 2009. **45**(3): p. 178-184.
14. Alexandre, M. and P. Dubois, *Polymer-layered silicate nanocomposites: preparation, properties and uses of a new class of materials.* Material Science and Engineering R, 2000. **28**.
15. Ray, S.S., K. Okamoto, and M. Okamoto, *Structure−Property Relationship in Biodegradable Poly(butylene succinate)/Layered Silicate Nanocomposites.* Macromolecules, 2003. **36**(7): p. 2355–2367.
16. Vaia, R.A. and E.P. Giannelis, *Polymer Melt Intercalation in Organically-Modified Layered Silicates: Model Predictions and Experiment.* Macromolecules, 1997. **30**: p. 8000-8009.
17. Nguyen, Q.T. and D.G. Baird, *An improved technique for exfoliating and dispersing nanoclay particles into polymer matrices using supercritical carbon dioxide.* Polymer, 2007. **48**(23): p. 6923-6933.
18. Zhang, Z., et al., *Synthesis and characterization of poly(butyl acrylate-co-methyl methacrylate) clay nanocomposites via emulsion polymerization.* International Journal of Nanoscience, 2006. **5**(2&3): p. 291-297.
19. Herrera-Alonso, J.M., et al., *Transport properties in polyurethane/clay nanocomposites as barrier materials: Effect of processing conditions.* Journal of Membrane Science, 2009. **337**(1-2): p. 208-214.
20. Patel, S., et al., *Effect of acrylic copolymer an terpolymer composition on the properties of in-situ polymer silica hybrid nanocomposites.* Journal of Materials Science, 2006. **41**(3): p. 927-936.
21. Xu, Y., et al., *Effect of clay type on morphology and thermal stability of PMMA-clay nanocomposites prepared by thermal heterocoagulation method.* Polymer, 2004. **45**(11): p. 3735-3746.
22. Yang, W.T., et al., *Preparation of polystyrene/clay nanocomposite by suspension and emulsion polymerization.* Polymer Composites, 2008. **29**(4): p. 409-414.
23. Diaconu, G., et al., *Macroinitiator and macromonomer modified montmorillonite for the synthesis of acrylic/MMT nanocomposite latexes.* Macromolecules, 2009. **42**(9): p. 3316-3325.
24. Donescu, D., et al., *Synthesis of polyvinylacetate-sodium montmorillonite hybrids by emulsion polymerization in the presence of anionic surfactants.* Journal of Dispersion Science and Technology, 2007. **28**(5): p. 671-679.
25. Ruggerone, R., et al., *Highly filled polystyrene-laponite nanocomposites prepared by emulsion polymerization.* European Polymer Journal, 2009. **45**(3): p. 621-629.
26. Negrete-Herrera, N., et al., *Aqueous dispersions of silane-functionalized laponite clay platelets. A first step toward the elaboration of water-based polymer/clay nanocomposites.* Langmuir, 2004. **20**(5): p. 1564-1571.

27. Diaconu, G., M. Paulis, and J.R. Leiza, *Towards the synthesis of high solids content waterborne poly(methyl methacrylate-co-butyl acrylate)/montmorillonite nanocomposites.* Polymer, 2008. **48**(10): p. 2444-2454.
28. Zhang, J., K. Chen, and H. Zhao, *PMMA colloid particles armored by clay layers with PDMAEMA polymer brushes.* Journal of Polymer Science A: Polymer Chemistry, 2008. **46**(8): p. 2632-2639.
29. Bon, S.A.F. and P.J. Colver, *Pickering miniemulsion polymerization using laponite clay as a stabilizer.* Langmuir, 2007. **23**(16): p. 8316-8322.
30. Guillot, S., et al., *Internally structred pickering emulsions stabilized by clay mineral particles.* Journal of Colloid and Interface Science, 2009. **333**(2): p. 563-569.
31. Voorn, D.J., W. Ming, and A.M. van Herk, *Polymer-clay nanocomposites latex particles by inverse pickering emulsion polymerization stabilized with hydrophobic montmorillonite platelets.* Macromolecules, 2006. **39**(6): p. 2137-2143.
32. Wu, Y., J. Zhang, and H. Zhao, *Functional colloidal particle stabilized by layered silicate with hydrophilic face and hydrophobic polymer brushes.* Journal of Polymer Science A: Polymer Chemistry, 2009. **47**(6): p. 1535-1543.
33. Ding, S., et al., *Amphiphilic mesoporous silica composite nanosheets.* Journal of Materials Chemistry, 2009. **19**: p. 3443 - 3448.
34. Cauvin, S., P.J. Colver, and S.A.F. Bon, *Pickering stabilized miniemulsion polymerization: preparation of clay armored latexes.* Macromolecules, 2005. **38**(19): p. 7887-7889.
35. Pickering, S.U., *Pickering: Emulsions.* Journal of the Chemical Society, Transactions, 1907. **91**: p. 2001-2021.
36. Binks, B.P., *Particles as surfactants--similarities and differences.* Current Opinion in Colloid & Interface Science, 2002. **7**(1-2): p. 21-41.
37. Lin, Y., et al., *Nanoparticle Assembly at Fluid Interfaces: Structure and Dynamics.* Langmuir, 2005. **21**(1): p. 191-194.
38. Herrera-Alonso, J.M., Z. Sedláková, and E. Marand, *Gas Barrier Properties of Nanocomposites Based on In situ Polymerized Poly(n-butyl methacrylate) in the Presence of Surface Modified Montmorillonite.* Journal of Membrane Science, 2009. **Submitted**.
39. Sedláková, Z., et al., *Polymer-clay nanocomposites prepared via in situ emulsion polymerization.* Polymer Bulletin, 2009. **63**(3): p. 365-384.
40. Crank, J., *The Mathematics of Diffusion*. Oxford Science Publications. 1979, New York: Oxford University Press.
41. Voorn, D.J., W. Ming, and A.M. van Herk, *Clay platelets encapsulate inside latex particles.* Macromolecules, 2006. **39**(14): p. 4654-4656.
42. Negrete-Herrera, N., et al., *Polymer/laponite composite colloids through emulsion polymerization: Influence of the clay modification level on particle morphology.* Macromolecules, 2006. **39**(26): p. 9177-9184.
43. Greesh, N., et al., *Impact of the clay organic modifier in the morphology of polymer-clay nanocomposites preprared by In Situ free-radical polymerization in emulsion.* Journal of Polymer Science A: Polymer Chemistry, 2008. **46**(11): p. 3619-3628.
44. Kilburn, D., et al., *Free volume in poly(n-alkyl methacrylate)s from positron lifetime and PVT experiments and its relation to the structural relaxation.* Polymer, 2006. **47**(22): p. 7774-7785.

45. Luna-Xavier, J.L., E. Bourgeat-Lami, and A. Guyot, *The role of initiation in the synthesis of silica/poly(methyl methacrylate) nanocomposites latex particles through emulsion polymerization.* Colloid and Polymer Science, 2001. **279**(10): p. 947-958.
46. Meneghetti, P. and S. Qutubuddin, *Synthesis, thermal properties and applications of polymer-clay nanocomposites.* Thermochimica Acta, 2006. **442**(1-2): p. 74-77.
47. Lin, R.Y., et al., *Preparation of porous PMMA/Na+–montmorillonite cation-exchange membranes for cationic dye adsorption.* Journal of Membrane Science, 2009. **326**(1): p. 117-129.
48. Daraboina, N. and G. Madras, *Thermal and photocatalytic degradation of poly(methyl methacrylate), poly(butyl methacrylate), and their copolymers.* Industrial & Engineering Chemistry Research, 2008. **47**(18): p. 6828-6834.
49. Demirelli, K., A. Kurt, and M. Coşkun, *Thermal degradation and synthesis of block copolymers of styrene and n-butyl methacrylate by atom transfer radical polymerization.* Polymer-Plastics Technology and Engineering, 2004. **43**(4): p. 1245-1263.
50. Milovanović, M., et al., *The thermal degradation of poly(diethyl fumarate).* Polymer Degradation and Stability, 2006. **91**(12): p. 3221-3229.
51. Novaković, K., L. Katsikas, and I.G. Popović, *The thermal degradation of poly(iso-butyl methacrylate) and polu (sec-butyl methacrylate).* Journal of Serbian Chemical Society, 2000. **65**(12): p. 867-875.
52. Laoutid, F., et al., *New prospects in flame retardant polymer materials: From fundamentals to nanocomposites.* Materials Science and Engineering: R: Reports, 2009. **63**(3): p. 100-125.
53. Kashiwagi, T., et al., *Flame retardant mechanism of polyamide 6–clay nanocomposites.* Polymer, 2004. **43**(3): p. 881-891.
54. Kashiwagi, T., et al., *Flame-Retardant Mechanism of Silica: Effects of Resin Molecular Weight.* Journal of Applied Polymer Science, 2002. **87**(9): p. 1541-1553.
55. Bandyopadhyay, S. and E.P. Giannelis, *Thermal and thermo-mechanical properties of PMMA nanocomposites.* Polymeric Materials Science and Engineering, 2000. **82**: p. 208-210.
56. He, X.D., et al., *The preparation of composite microsphere with hollow core/porous shell structure by self-assembling of latex particles at emulsion droplet interface.* Journal of Colloid and Interface Science, 2006. **299**(2): p. 791-796.
57. Riess, G., *Block copolymers as polymeric surfactants in latex and microlatex technology.* Colloids and Surfaces A: Physicochemical and Engineering Aspects, 1999. **153**(1-3): p. 99-110.
58. Zhang, M.-G., et al., *Effects of monomer polarity on MMA/BA/NaMA emulsifier-free emulsion copolymerization.* European Polymer Journal, 1998. **34**(9): p. 1243-1247.
59. Jonquières, A., R. Clément, and P. Lochon, *Permeability of block copolymers to vapors and liquids.* Progress in Polymer Science, 2002. **27**(9): p. 1803-1877.
60. Naylor, T.V., ed. *Permeation Properties*. Comprehensive Polymer Science, ed. A. Geoffrey. 1989, Pergamon Press Inc. 643-668.
61. Ronova, I.A., et al., *Occupied and Accessible Volumes in Glassy Polymers and Their Relationship with Gas Permeation Parameters.* Macromolecular Theory and Simulation, 2003. **12**(6): p. 425-439.
62. Koros, W.J., et al., *Polymeric membrane materials for solution-diffusion based permeation separations.* Progress in Polymer Science, 1998. **13**(4): p. 339-401.

63. Bharadwaj, R.K., *Modeling the Barrier Properties of Polymer-Layered Silicate Nanocomposites.* Macromolecules, 2001. **34**(26): p. 9189-9192.
64. Cussler, E.L., et al., *Barrier Membranes.* Journal of Membrane Science, 1988. **38**(2): p. 161-174.
65. Eitzman, D.M., R.R. Melkote, and E.L. Cussler, *Barrier membranes with tipped impermeable flakes.* AIChE Journal, 1996. **42**(1): p. 2-9.
66. Falla, W.R., M. Mulski, and E.L. Cussler, *Estimating diffusion through flake-filler membranes.* Journal of Membrane Science, 1996. **119**(1): p. 129-138.
67. Lape, N.K., E.E. Nuxoll, and E.L. Cussler, *Polydisperse flakes in barrier films.* Journal of Membrane Science, 2004. **236**(1-2): p. 29-37.
68. Nielsen, L.E., *Models for the permeability of filled polymer systems.* J. Macromol. Sci., Chem., 1967. **A1**.
69. Yang, C., W.H. Smyrl, and E.L. Cussler, *Flake alignment in composite coatings.* Journal of Membrane Science, 2004. **231**(1-2): p. 1-12.
70. Liu, Q. and E.L. Cussler, *Barrier membranes made with lithographically printed flakes.* Journal of Membrane Science, 2006. **285**(1-2): p. 56-67.
71. Wright, C.T. and D.R. Paul, *Gas sorption and transport in poly(tertiary-butyl methacrylate).* Polymer, 1997. **38**(8): p. 1871-1878.

Chapter 7 Final Conclusions and Future Work

7.1 Overall Conclusions

The characterization results for the polyurethane/clay nanocomposites series indicate that complete exfoliation of the silicate platelets was not achieved via solution casting. One of the interesting results seen in this work was the interactions of the different surfactants used to organically modify the surface of the silicate platelets. The organic modification of the silicate platelets had a direct effect on the dispersion of the platelets in the polymer matrix. For example, modification of the silicate platelets with alkyl ammonium groups with two tallow tails, such as the Cloisite ® 20A, introduced steric hindrance and prevented penetration of the polyurethane in the gallery space, thus limiting the exfoliation of the silicate platelets. The structure of the Cloisite ® 20A is seen in Figure 1. On the other hand, the use of alkyl ammonium groups with only one tail, such as Cloisite ® 10A and Cloisite ® 30B, did improve the dispersion properties of the platelets in the matrix, although the simple mixing process was not enough to achieve a fully exfoliated morphology in the matrix. The chemical structure of Cloisite ® 10A can be seen in Figure 2.

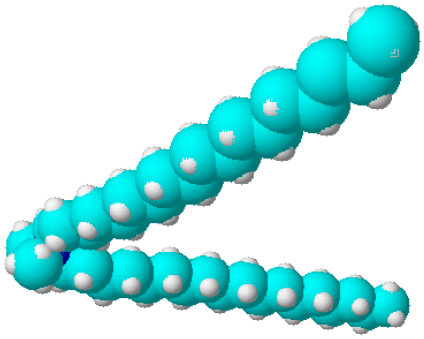

Figure 7.1 Chemical structure of Cloisite ® 20A, where the hydrogenated tallow is (~65% C18; ~30% C16; ~5% C14).

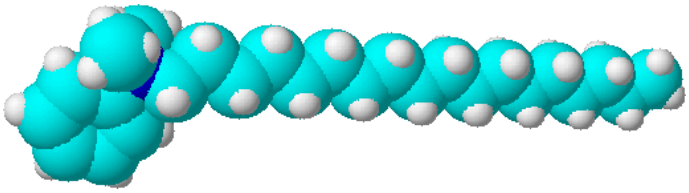

Figure 7.2 Chemical structure of Cloisite ® 10A, where the hydrogenated tallow is (~65% C18; ~30% C16; ~5% C14).

Another interesting result of this work was the use of sonication to disperse clay platelets in the matrix. Permeation results suggested that sonication enhanced the barrier properties of the membranes by improving the dispersion properties of the silicate platelets. Permeation data from the sonication series also suggest that gas molecules take a more tortuous pathway during permeation. Polyurethane/clay nanocomposites showed a significant decrease in diffusivity coefficient of permeating VOC molecules, although the decrease occured at the high content of clay in the matrix. Diffusivity coefficients for the sonciated series suggest that this method improved the barrier properties of the membranes. Results from the sorption coefficient or

partition coefficient (K) suggest that the permeating VOC molecules interact with the polymer matrix on a molecular level, and that partition coefficient is dominated by thermodynamic interactions and not by the morphology of the nanocomposite.

The evolutionary process of the research led us to consider alternative preparation methods that would lead to an improvement in the barrier properties. According to the review by Ray and Okamoto [1], another possible synthesis method to obtain polymer/clay nanocomposites is the synthesized via *in situ* polymerization. The *in situ* polymerization of poly(n-butyl methacrylate)/clay nanocomposites yielded barrier membranes with exfoliated morphologies as seen via XRD diffractograms. The grafting reaction of the monomer n-butyl methacrylate with the tether group on the surface of the clay platelets allowed for the complete exfoliation of the platelets, thus producing well dispersed silicate platelets in the matrix. The dispersion of the clay platelets in the matrix was also enhanced by the organically modified clay. Organic modification of natural montmorillonte Cloisite ® Na^+, was done via two different methods, sonication and stirring. Permeation results for barrier membranes obtained with sonicated clay indicate enhanced barrier properties. Phenomenological models used to predict permeation values indicate that sonication of the modified clay helped the barrier membranes to approach the ideal distribution of the platelets in the matrix. Figure 7.3 corresponds to the ideal distribution of the platelets in a 3D environment, on which the phenomenological models are based.

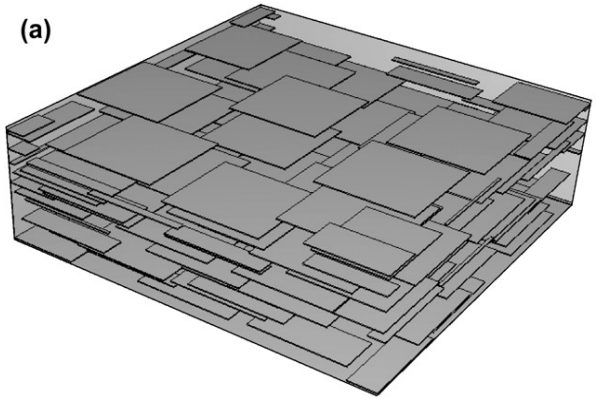

Figure 7.3. Ideal distribution of silicate platelets in the matrix. The silicate platelets are perpendicularly aligned in the direction of the gas permeating molecules. Also there is a regular spacing in the x and y directions.

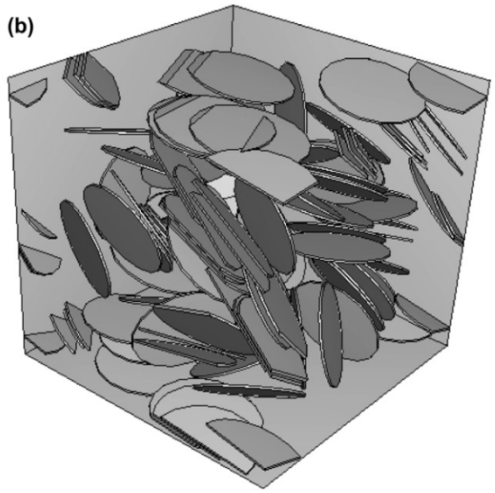

Figure 7.4 Platelets throughout the matrix are randomly dispersed and not aligned.

Figure 7.4, can be considered the “real” distribution of the platelets in the matrix. The random arrangement of the individual silicate platelets in the matrix in the x, y and z directions maybe the cause for the discrepancies with the experimental results and the values predicted by the phenomenological models.

In the last stage of this dissertation, polymer/clay nanocomposites were synthesized via emulsion polymerization. Greener and more environmentally friendly procedures prompted the use of this synthesis method. Since the final application of these barrier membranes would be in the form of paints and coatings, we have chosed to employ polymethacrylates as the matrix. N-butyl methacrylate was used as monomer in the emulsion polymerization of the nanocomposites. XRD diffractograms of the resulting nanocomposite membranes suggest intercalation and possible exfoliation of the clay platelets in the matrix. Permeation data of the barrier membranes obtained via emulsion polymerization suggested improved barrier properties when compared to the pristine poly(n-butyl methacrylate). Furthermore, the permeation values of nanocomposites obtained via emulsion polymerization were higher than those obtained via *in situ* polymerization at the same clay content. These results prompted the prompted the use copolymers of poly(butyl methacrylate) and poly(methyl methacrylate) to decrease permeability. SEM micrographs of the colloidal solutions suggest that the presence of the silicate platelets restricts the size of the polymer particles. These micrographs also suggest that more than one silicate platelet may be attached to the surface of the polymer particles. The use of the copolymer PMMA/PBMA with high PMMA content in fact enhanced the barrier properties of the membranes. The addition of the copolymer produced a decrease in gas permeability of up to 85%, in comparison to the pristine PBMA/clay polymer. The interaction of the PMMA with the silicate layers further restricted the molecular chain motion in the matrix, which was corroborated by the increase in T_g for the copolymer series. The copolymers also enhanced the physical properties of the barrier membranes. Experimental permeation data was analyzed by the use of phenomenological models such as those of Nielsen [2], and Cussler [3], and the further modifications of Cussler's original equation [4, 5]. Fitting these phenomenological models to the experimental permeation data

yieled the aspect ratio of the clay particles. For the poly(n-butyl methacrylate)/clay nanocomposite series, the apparent aspect ratio was around 50. This is the same value as reported by the manufacturer, Southern Clay Products, for natural montmorillonite. These phenomenological models suggest a good dispersion of the layered materials in the matrix.

7.2 Future considerations

The main aim of the research project was to develop polymer/clay nanocomoposites that may act as barrier membranes for structural insulated panels. These barrier membranes may be applied as a coating, which lead our group to consider emulsion based on polyacrylates, which are known to be used in the paint industry [6, 7]. The synthesis of the barrier membranes via emulsion polymerization was an initial step towards developing a product aimed at the paint and coating industry. One of the problems encountered through the synthesis of the colloidal solutions was the flocculation of the polymer/clay particles at high water to monomer ratios. In our work we experienced problems obtaining stable colloidal solutions at high water to monomer ratios. We tried the synthesis of polymer/clay nanocomposites via emulsion polymerization at water to monomer ratios of 1:1, 2:1 and 5:1. At these high water to monomer ratios, the latex presented coagulum, thus indicating a poor colloidal stability. This poor colloidal stability was caused by the clustering of the aggregates in the emulsion. The attractive forces between the nanocomposites particles proved to be stronger at a high monomer concentration. The 10:1 water to monomer ratio, did not present coagulation in the colloidal solution, thus providing enhanced colloidal stability. With these problems in mind future work may be directed towards developing stable colloidal solutions with a high monomer to water ratios. The combined effect of a higher monomer to water ratios, and the synthesis of polymer/clay nanocomposites in the colloidal

solution will prove attractive to the paint and coating industry [8]. The foreseeable application for this technology would be a paint or coating that decreases of VOC content emitted from structural insulated panels (SIPs). The commercialization of these types of emulsions are mainly targeted to improve indoor air quality, although this technology does not have to be limited to only VOC emitting SIPs. The application may be extrapolated to various polymer products, such as vinyl flooring [9], and wood derived products [10], which has been known to be a primary emission source of VOCs. A possible study may be in the direction of coating small amounts of oriented strand boards and/or polystyrene/polyurethane foam used in SIP and measuring the decrease in source emission via use of microbalance characterization. The initial study would be oriented to obtaining sink/source diffusivity coefficient profiles for the materials coated with the barrier membrane. This study would help quantify the decrease in diffusivity coefficients for the individual materials when coated with the barrier membranes. Once the decrease in diffusivity profiles has been confirmed by the use of coating barrier membranes, the second stage of the proposed research project would be a characterization of VOCs emitted in extended time periods. Gravimetric sampling may be carried out on a daily basis during a 30 to 50 day interval. This study would help predict the long term effects of the coating as a barrier membrane. The long term measurements have been carried out by Little el al. [11].

Future work related to *in situ* polymerization of acrylates may be aimed at incorporating layered materials such as aluminophosphates into the polymer matrix. In previous years, our group [12, 13], has worked with aluminophosphates as mixed matrix membranes in order to improve gas separation. Once exfoliated the aluminophosphates can separate gases via a molecular sieve mechanism [14]. The crystal structure of the aluminophosphates may allow for increased selectivity in the matrix. According to these studies done by our group, layered

materials such as aluminophosphates present problems in the degree of exfoliation of the platelets in the polymer matrix. Vaughan et al. [12, 13], suggest that aluminophosphates may be modified to change the surface properties of the layered materials. Ion exchange reactions may tether reactive groups on the surface of the layered material, thus providing a seed surface for grafting of polymer chains. The polymer grafting will facilitate the exfoliation/intercalation effect. Further study would be aimed at evaluating the amount of surfactant used in the surface modification and the possible impact this may have on the total amount of polymer grafted on the surface of the aluminophosphates layers. The amount of polymer grafted to the surface of the aluminophosphates layers may be determined by thermogravimentric analysis [15].

Theoretically, the packing density of the polymer chains in the matrix affects the permeability of the mixed matrix membrane, which may ultimately affect the selectivity of the mixed matrix [16, 17], thus limiting the effective separation properties of the membrane. Another element worth evaluating would be the type of monomer used in the *in situ* polymerization reaction. Our study with different copolymers indicated that the different acrylate groups used as the polymer matrix made a difference in the permeation properties of the polymers. Although free volume studies were not carried out, it would be interesting to evaluate the free volume in the mixed matrix and the effect that different side groups have may have on permeation properties[18, 19], as well as thermal stability properties of the polymers/clay nanocomposites. The packing density would also be an interesting topic to study, due to possible phase separation with the polymer and the layered materials. According to Giannelis [20], there may be certain incompatibilities of the layered materials with the polymers and/or the surfactant than may lead to a decrease in gas separation properties.

The contribution of improving indoor air quality and the environment maybe just the starting point for these polymer/clay nanocomposites. With the packing industry in mind [21], the production of barrier membranes based on biodegradable polymers may also be an attractive area. These biodegradable polymers would help decrease the amount landfills used to dispose of plastic waste and also prevent the possible incineration of these materials. Ray and Bousmina [22], indicated that the desired properties of "greener" and more environmentally friendly polymers such as biodegradable polymers are low melt viscosity, gas barrier properties, improved thermal and mechanical stability and a slow biodegradation rate. In order to achieve these properties, layered materials such as montmorillonite and laponite have been used to modify the properties of the pristine polymers [23, 24]. A possible synthesis alternative to produce "greener" biodegradable polymer/clay nanocomposites may be via emulsion polymerization [25].

References

1. Ray, S.S. and K. Okamoto, *Polymer/layerd silicate nanocomposites: a review from preparation to processing.* Progress in Polymer Science, 2003. **28**(11): p. 1539-1641.
2. Nielsen, L.E., *Models for the permeability of filled polymer systems.* J. Macromol. Sci., Chem., 1967. **A1**.
3. Cussler, E.L., et al., *Barrier Membranes.* Journal of Membrane Science, 1988. **38**(2): p. 161-174.
4. Lape, N.K., E.E. Nuxoll, and E.L. Cussler, *Polydisperse flakes in barrier films.* Journal of Membrane Science, 2004. **236**(1-2): p. 29-37.
5. Yang, C., W.H. Smyrl, and E.L. Cussler, *Flake alignment in composite coatings.* Journal of Membrane Science, 2004. **231**(1-2): p. 1-12.
6. TiglI, R.S. and V. Evren, *Synthesis and characterization of pure poly(acrylate) latexes.* Progress in Organic Coatings, 2005. **52**(2): p. 144-150.
7. Bauer, F., et al., *Trialkoxysilane grafting onto nanoparticles for the preparation of clear coat polyacrylate systems with excellent scratch performance.* Progress in Organic Coatings, 2003. **47**(2): p. 147-153.

8. Lai, M.-C., et al., *Advanced environmentally friendly anticorrosive materials prepared from water-based polyacrylate/Na+-MMT clay nanocomposite latexes.* European Polymer Journal, 2007. **43**(10): p. 4219-4228.
9. Cox, S.S., D. Zhao, and J.C. Little, *Measuring partition and diffusion coefficients for volatile organic compounds in vinyl flooring.* Atmospheric Environment, 2001. **35**(22): p. 3823-3830.
10. Hodgson, A.T., D. Beal, and J.E.R. McIlvaine, *Sources of formaldehyde, other aldehydes and terpenes in a new manufactured house.* Indoor Air, 2002. **12**(4): p. 235-242.
11. Yuan, H., J.C. Little, and A.T. Hodgson, *Transport of polar and non-polar volatile compounds in polystyrene foam and oriented strand board.* Atmospheric Environment, 2007. **41**(15): p. 3241-3250.
12. Vaughan, B.R. and E. Marand, *Transport properties of polymer-aluminophosphate nano-composites prepared by simple mixing.* Journal of Membrane Science, 2008. **310**(1-2): p. 197-207.
13. Vaughan, B., et al., *Transport properties of aluminophosphate nanocomposite membranes prepared by in situ polymerization.* Journal of Membrane Science, 2008. **316**(1-2): p. 153-163.
14. Jeong, H.-K., et al., *Fabrication of Polymer/Selective-Flake Nanocomposite Membranes and Their Use in Gas Separation.* Chemistry of Materials, 2004. **16**(20): p. 3838-3845.
15. Negrete, et al., *Aqueous Dispersions of Silane-Functionalized Laponite Clay Platelets. A First Step toward the Elaboration of Water-Based Polymer/Clay Nanocomposites.* Langmuir, 2004. **20**(5): p. 1564-1571.
16. Pinnau, I., Z. He, and A. Morisato, *Synthesis and gas permeation properties of poly(dialkylacetylenes) containing isopropyl-terminated side-chains.* Journal of Membrane Science, 2004. **241**(2): p. 363-369.
17. Espeso, J., et al., *Effect of substituents on the permeation properties of polyamide membranes.* Journal of Membrane Science, 2006. **280**(1-2): p. 659-665.
18. Kilburn, D., et al., *Free volume in poly(n-alkyl methacrylate)s from positron lifetime and PVT experiments and its relation to the structural relaxation.* Polymer, 2006. **47**(22): p. 7774-7785.
19. Ronova, I.A., et al., *Occupied and Accessible Volumes in Glassy Polymers and Their Relationship with Gas Permeation Parameters.* Macromolecular Theory and Simulations, 2003. **12**(6): p. 425-439.
20. Giannelis, E.P., *Polymer layered silicate nanocomposites.* Advanced Materials, 1996. **8**(1): p. 29-35.
21. Azeredo, H.M.C.d., *Nanocomposites for food packaging applications.* Food Research International. **In Press, Corrected Proof**.
22. Sinha Ray, S. and M. Bousmina, *Biodegradable polymers and their layered silicate nanocomposites: In greening the 21st century materials world.* Progress in Materials Science, 2005. **50**(8): p. 962-1079.
23. Huang, M., J. Yu, and X. Ma, *High mechanical performance MMT-urea and formamide-plasticized thermoplastic cornstarch biodegradable nanocomposites.* Carbohydrate Polymers, 2006. **63**(3): p. 393-399.
24. Bordes, P., E. Pollet, and L. Avérous, *Nano-biocomposites: Biodegradable polyester/nanoclay systems.* Progress in Polymer Science, 2009. **34**(2): p. 125-155.

25. Vladisavljevic, G.T. and R.A. Williams, *Recent developments in manufacturing emulsions and particulate products using membranes.* Advances in Colloid and Interface Science, 2005. **113**(1): p. 1-20.